

100 (AFSC)
and is
100-12
3-1-82

FUNDAMENTAL STUDIES ON AMBIENT TEMPERATURE
CREEP DEFORMATION BEHAVIOR OF ALPHA AND
ALPHA-BETA TITANIUM ALLOYS

DISTRIBUTION STATEMENT A

Approved for public release,
distribution unlimited



Charles Arthur Greene, Doctor of Philosophy, 1994

Dissertation Directed by

Dr. Sreeramamurthy Ankem, Associate Professor

Department of Materials and Nuclear Engineering

Engineering Materials Program

College of Engineering

University of Maryland

College Park

19980115 173

PII Redacted



UNIVERSITY OF MARYLAND AT COLLEGE PARK
GRADUATE STUDIES AND RESEARCH

February 15, 1994

Report of Examining Committee

Name of degree candidate: Charles Arthur Greene

Degree sought: Ph.D.

Date of Oral Examination: ☒ June 6, 1994

The examination and thesis or dissertation has been approved by the following committee. Signatures of the committee indicate that all thesis or dissertation corrections have been made.

Chairperson:

Sheila M. Anderson
A. Ray Bourd
L. L. L. L.
Ronald H. Armstrong
J. R. Yoder

Representative of the Graduate Dean (dissertation only):

Ronald H. Armstrong

(To be returned to Graduate Records Office as soon as signed by the Committee)

9/90

ABSTRACT

Title of Dissertation: FUNDAMENTAL STUDIES ON AMBIENT
TEMPERATURE CREEP DEFORMATION
BEHAVIOR OF ALPHA AND ALPHA-BETA
TITANIUM ALLOYS

Charles Arthur Greene, Doctor of Philosophy, 1994

Dissertation directed by: Dr. Sreeramamurthy Ankem, Associate
Professor, Department of Materials and
Nuclear Engineering

Systematic studies were undertaken to determine the ambient temperature tensile and creep deformation behavior, including mechanisms, of α Ti-Mn, and α - β and β Ti-Mn and Ti-V alloys. In regard to the α Ti-Mn alloy, it was found that when creep tested at 95% of the 0.2% Yield Stress (YS) the creep strain of the coarse grained (500 μ m) material was significantly higher than the fine grained (45 μ m) material. This effect was found to be due to the scientifically interesting phenomenon of time dependent twinning in coarse grained α phase. Such a phenomenon has never been reported before. Based on optical and scanning electron microscopic observations of displacements of the grid lines obtained by electron lithography and transmission electron microscopic observations, it was found that there are strong slip/twin,

twin/slip and twin/twin interactions during creep deformation. The tensile deformation of β titanium alloys depended on the alloying elements. In the β Ti-Mn alloy the tensile deformation mechanisms were found to be coarse and wavy slip whereas in the β Ti-V alloy the deformation mechanisms were found to be coarse and wavy slip as well as twinning. This difference was attributed to the difference in stability of the β phase. In contrast to the α Ti-Mn alloy the creep deformation in the β Ti-Mn alloy was found to be negligibly small at a stress level of 95% YS. With respect to α - β titanium alloys, for similar volume percent and morphology of phases, the tensile and creep deformation mechanisms were also found to depend on the alloying elements. In regard to the α - β Ti-Mn alloy, the deformation mechanisms were found to be predominately fine slip in α and β phases and occasional interface sliding. In the case of the α - β Ti-V alloy the deformation mechanisms were found to be fine slip as well as very coarse slip bands traversing across many α - β interfaces in a given colony. This difference in deformation mechanisms appears to be related to the relatively higher unstable nature of the Ti-V β phase. These results have far reaching implications for selection and design of titanium alloys for various applications. Based on these results it is reasonable to suggest for those applications where ambient temperature creep is an important factor, when selecting α titanium alloys a fine grained microstructure is preferred, this is opposite to what is preferred at high temperatures

where large grain sizes are preferred for high creep resistance. In addition, these results suggest that, when selecting an α - β titanium alloy with Widmanstatten microstructure, an α - β alloy with stable β phase is preferred. To design new alloys or improve the properties of existing alloys wherever ambient temperature creep is an important factor it is essential to understand the creep deformation mechanisms. This investigation addresses this fundamental aspect.

FUNDAMENTAL STUDIES ON AMBIENT TEMPERATURE CREEP
DEFORMATION BEHAVIOR OF ALPHA AND
ALPHA-BETA TITANIUM ALLOYS

by

Charles Arthur Greene

Dissertation submitted to the Faculty of the Graduate School
of The University of Maryland in partial fulfillment
of the requirements for the degree of
Doctor of Philosophy
1994

Advisory Committee:

Associate Professor Sreeramamurthy Ankem, Chairman/Advisor
Professor Alexander Roytburd
Professor Ronald W. Armstrong
Associate Professor Lourdes Salamanca-Riba
Dr. George R. Yoder, Office of Naval Research

© Copyright by
Charles Arthur Greene
1994

PREFACE

In the spring of 1990, Dr. Ankem approached me with an exciting research program that he was about to embark on. At the time, I was a student in one of his courses. He proposed the idea of working together on an in depth study of the room temperature creep of titanium alloys. I was immediately interested because of the relative lack of scientific knowledge in this area and together with one other graduate student began to research the fundamental behavior of α , β , and α - β Ti-Mn and Ti-V alloys. The original goal was to be able to predict creep behavior based on the microstructure and composition of an alloy and recommend ways to improve its creep resistance.

Throughout the investigation many sophisticated and simple techniques were utilized. We found out that the simple techniques can often yield more information than more complicated, time consuming and expensive ones. It also became evident through the course of this investigation that one never knows what will be found until one looks, or polishes, etches, probes and prods. It also helps to be prepared, as Louis Pasteur so famously noted in the nineteenth century, so that when a never before reported phenomenon occurs the careful observer will see it. In our case we discovered the scientifically interesting and practically important phenomenon of **Time dependent twinning**, which is the growth and nucleation of twins over long periods of time under constant stress.

The results of this investigation are important to consider when using existing titanium alloys or designing new titanium alloys for use in ambient conditions. However, this dissertation should be read not only by titanium users and metallurgists, but also materials scientist and engineers in general due to the useful techniques and wide reaching results presented.

In the end, my work concentrated on the creep deformation mechanisms of small and large grained α Ti-Mn alloy, α - β Ti-Mn and Ti-V with Widmanstatten type microstructure and β Ti-Mn alloys. In addition, the tensile deformation behavior of these alloys was studied as well as that of β Ti-V alloy. This dissertation does not answer all the questions raised by this investigation. However, work will continue since the original goal is still as important as ever though requiring more work than anticipated due to the many significant findings, each leading to its own exciting and eventful scientific investigation.

DEDICATION

To Gretchen and Benjamin

ACKNOWLEDGMENTS

I would like to especially thank my advisor of the past four years, Dr. Ankem, for believing in me and my ideas, for allowing me room to learn, for constant guidance and wisdom when I needed it most, and for his warm friendship, without whom this dissertation would not have materialized.

I would like to thank Milton Shapiro for his special interest in the project and his careful workmanship, Gene Taylor and Helaleh Maghsoudlou of the Microscopy Facility, the Faculty of the Materials Engineering Group for imparting valuable wisdom, the Staff who were very supportive and Fellow students in the Materials Engineering Group. For valuable assistance I am indebted to Beesabathina D. Prasad, Li-Hsin Kuo, Xuwei Zhou, Len Wang, Kang Xu, Xiaodu Liu and M. N. Vijayshankar. I can not express my gratitude adequately for the assistance I received from Fellow Colleagues who worked on this project, Surjit Singh and Deepak Sil. I would like to acknowledge the help of Dr. Behnan Pourdeyhimi and Dr. James S. Sirkis for the free use of their laboratories, as well as Bob Wilson and Dave Evans and the Electrical Engineering Clean Room Facility.

I would like to thank the Committee members for taking the time out of their busy schedules to review this work. I am deeply appreciative to Dr. George Yoder for his genuine interest and valuable suggestions throughout the entire course of this project.

I would like to thank my wife, Gretchen, for constant inspiration, moral support and endless sacrifices throughout the course of my graduate studies and I would like to acknowledge my parents for, well, being great parents.

I Gratefully acknowledge Mr. J. R. Wood and Stan Seagle of RMI Co. for their interest in the project and for supplying the material used in this investigation. Finally, I am grateful for major financial support of Office of Naval Research (ONR) under Grant No. N00014-90-J-1907 and the National Defense Science and Engineering Graduate Fellowship (NDSEG) Program.

TABLE OF CONTENTS

<u>Section</u>	<u>Page</u>
List of Tables.....	x
List of Figures.....	xi
List of Abbreviations and Symbols.....	xvi
1. Introduction.....	1
2. Experimental.....	6
2.1. Materials and Heat Treatments.....	6
2.2. Attaching Fiducial Grid of Au to the Titanium Specimens.....	8
2.3. Scanning Electron Microscopy.....	15
2.4. Online Computerization of Zeiss ICM 405.....	17
2.5. Transmission Electron Microscopy.....	19
2.6. Tensile Testing.....	21
2.7. Creep Apparatus and Testing.....	22
2.8. Experimental Variation.....	23
3. Results.....	24
3.1. Alpha Ti-0.4Mn Alloy.....	24
3.1.1. Tensile Deformation of Small Grained Material.....	24
3.1.2. Creep Deformation of Small Grained Material.....	24
3.1.3. Tensile Deformation of Large Grained Material.....	25
3.1.4. Creep Deformation of Large Grained Material.....	25
3.2. Beta Ti-13.0Mn Alloy.....	28
3.2.1. Tensile Deformation.....	28

TABLE OF CONTENTS (Continued)

<u>Section</u>	<u>Page</u>
3.2.2. Creep Deformation.....	28
3.3. Beta Ti-14.8V Alloy.....	29
3.3.1. Tensile Deformation.....	29
3.4. Alpha-Beta Ti-6.0Mn Alloy.....	29
3.4.1. Tensile Deformation.....	29
3.4.2. Creep Deformation.....	30
3.5. Alpha-Beta Ti-8.1V Alloy.....	31
3.5.1. Tensile Deformation.....	31
3.5.2. Creep Deformation.....	31
4. Discussion.....	33
4.1. Alpha Ti-0.4Mn Alloy.....	33
4.1.1. Tensile Deformation Behavior.....	33
4.1.1.1. Small Grained Material.....	33
4.1.1.2. Large Grained Material.....	34
4.1.2. Creep Deformation Behavior.....	34
4.1.2.1. Small Grained Material.....	34
4.1.2.2. Large Grained Material.....	36
4.2. Beta Ti Alloys.....	41
4.2.1. Tensile and Creep Deformation Behavior of Ti-13.0Mn Alloy.....	41
4.2.2. Tensile Deformation Behavior of Ti-14.8V Alloy.....	43

TABLE OF CONTENTS (Continued)

<u>Section</u>	<u>Page</u>
4.3. Alpha-Beta Ti-6.0Mn and Ti-8.1V Alloys.....	45
4.3.1. Tensile Deformation Behavior.....	45
4.3.2. Creep Deformation Behavior.....	46
5. Suggestions For Future Studies.....	51
6. Conclusions.....	53
7. Appendices.....	57
A. Typical Tensile Test Data.....	57
B. Typical Creep Test Data.....	70
8. Tables.....	78 - 82
9. Figures.....	84 - 188
10. References.....	189

LIST OF TABLES

<u>Number</u>	<u>Page</u>
A.1. Typical Tensile Test Data.....	57
B.1. Typical Creep Test Data.....	70
1. Chemical Composition of Various Titanium Alloys Used in this Investigation.....	78
2. Electropolish and Etching Solutions.....	79
3. Example of Point Table for 20 μm Line Spacing.....	80
4. Dilute Titanium Etchant.....	81
5. Twinning Rotation Angle and Rotation Axis.....	81
6. Creep Curve Parameter n , Time Exponent.....	82

LIST OF FIGURES

<u>Number</u>	<u>Page</u>
Fig. 1 Typical microstructure of Ti-0.4 wt % Mn (~100% α) alloy.....	84
Fig. 2 Typical Widmanstatten type microstructure of Ti-6.0Mn (~46% α - 54% β) alloy.....	85
Fig. 3 Typical Widmanstatten type microstructure of Ti-8.1V (~51% α - 49% β) alloy.....	86
Fig. 4 Typical microstructure of small grained Ti-0.4Mn (~100% α) alloy.....	87
Fig. 5 Typical microstructure of Ti-13.0Mn (~100% β) alloy.....	88
Fig. 6 Typical microstructure of Ti-14.8V (~100% β) alloy.....	89
Fig. 7 Partial Ti end of the Ti-Mn phase diagram [45].....	90
Fig. 8 Partial Ti end of the Ti-V phase diagram [46].....	91
Fig. 9 Diagram of (a) room temperature creep and tensile specimens.....	92
Fig. 10 Vacuum spinner and specimen holder.....	93
Fig. 11 A schematic of the entire process for producing fiducial grids.....	94
Fig. 12 Schematic of specimen holder for electron beam writing.....	95
Fig. 13 Deformation twinning in a coarse grained α Ti-0.4Mn alloy crept to 2.7% at 298 K: (a) Bright field TEM.....	96
Fig. 14 Transmission electron micrograph of 500 μm grain size α Ti-0.4 wt% Mn alloy after room temperature creep.....	99

LIST OF FIGURES (Continued)

<u>Number</u>	<u>Page</u>
Fig. 15 Typical microstructure of Ti-0.4Mn (~100% α) alloy: (a) before tensile deformation and, (b) after.....	101
Fig. 16 Ambient temperature true stress - true strain curves of Ti-0.4Mn (~100% α) alloy.....	103
Fig. 17 Microstructure of Ti-0.4Mn (~100% α) alloy: (a) before tensile deformation and, (b) after.....	104
Fig. 18 Optical micrograph of α Ti-0.4Mn alloy after tensile.....	106
Fig. 19 Creep test and data acquisition setup.....	107
Fig. 20 Ambient temperature creep curve for Ti-0.4Mn.....	108
Fig. 21 SEM micrographs of Ti-0.4Mn (~100% α) alloy: (a) before creep deformation and, (b) after.....	109
Fig. 22 SEM micrographs of Ti-13.0Mn (~100% β) alloy: (a) before creep deformation and, (b) after	112
Fig. 23 Optical micrograph of α Ti-0.4Mn alloy after creep.....	114
Fig. 24 Optical micrograph of β Ti-13.0Mn alloy after creep.....	115
Fig. 25 Typical microstructure of Ti-0.4Mn (~100% α) alloy: (a) before creep deformation, (b) after.....	116
Fig. 26 Microstructure of α Ti-0.4Mn alloy, grain size ~ 0.5 mm. Note that the twinning length and width increase with creep time: (a) before deformation, (b) after.....	118
Fig. 27 Microstructure of Ti-0.4Mn (~100% α) alloy: (a) before tensile deformation and, (b) after.....	120

LIST OF FIGURES (Continued)

<u>Number</u>	<u>Page</u>
Fig. 28 Microstructure of Ti-0.4Mn (~100% α) alloy: (a) before creep deformation and, (b) after.....	122
Fig. 29 Microstructure of Ti-0.4Mn (~100% α) alloy: (a) before tensile deformation and, (b) after.....	124
Fig. 30 Microstructure of Ti-0.4Mn (~100% α) alloy: (a) before tensile deformation and, (b) after.....	127
Fig. 31 Instantaneous plastic + creep strain vs. time for α Ti-0.4Mn alloy. Creep stress: 95% YS.....	129
Fig. 32 Microstructure of Ti-0.4Mn (~100% α) alloy: (a) before creep deformation, (b) after.....	130
Fig. 33 Optical micrographs of (a) undeformed, (b), (c), and (d) deformed α Ti-0.4Mn alloy, Specimen B.....	133
Fig. 34 Optical micrographs of a different area of specimen B. (a) Undeformed, (b) creep strain = 0.61%.....	136
Fig. 35 Optical micrograph of another area of Specimen B.....	138
Fig. 36 Ambient temperature true stress - true strain curve of β Ti-13.0Mn alloy.....	140
Fig. 37 SEM micrographs of Ti-13.0Mn (~100% β) alloy: (a) before tensile deformation and, (b) after.....	141
Fig. 38 Optical micrograph of β Ti-13.0Mn alloy after tensile.....	144
Fig. 39 Ambient temperature creep curve of β Ti-13.0Mn alloy.....	145
Fig. 40 SEM micrographs of Ti-13.0Mn (~100% β) alloy (a) before creep deformation and, (b) after.....	146

LIST OF FIGURES (Continued)

<u>Number</u>	<u>Page</u>
Fig. 41 Ambient temperature creep curve of β Ti-13.0Mn crept at 100% YS.....	148
Fig. 42 Ambient temperature true stress - true strain curve of β Ti-14.8V alloy.....	149
Fig. 43 SEM micrographs of Ti-14.8V (~100% β) alloy: (a) before tensile deformation and, (b) after.....	150
Fig. 44 Optical micrograph of β Ti-14.8V alloy after tensile.....	153
Fig. 45 Ambient temperature true stress - true strain curves of α - β Ti-6.0Mn and Ti-8.1V alloys.....	155
Fig. 46 SEM Microstructure of Ti-6.0Mn (~46% α - 54% β) alloy: (a) before tensile deformation.....	156
Fig. 47 Optical micrograph of α - β Ti-6.0Mn alloy after tensile deformation.....	159
Fig. 48 Ambient temperature creep curves of α - β Ti-6.0Mn and Ti-8.1V alloys at 95% and 100% yield stress.....	161
Fig. 49 SEM micrographs of Ti-6.0Mn (~ 46% α - 54% β) alloy: (a) before creep deformation, (b) after.....	162
Fig. 50 SEM micrographs of Ti-6.0Mn (~ 46% α - 54% β) alloy: (a) before creep deformation and (b) after.....	165
Fig. 51 Optical micrograph of α - β Ti-6.0Mn alloy after creep.....	167
Fig. 52 SEM Micrograph of Ti-8.1V (~ 51% α - 49% β) alloy: (a) before tensile deformation and (b) after.....	168
Fig. 53 A different area of the same α - β Ti-8.1V alloy.....	170

LIST OF FIGURES (Continued)

<u>Number</u>	<u>Page</u>
Fig. 54 Optical micrograph of α - β Ti-8.1V alloy.....	173
Fig. 55 Microstructure of Ti-8.1V (~ 51% α - 49% β) alloy: (a) before creep deformation and (b) after.....	174
Fig. 56 Optical micrograph of Ti-8.1V (~ 51% α - 49% β) alloy after creep deformation.....	177
Fig. 57 Log-log plot of creep strain, ϵ_c vs. time, t . Slope.....	179
Fig. 58 Optical micrograph of another area of Specimen B.....	181
Fig. 59 Transmission electron micrograph of 500 μm	183
Fig. 60 Pre ω phase streaking in the SADP of the β phase.....	185
Fig. 61 Athermal ω phase in the SADP of the β phase.....	186
Fig. 62 Ambient temperature true stress - true strain curve of α Ti-1.5V alloy [98].....	187
Fig. 63 A stereographic projection showing the interface.....	188

LIST OF ABBREVIATIONS AND SYMBOLS

A/D	Analog to Digital
A-etch	Titanium etchant, composition listed in Table 2
α	The hexagonal close packed crystal structure phase of titanium
Al	Elemental aluminum
Å	Angstrom(s), 10^{-10} meters
ASTM	American Society for Testing and Materials
ATS	Applied Test Systems
Au	Elemental gold
bcc	Body Centered Cubic
BCC	Body Centered Cubic
β	The body centered cubic crystal structure phase of titanium
C	Celsius (or Centigrade), Elemental carbon
CCD	Charged Coupled Device
cm	centimeter(s)
CP	Commercial Purity
d_{hkil}	distance between $hkil$ planes
δ	misfit parameter
dpi	dots per inch
DOS	Disk Operating System
FC	Furnace Cool or Furnace Cooled
Fe	Elemental iron
ϕ	Twin rotation angle
h	hour(s)
hcp	hexagonal close-packed
HREM	High Resolution Electron Microscopy
in	inch(es)
k	$\times 10^3$
K	Kelvin(s)
K_1	Twin Plane
K_2	Second invariant plane
kg	kilogram(s), 10^3 grams
kV	kilovolt(s), 10^3 volts
ln	Natural logarithm
MB	Mega byte
μm	micron(s), 10^{-6} meters

LIST OF ABBREVIATIONS AND SYMBOLS (Continued)

m m	millimeter(s), 10^{-3} meters
Mn	Elemental manganese
Mo	Elemental molybdenum
MPa	Mega Pascal(s), 10^6 Pa
m V	millivolt(s), 10^{-3} volts
n	time exponent
N	Elemental nitrogen
nA	nano Amperes
Nb	Niobium
η_1	Twinning shear direction
η_2	Direction of intersection of plane of shear with K_2
O	Elemental oxygen
ω	Greek letter omega represents the omega phase of titanium
Pa	Pascal(s)
PC	Personal Computer (desktop computer)
r	distance from transmitted beam to a diffracted spot in SADP
RAM	Rapid Access Memory
R-etch	Titanium etchant, composition listed in Table 2
rpm	Rotation(s) per minute
s	second
SADP	Selected Area Diffraction Pattern
SEM	Scanning Electron Microscope
Sn	Elemental tin
t	time
T	temperature
Ta	Elemental Tantalum
TEM	Transmission Electron Microscope
Ti	Elemental titanium
Ti-6211	Ti-6Al-2Nb-1Ta-0.8Mo
Ti-64	Ti-6Al-4V
TIFF	Tagged Image Format File
T_m	Melting Temperature
V	Elemental vanadium
VCR	Video Cassette Recorder
VGA	Video Graphics Adapter
vol%	volume percent
wt%	weight percent

LIST OF ABBREVIATIONS AND SYMBOLS (Continued)

WQ	Water Quench or Water Quenched
x	multiplication, as in <i>Magnification of 30x</i>
x,y,z	space coordinates
YS	Yield Stress

1. INTRODUCTION

Titanium alloys are technologically important. Titanium has a high strength to weight ratio, excellent resistance to corrosion, good weldability and it is biocompatible, making titanium and titanium alloys important materials in the aerospace, chemical processing, marine and biomedical industries. Titanium and titanium alloys are technologically important because of their extensive desirable qualities. Titanium alloys resist corrosion by many acids making them ideal materials for use in, for example, industrial flue gas scrubbers, down hole pipes for sour gas wells, heat exchangers and holding vessels in corrosive environments [1]. The excellent sea water corrosion resistance of titanium is useful in ship and marine applications where high initial costs are offset by longer service life times and lower maintenance costs. In the aerospace industry titanium is used extensively due to its high strength-to-weight ratio, its high strength even at high temperatures and its resistance to creep and fatigue, where it is used in fuselage and engine components. In the biomedical industry titanium is used because it is inert when in contact with biological fluids and because of its reliability it can be used in fabricating human implants. Titanium is biocompatible, the human immune system tends not to reject implants made of titanium. The implants, whether structural, as in bone substitution, or moving, as in heart pacemakers, must be reliable, and ideally maintenance free, making titanium a material of choice in this industry [2,3]. Titanium is

also a model for two-phase materials. Experimental research and modeling of alpha, beta and alpha-beta titanium alloys can lead to a deeper understanding of other systems with two phases in equilibrium.

Because titanium is such a technologically important material with many widespread applications, it would be expected that the room temperature tensile deformation behavior amongst its other properties, would be thoroughly studied. This is indeed the case, beginning in the 1940's and 50's, see for example reference [4], extensively thereafter [5,6] and on into the present [7,8] the room temperature tensile deformation behavior of α , β and α - β titanium alloys has been the subject of countless publications.

Since the room temperature tensile deformation mechanisms of α , β and α - β titanium alloys are of significance in the current study these mechanisms are briefly reviewed. It was reported in the past that α titanium alloys deform at room temperature by prismatic slip [9], basal slip [10], and prismatic slip of $c + a$ dislocations [11-14]. Twinning [10,15,16] and occasional grain boundary sliding [6,17] have also been reported as deformation mechanisms in α titanium alloys. The α - β titanium alloys have been found to deform by slip across phases due to the Burgers orientation relationships, twinning in the α phase, interphase interface sliding and individual slip in the α and β phases[18,19]. In regard to the beta titanium alloys, investigators report deformation mechanisms to be coarse planar and wavy slip [6,17,19] and

stress induced plate formation. There is still some confusion surrounding the nature of the plates formed in β phase Ti-V alloys under room temperature deformation. The plates have been reported to be twins [8], martensite [20], and one orientation of the ω phase [21].

In contrast to the tensile deformation mechanisms of titanium alloys, very little work has been done on their room temperature creep deformation mechanisms even though creep behavior is an important property. Many of the ambient temperature applications for titanium alloys involve high stresses for extended periods of time. For example, the main landing gear of the new Boeing 777 will be made entirely from Ti-10V-2Fe-3Al alloy [22] and must support the aircraft while it is on the ground or in the case of pressure hulls made of titanium for deep sea submersibles. In these instances the creep behavior of titanium alloys must be well understood since it has been known for some time that titanium alloys do creep at ambient temperatures [23-34].

Numerous investigators in the past have understood the importance of determining the creep behavior of titanium. The earliest work is attributed to Heinrich Adenstedt in 1949 [35]. He found in commercial purity (CP) titanium that cold working improved the creep resistance as well as raised the yield strength. Adenstedt also guessed that alloyed titanium would have a "more favorable creep behavior" than the CP titanium. Kiessel and Sinnott [36] and others [37] also performed early investigations on the creep of CP titanium. Much of this early work and the following investigations [38-41] concentrated on

the temperature dependence of the creep rate of CP titanium with minimal attention to fundamental mechanisms of creep behavior.

More recently, there has been additional work carried out on the room temperature creep of titanium, but concentrating only on specific titanium alloys. One titanium alloy in particular which has been the subject of extensive creep studies at room temperature due to its wide use, especially in space and aeronautical applications, is the near alpha alloy Ti-6Al-4V, or Ti-64 [24,26,33,34,42,43]. Chu [23] and Miller and co-workers [25] on the other hand, chose to study the room temperature creep properties of Ti-6Al-2Nb-1Ta-0.8Mo alloy, known as Ti-6211. Thompson and Odegard have suggested a method of producing a creep resistant microstructure for the alloy of their investigation, Ti-5Al-2.5Sn [44]. However, no systematic investigation has been undertaken to determine the effect of alloying element and microstructure on the room temperature creep mechanisms of titanium alloys. Most of the earlier investigations were concerned with determining creep properties of specific alloys and little emphasis was placed on fundamental understanding of creep deformation mechanisms.

In contrast to the extensive work on CP titanium and near alpha titanium alloys, the amount of research on the ambient temperature creep of near beta or beta titanium alloys other than investigations by the author and co-workers [7], is minimal and no significant information is available.

It is very important to understand creep deformation

mechanisms to improve the creep resistance of existing titanium alloys and to develop new titanium alloys with improved creep resistance at ambient temperature. To understand the creep of two-phase, i.e. α - β , titanium alloys one must first understand the creep of the individual phases and how it is altered by alloying element and microstructure. For example, if two alloys with the same microstructure have different alloying elements will the creep deformation mechanism and the creep strain be the same? This deceptively simple question cannot be answered by the current breadth of literature on the ambient temperature creep of specific alloys. Therefore, this investigation was undertaken to systematically study the effect of microstructure and alloying elements on the room temperature tensile and creep deformation mechanisms of α , α - β and β Ti-Mn and Ti-V alloys. Presented herein are results on the ambient temperature tensile and creep deformation mechanisms of α , β and α - β Ti-Mn and α - β Ti-V alloys as well as the ambient temperature tensile deformation mechanisms of β Ti-V alloys.

2. EXPERIMENTAL

2.1. Materials and Heat Treatments

For this investigation three Ti-Mn alloys and two Ti-V alloys were used. All five alloys were melted as 13.6 kg ingots and processed to 1.74 cm diameter bars at the RMI Company in Niles, Ohio. The final step (rolling) was carried out in the $\alpha + \beta$ field at 973 K and a 60% reduction in area was given for all of the alloys. This work was found to be sufficient to recrystallize all of the alloys within 12 hours at 973 K.

The mechanisms of room temperature tensile and creep deformation were studied for two different grain size α Ti-Mn alloys and one grain size of the β Ti-Mn and β Ti-V alloys. In addition, the two-phase α - β Ti-Mn and Ti-V alloys were studied with a Widmanstätten type microstructure.

To obtain the coarse grain size (500 μm) for the α Ti-Mn alloy and the Widmanstätten type microstructure for the α - β Ti-Mn and Ti-V alloys, the bars were vacuum sealed in quartz tubes at 10^{-3} to 10^{-4} Pa, then heat treated for 2 h at 1173 K, furnace cooled to 963 K and annealed for 200 h at 963 K followed by a water quench. Typical microstructure of this coarse grained α Ti-Mn alloy is shown in Fig. 1. Typical α - β Ti-Mn and Ti-V alloys with Widmanstätten type microstructure are shown in Figs. 2 and 3. To obtain the smaller grain size microstructure of the α

and β Ti-Mn and β Ti-V alloys, as shown in Figs. 4, 5 and 6 respectively, the bars were heat treated in a vacuum of 10^{-3} to 10^{-4} Pa for 200 h at 963 K followed by a water quench.

The alloys, their compositions and volume percent of phases are given in Table 1 and are also indicated in the phase diagrams of Figs. 7 [45] and 8 [46]. The chemical compositions are actual chemical compositions of the alloys after fabrication as determined by the wet chemistry method at RMI Co. in Niles, OH. Although the alloy composition in the Ti-Mn system varies from 0.4% Mn for alloy 1 to 13% Mn for alloy 2, the chemical compositions of the α and β phases remain fairly constant. The chemical compositions of the α and β phases are given by the points of intersection of the tie line in Fig. 7 with the α and β solvus respectively. The same is true for the chemical composition of the β phase in the two alloys of the Ti-V system.

Tensile and creep specimens were carefully machined from the quenched bars so that no undesirable oxide from the processing and heat treatment remained. Multiple passes and small cuts were taken with the lathe and mill to introduce the least amount of surface deformation as possible to the samples while machining. The samples were machined with threaded, 1.23 cm (0.485 in) diameter, ends to fit threaded grips and gauge sections 2.86 cm (1.125 in) in length. Flats were milled on the gauge sections, see Fig. 9 (a). Fiducial lines were put on the flats as described in the following section.

2.2. Attaching Fiducial Grid of Au to the Titanium Specimens

Initially a technique was developed to attach a reference grid of micron sized lines to the titanium alloy specimens using laser interferometry. Though the technique met with success in producing a fiducial grid of $1.5\text{ }\mu\text{m}$ wide lines spaced $1.5\text{ }\mu\text{m}$ apart on holographic film, the transfer to the metal specimen was more difficult than originally anticipated. The liquid emulsion being used needed a more powerful laser with a higher frequency than was conveniently available. The new technique developed only requires equipment readily available at any university.

A brief overview on making fiducial grids of evaporated Au using a simple electron beam writing technique is presented here. The technique was developed to provide an inexpensive way to fix fiducial lines on unique shaped specimens that would not fit into standard photolithography equipment.

Actual electron beam writing has many uses and requires high resolution electron resists [47]. The objective in this case was to develop a simple and inexpensive way to make a reference grid to keep track of interphase sliding, grain boundary sliding and fine slip during tensile and creep strain of two-phase titanium alloys as well as fine slip and grain boundary sliding of single phase titanium alloys [18,25]. In the literature broad descriptions are given as to fixing fiducial grids to various substrate [48], but no detailed, step by step, procedure can be

found. This technique was developed to provide a complete procedure that can be easily duplicated by subsequent investigators.

Titanium samples used as the substrate were mechanically polished with progressively finer special silicon carbide grinding paper. Cylindrical cross sections of a rolled titanium alloy bar were used to develop the technique before applying it to the actual test specimens, see Fig. 9 (b). After hand polishing with 600 grit grinding paper the samples were electropolished at -60°C to yield a mirror like surface. The electropolish solution is given in Table 2. The two-phase and β phase titanium alloys were then etched to reveal grain boundaries and interphase boundaries using R etch [49] followed by A etch [49] with water rinse after each etch. The α titanium alloys were etched very lightly with A etch followed by R etch. Etchants are also listed in Table 2.

Using a vacuum spinner (Headway Research Inc.) the substrate flooded with photo resist was spun at speeds between 3k and 5k rpm. Faster spin speeds yielded thinner coatings of photo resist. The variation in final thickness of photo resist between these speeds was less than $0.5\text{ }\mu\text{m}$. A thicker coating was desired to facilitate removal later in the procedure so a spin speed of 3000 rpm was used. The tensile and creep test specimens were spun using a specially designed holder which is shown in Fig. 10. The photo resist used was Shipley Microposit[®] 2400 Series Photo Resist. This particular resist was chosen because it is a positive photo resist of relatively low cost and high resolution.

Under yellow safe light the substrate was flooded with the photo

resist using an eye dropper then accelerated to 3000 rpm and spun for 30 seconds. A primer can be used to aid with adhesion, however the photo resist was applied directly to the polished and etched titanium substrate with very good results. In addition, it is suspected that the primer was causing problems later in the procedure preventing the evaporated Au from depositing directly on the titanium substrate.

Following the manufacturer's directions [50], the substrate with a new layer of photo resist, approximately $1.5\text{ }\mu\text{m}$ thick, as schematically shown in Fig. 11 (a), was baked in an oven at 90°C for twenty minutes. The samples were then placed in a black film box which was then placed in a black film bag and transported to the scanning electron microscope lab for exposure to the electron beam.

The Jeol 840 Scanning Electron Microscope (SEM) with Microprobe was used for all beam writing using a custom designed specimen holder, see Fig. 12. The Jeol 840 has a computer to store tables of points -- coordinates in x, y, and z. To begin beam writing, a table of ninety-nine points was entered and stored on disk, with x and z constant but increasing y by $20\text{ }\mu\text{m}$ with each point, see Table 3. In this way, approximately 2 mm of the sample could be covered. When the electron beam is in line mode the length of the line swept on the sample depends on the magnification. At a magnification of 30x the line is approximately 5 mm long. At a magnification of 50x the line is 2 - 3 mm long. By adjusting the magnification, setting the microscope on line mode, and executing each point in the point table, an area which

has an x dimension dependent on magnification and y dimension dependent on the point spacing and the number of points executed, was covered by parallel lines. However, the beam had to be "blocked" when moving to each successive point in the y direction. This was accomplished by using the Faraday Cup. When the Faraday Cup is in (reading the incident beam current) the beam is blocked thus allowing movement of the stage to the next point in the point table. After the ninety-nine points were executed, blocking the beam while moving and unblocking the beam for a short exposure time in line mode while stationary, the stage was moved to its center and rotated 90°. The ninety-nine points were then executed again with blocking and unblocking at the appropriate time. The time the beam is unblocked is the exposure time. Fig. 11 (b) illustrates the electron beam exposing the photo-resist.

If more than 2 mm² of grid area, using a 20 µm line spacing, was desired then a second table containing ninety-nine points was loaded from the computer and executed before rotating the stage about its center, which also corresponded to the center of the parallel lines. The tables were executed again after rotation thus yielding a 4 mm² area of 20 µm spaced grid lines.

Before placing the specimen coated with photo resist into the scanning electron microscope (SEM) a blank specimen was needed to focus the beam and center the specimen. Centering was necessary so

that upon rotation the parallel lines would cross. Focusing the beam was done at a high magnification and at the accelerating voltage to be used for beam writing, however the beam writing current was adjusted after focusing. After focusing and adjusting the beam current the accelerating voltage was left on and the Faraday Cup was used to block the beam while the specimen with the photo resist was exchanged for the blank specimen in the microscope. The exchange was done in the dark and a yellow safe light was not needed. The purpose of leaving the accelerating voltage and filament current on is twofold: one, to allow the beam to stabilize and two, to prevent the automatic chamber light inside the microscope from switching on.

A beam current of 1.5 to 2 nA, an accelerating voltage of 20 kV, and an exposure time of 1 s were used for the specimens coated at 3,000 rpm.

Shipley Microposit[®] 2401 Developer was used to develop the exposed samples. Following the manufacturer's directions, a develop time of one minute with agitation was used followed by vigorous rinsing with distilled water. The developer removed the exposed photo-resist as illustrated in Fig. 11 (c). After developing, the sample can be exposed to normal light. At this point samples were viewed in the Zeiss 405M light microscope at magnifications up to 500x. A clean exposure and development could be discerned under the light microscope by noting if photo resist was still evident in the lines where no photo resist was desired. A successful sample had squares of unexposed photo resist

separated by two sets of parallel lines or avenues of bare substrate running perpendicular to each other.

In order to later remove the unexposed photo resist it was necessary to etch the titanium substrate with a very dilute etchant that did not contain alcohol or acetone which would attack the remaining photo resist, as shown in Fig. 11 (d). The etchant insured that the evaporated Au coated the exposed titanium yet left an overhang of photo resist facilitating its removal, see Fig. 11. The etchant used is given in Table 4. The sample was etched for 15 - 25 s. The sample was then rinsed with water, air dried and vacuum sputter coated with up to 500 Å of Au.

Shipley Microposit[®] Remover 1165 was used to strip the unexposed photo resist, as in Fig. 11 (e). The sample was submerged in the remover and placed in an ultrasonic agitator for 10 minutes. Then rinsed with water. Gold grid lines 1 - 2 µm wide spaced 20 µm apart covering an area 2 mm x 2 mm in the center of the gauge length were obtained, see Fig. 11 (f). Typical grid lines can be seen in Fig. 1.

The problem of desired Au lines delaminating from the substrate occurred when the sample was left in the ultrasonic agitator too long. This problem was avoided by choosing a high enough beam current and long enough exposure time so that the entire depth of the photo resist in the exposed areas was developed away. Exposure time seems to be the more critical parameter since there is a finite time for the current to reach its peak amperage when the Faraday cup is removed.

The three critical parameters for beam writing are beam current, exposure time, and accelerating voltage. It was important to use high enough values of all three parameters to begin with. After success with high values this technique was tuned to yield high resolution lines. The process resulted in thin and continuous lines.

This technique is very similar to techniques used in the preparation of semiconductors. It should work well with other scanning electron microscopes and other substrate, metals or semiconductors. The materials used for obtaining the grid lines are inexpensive yet produce very fine lines. However, there are other expensive higher resolution photo-resists which can produce even better lines when used with this procedure.

The grid lines served three purposes. First, very fine homogeneous slip was monitored by noting any distortion in the grids. Second, it was possible to keep track of grain boundary sliding where the grid lines became displaced at the grain boundaries. Third, interface sliding could be discerned by noting where grid lines became displaced at interface boundaries between the α and β phases.

2.3. Scanning Electron Microscopy

A Jeol 840 Scanning Electron Microscope (SEM) with Microprobe was used to examine tensile and creep specimens. The Jeol 840 uses a vacuum lock to insert and remove specimens for examination restricting the length of samples to 3.5 in. The holder illustrated in Fig. 12 was utilized for all SEM studies. Typical SEM micrographs are shown in Figs. 1 through 6. Typically, the flat of a creep or tensile specimen would be examined before testing by selecting up to six different regions covered by the fiducial grid. At each region low magnification, 200 x, Black and White (B/W) Polaroid pictures with negatives, type 55 film, would be taken. About four areas in each of these low magnification regions would be subsequently photographed at 500 x, 1000 x and 2000 x, yielding detailed information about the microstructure that could be compared with the same exact region and area after deformation.

Basically, scanning electron microscopy reveals features on the surface of the samples by scattering of electrons. Features that are stronger scatters of electrons appear brighter, also features that accumulate electrons, such as pits appear brighter in the micrographs. Contrast is also achieved by differences in orientation of neighboring grains as well as height differences on the sample surface, both of which effect the electron scattering intensity.

Therefore, the SEM pictures presented here appear much differently than the optical, i.e. light, microscopy pictures. The contrast

is inverted. The α phase in the two-phase alloys scatters electrons more strongly than the β phase and usually appears much lighter in the micrographs. The identity of the phases was verified using the microprobe. Slip lines and grain boundaries also are usually lighter than the surrounding material. The gold grid lines offer an excellent contrast in SEM, appearing bright white in most cases, whereas a material such as aluminum or copper would not have shown up nearly as well.

2.4. Online Computerization of Optical Microscopy

The Zeiss ICM 405 Inverted Metallographic Light Microscope was adapted to transfer a real time black and white image seen at the eyepiece directly to a 80386SX desktop computer while simultaneously displaying the image on a high resolution monitor. The microscope was fitted with a standard C-mount adapter allowing a solid state Charged Coupled Device (CCD) camera to be mounted directly to the microscope housing. A 4815 series monochrome CCD video camera from COHU, Inc. [51] with a pickup area of 8.8 mm x 6.6 mm, active picture elements of 754 (H) by 488 (V) and a resolution of 565 tv lines (H) and >350 tv lines (V) was used.

The video camera relays an image to a PCVISIONplus™ Frame Grabber board [52] installed in a 386SX desktop computer equipped with 2 Megabytes (MB) of Rapid Access Memory (RAM), a 80387 Math Coprocessor, 40 MB hard drive, two high density floppy drives and super VGA 1024 x 726 monitor. The frame grabber digitizes the image at a rate of 30 interlaced frames per second, storing the resulting picture in frame memory and displaying it on the high resolution Electrohome ECM 1310 monitor. Each picture is made up of 640 by 512 pixels and each pixel is one of 256 possible intensities of gray scale. The interlaced video signal produces a flicker free real time image for focusing and moving of the sample with no detectable abnormality to the observer. PCplus™ software, included with the frame grabber board which performs basic

initialization and testing capabilities was installed on the hard drive.

The software used for image analysis and storage was Microsoft[®] DOS 5 compatible JAVA[®] from Jandel Scientific [53]. Images were printed using the Mitsubishi CP1000U color video copy processor which has a resolution of 1280 dots (H) by 960 lines (V) with 256 gradations for each color, yellow, magenta and cyan. Images were also printed at Maryland Media on a 3200 dots-per-inch (dpi) imagesetter.

The image processing capabilities of the JAVA software were utilized to make volume percent of phases measurements as follows. An image of the two-phase alloy was captured in memory directly from the microscope. The total number of pixels, number of pixels with dark gray levels and the number of pixels with light gray levels were counted. The number of pixels with dark gray levels divided by the total number of pixels was taken as the volume percent of α phase and the number of pixels with light gray levels divided by the total number of pixels was taken as the volume percent of β phase.

By running a video cable from any of the other microscopes in the microscopy facility or from a Video Cassette Recorder (VCR), live images can be captured and stored on computer disk as Tagged Image Format (TIF) files by the Online computerized microscopy setup. This system works well, but due to the large amounts of information contained in high resolution images improvement can be made to it by adding more memory to the computer as well as a higher capacity hard drive.

2.5. Transmission Electron Microscopy

To study the mechanisms of room temperature tensile and creep deformation, thin foils of specimens before and after testing were prepared by the method following Spurling [54]. Thin sections were cut from the undeformed specimens and the gauge section of the deformed test specimens using a low speed diamond wafering saw. Using a slurry disk cutter, 3 mm diameter disks were cut from these thin sections, then the disks were cryogenically jet polished with a twin jet electropolisher until a hole was detected. The resultant foils were then examined in the Transmission Electron Microscope (TEM).

Thin areas of the specimen foils were located and studied in the Jeol Jem-2000FX II TEM. The Jeol Jem-100CX was also used for a short time when a lens in the 2000FX was over heating during use. Bright field images of relevant features were recorded on micrograph negatives. Typical TEM photographs are shown in Figs. 13 and 14. Selected Area Diffraction Patterns (SADP) of the individual phases in the single and two-phase alloys were obtained by tilting the samples. Extra twin spots were noted in the SADP of α Ti-0.4Mn alloy at the twin/matrix interface and identified as outlined below.

A good description of the method used to identify the twins in α Ti-0.4Mn alloy is given by Edington [55] and follows the stereographic technique described by Partridge [56]. In brief, the trace of the zone axis of the parent material in the SADP containing twin spots was drawn on a

(0001) stereogram. To determine the type of twin, the planes producing the extra spots in the SADP were identified. If the poles of those planes landed on the trace of the parent zone when the (0001) projection was rotated about the normal to the plane of shear through an angle 2ϕ , where ϕ is the angle between the twin plane and the basal plane, (0001), then the twin plane was determined. Table 5 lists the common twins in titanium, their rotation angles and their rotation axes. The plane of shear is also referred to as the plane containing η_1 , twinning shear direction, and η_2 , direction of intersection of plane of shear with K_2 , the second invariant plane, or the plane perpendicular to K_1 , the twin plane, and K_2 .

2.6. Tensile Testing

Scanning electron micrographs using a secondary electron detector were taken of the samples before and after tensile testing. It was important to take pictures before as well as after deformation since it was difficult in some cases to discern if a twin or other deformation mechanism was present before testing. Many pictures were taken before testing since it was not possible to predict where a deformation mechanism would act. Typical before and after tensile deformation pictures are shown in Fig. 15 (a) and 15 (b), respectively.

Specimens with gold grid lines were tensile tested on a floor model INSTRON machine at room temperature (298 K) at an initial strain rate of 3.28×10^{-5} per second. For each tensile test two to four specimens were used and the results averaged. Individual test results varied at maximum by 4%. The samples were strained to 3% total strain. Typical true stress-strain curves are shown in Fig. 16. Typical tensile test data is shown in Appendix A. SEM pictures taken after testing are shown in Figs. 15 (b) and 17 (b). Optical pictures at 500x were also taken after testing since, for the α Ti-Mn alloy and the β Ti-V alloy, the twins are more easily recognized in the light microscope, see Fig. 18. The Zeiss ICM 405 inverted metallographic light microscope was used for optical pictures using extended focal length Nikon 141360 and Leitz 519760 objective lenses. The extended focal length lenses were necessary due to the size and shape of the test specimens.

2.7. Creep Apparatus and Testing

During the course of this project creep test apparatus was acquired and setup as illustrated in Fig. 19. As shown, the computer acquires data from both lever arm testing machines simultaneously. The modules convert the resistance measured at the strain gauges into a voltage between 0 and 10 V for the analog to digital (A/D) board. On full range a 10 V reading by the A/D board equals a 0.1 inch displacement at the strain gauge, a 10% strain since the gauge length is 1 inch.

Specimens with grid lines were creep tested at room temperature in air on an Applied Test Systems (ATS) Lever Arm Tester as described. The strain was measured by a clip on extensometer and strain module, calibrated in accordance with ASTM E83A. The strain data was recorded on a PC using an Analog Connection™ ACJr™ A/D board and Quicklog PC™ Software, both from Strawberry Tree Incorporated [57].

The specimens were creep tested at 95% of their respective 0.2% Yield Stresses. The tests were conducted under constant load conditions, however the reduction in cross sectional area was minimal, thus approximating constant stress creep tests. Typical creep curves are shown in Fig. 20. Typical creep test data is shown in Appendix B. SEM pictures of the alloys were taken before and after testing as shown in Figs. 21 and 22. As in the case of tensile tests, optical pictures at 500x were also taken after creep testing and examples of these pictures are shown in Figs. 23 and 24.

In the case of the large grain size α Ti-Mn alloy, observation of the specimen crept to a creep strain of $\sim 2.7\%$ showed extensive twinning, see Fig. 25. To systematically determine the role of twinning on creep, several areas of another specimen of this material were photographed and it was crept with interruptions at predetermined creep strains of approximately 0.1, 0.2, 0.4, 0.6, 0.9, 1.2, 1.7, 2.2, and finally, 2.7 percent. The same areas of the specimen were photographed after each interval of strain to determine the creep deformation mechanisms and the role of twinning on creep. Typical creep interrupt sequence is shown in Fig. 26.

2.8. Experimental Variation

The experimental variation of interest is that which contributes to an uncertainty in the creep strain during a creep test. Due to the long times in a single test some tests were conducted only once. The tests that were repeated, for example, those of the large and small grained α Ti-0.4Mn alloys showed very good correlation in creep strain for equal amounts of time and the variation was insignificant.

Based on standard data reduction and error analysis methods [58], we expect a probable 3% relative uncertainty in the creep strain. This is an acceptable level which does not interfere with the conclusions of the investigation.

3. RESULTS

3.1. Alpha Ti-0.4Mn Alloy

3.1.1. Tensile Deformation of Small Grained Material

The ambient temperature true stress - true strain curve shown in Fig. 16 for α Ti-0.4Mn with grain size $\sim 45 \mu\text{m}$ has a 0.2% YS of 235 MPa and shows work hardening. This result agrees well with previous investigations [6,17]. The deformation mechanisms are twinning as shown in Figs. 17 and 18, fine slip as shown in Fig. 15, and rare grain boundary sliding, see Fig. 27.

3.1.2. Creep Deformation of Small Grained Material

The ambient temperature creep curve of α Ti-0.4Mn crept at 95% of 0.2% YS is presented in Fig. 20. The slope of the curve is decreasing with time, i.e. the curve is approaching a plateau, indicating an exhaustion type creep mechanism [25]. Comparison of the photomicrographs of before and after creep deformation indicate that the tensile and creep deformation mechanisms are similar in spite of significant differences in strain rates. Fig. 21 (b) in comparison with Fig. 21 (a) shows elongation of grid lines in the direction of loading indicating very fine slip (not seen in the photomicrograph). Fig 28 (b)

shows distortion of the fiducial grid by fine slip. In Fig. 21 (b) grain boundary sliding is noticeable, but it is to be noted that this is not a common occurrence. Twinning also occurs in this alloy, see Figs. 21 (c) and 23, it is noted that for some twins there is an associated grid distortion.

3.1.3. Tensile Deformation of Large Grained Material

Two tensile specimens of the coarse grain α Ti-Mn alloy were tested and the variation in the yield stress was found to be less than 2%. From these tests an average value of the 0.2% YS was determined to be as 262 MPa. A typical tensile true stress vs. true strain curve is shown in Fig. 16. Considerable strain hardening is indicated. No serrations were observed in the tensile curve. Observation of specific areas before and after deformation indicated coarse slip and extensive twinning as shown in Figs. 29 and 30. Such behavior has been noted by earlier investigators [6,9,11,59,60].

3.1.4. Creep Deformation of Large Grained Material

The creep tests were conducted at 95% of the YS which was 249 MPa. The first specimen, specimen A, was crept continuously to approximately 2.7% creep strain. The creep curve for this first specimen is shown as the solid line in Fig. 31. Typical before and after creep

deformation micrographs are shown in Fig. 32. Deformation by extensive twinning and some coarse slip can be seen to have occurred in these figures. A second specimen, specimen B, was crept for different amounts of strain with predetermined interruptions, as mentioned in section 2.7, and the creep curve constructed from this data is shown as the dotted curve in Fig. 31. The triangles and the associated numbers indicated in Fig. 31 correspond to the points of test interruption. At strains corresponding to these points, the specimen was unloaded and the same areas of the specimen photographed prior to testing were photographed again and the specimen was reloaded. This process was repeated until an instantaneous plastic + creep strain of 2.8% was obtained. The instantaneous plastic strain is that plastic strain which can be measured from the true stress vs. true strain curve at 95% YS, which is a strain of about 0.1% for this alloy. The creep curve constructed from interrupt data of specimen B very nearly equals the creep curve of the uninterrupted data of specimen A.

Typical areas before and after creep deformation are shown in Figs. 33 and 34. Observation of these figures indicate fine slip. However, after large amounts of strain coarse slip lines were observed in a few areas as seen in Fig. 35 (c). Since fine slip could not be seen directly, grid line spacing was compared before and after deformation and based on the grid line elongation in the direction of loading it was concluded that fine slip did occur, for example, compare location "B" in Fig. 34 (a) with the same location in 34 (b). Comparison of the grid line spacing before

and after deformation also indicates that the deformation is non-uniform. The loading direction is from top to bottom as indicated in Figs. 33 and 34. Slip in α titanium is known to occur predominately on the prism planes and to a lesser extent on the basal and pyramidal planes with $\langle 11\bar{2}0 \rangle$ as the slip direction [9,11]. Additionally, slip can occur by movement of $c+a$ dislocations [12,13]. Most of the deformation in the earlier stages of creep appears to be due to slip even though some twins are seen to form instantaneously. Slip also continuously contributes to strain while the twins nucleate and grow at later stages as creep progresses. If there is little or no twinning, as in the case of the small grained (45 μm) α Ti-Mn alloy [7], then the creep strain should be progressing by slip leading to creep exhaustion where a plateau should be observed in the creep vs. time curve in a short time, see Fig. 20. However, since twinning occurs in this coarse grained (500 μm) alloy, creep continues to very long times followed by creep saturation. The effect of grain size during the room temperature creep deformation observed in this investigation does not correlate with the grain size effects reported earlier for high temperature creep [61,62]. Such a correlation is not expected because the creep mechanisms at room temperature can be quite different from those at high temperature.

Transmission electron microscopy studies of the deformed regions of this large grained α Ti-Mn alloy showed additional spots in the selected area diffraction patterns. The spots were attributed to twinning as shown in Figs. 13 and 14, thus confirming the twinning

process conclusively.

3.2. Beta Ti-13.0Mn Alloy

3.2.1. Tensile Deformation

The ambient temperature true stress - true strain curve shown in Fig. 36 for β Ti-13.0Mn with grain size $\sim 200 \mu\text{m}$ shows very little strain hardening and it has a yield strength of 940 MPa. The deformation mechanism appears to be very coarse planar and wavy slip as shown in Figs. 37 and 38. No twinning was observed. Similar results were also reported in previous investigations by Ankem and Margolin [6,17-19].

3.2.2. Creep Deformation

The ambient temperature creep curve of β Ti-13.0Mn crept at 95% YS is presented in Fig. 39. This curve shows very little creep strain in contrast to the α phase. The creep strain was only 0.03% in ~ 400 hr. Despite the fact that there is very little creep strain, coarse slip was observed in a few grains as shown in Figs. 22, 24 and 40. No twinning was detected. This alloy was also crept at 100% of the 0.2% YS as shown in Fig. 41. The higher creep stress level raised the amount of plastic strain as would a normal tensile test at this stress and due to the lack of work hardening in this alloy, the resultant instantaneous strain can be

much higher than that observed at a creep stress of 95% YS. However, even at 100% YS the β Ti-Mn alloy did not creep significantly.

3.3. Beta Ti-14.8V Alloy

3.3.1. Tensile Deformation

The ambient temperature true stress - true strain curve for β Ti-14.8V, at a grain size of $\sim 35 \mu\text{m}$ is shown in Fig. 42. The YS of this alloy is 790 MPa. Note that this is a lower strength than the YS of β Ti-13.0Mn alloy. As in the β Ti-Mn case, there is very little strain hardening [20]. However, in contrast to the β Ti-Mn alloy, in addition to coarse planar and wavy slip, another mechanism, what appears to be twinning, was also observed, see Figs. 43 and 44. Profuse twinning in Ti-15.5V deformed between 4-9% by cold rolling has been reported by Oka and Taniguchi [63].

3.4. Alpha-Beta Ti-6.0Mn Alloy

3.4.1. Tensile Deformation

The α - β Ti-6.0Mn alloy with Widmanstätten microstructure when deformed at room temperature in a tensile test yielded at 623 MPa followed by strain hardening as shown by the true stress - true strain

curve of Fig. 45. The tensile deformation mechanisms were found to be anisotropic two-phase interface sliding, slip in the α and β phases and twinning in the alpha phase. For illustration, the anisotropic interface sliding is shown in Fig. 46 (b). Twinning in the α phase can be seen in Fig. 46 (d). Coarse slip in the β phase and slip in the α phase can be seen in Fig. 47. These results agree with previous investigations on two-phase titanium alloys in the Ti-Mn system [18].

3.4.2. Creep Deformation

The α - β Ti-6.0Mn alloy with Widmanstätten microstructure was creep tested at room temperature. Two creep stresses were used, 95% and 100% of the 0.2% YS. The creep curves are shown in Fig. 48. As in the case of the α Ti-Mn alloys, creep exhaustion was observed. The creep deformation mechanisms were the same for these two creep stress levels. They were found to be anisotropic two-phase interface sliding, coarse slip in the β phase, and slip and twinning in the α phase as in the case of tensile deformation. However, the maximum creep strain is much lower than the tensile strain so it was more difficult to observe the deformation mechanisms. Interface sliding is shown in Fig. 49 (b) and (c). Before and after creep deformation micrographs are shown in Fig. 50 where fine slip is discerned from grid line displacement measurement.

3.5. Alpha-Beta Ti-8.1V Alloy

3.5.1. Tensile Deformation

The α - β Ti-V alloy with Widmanstätten type microstructure as shown in Fig. 3, was tensile tested at room temperature in the same manner as the previous alloys. It was found to yield at 597 MPa and work harden only slightly as shown in Fig. 45. This is in contrast to the α - β Ti-Mn alloy which work hardens considerably and has a higher yield point. Also in contrast to the Ti-Mn alloy, the Ti-V alloy deforms by continuous slip in both the α and β phases and across the α - β interface. This is shown in Figs. 52-54.

3.5.2. Creep Deformation

The ambient temperature creep curves of α - β Ti-V alloy with Widmanstätten type microstructure crept at 95% and 100% of 0.2% YS are shown in Fig. 48. These curves exhibit creep exhaustion and a higher creep strain for α - β Ti-V alloy in the same amount of time than that shown by the curve in the same figure for α - β Ti-Mn alloy crept at the same percent of yield stress. The creep deformation mechanisms for α - β Ti-V alloy are slip in the α and β phases and continuous slip across the α - β interfaces this is in contrast to the α - β Ti-Mn alloy where rarely

slip was seen to cross the α - β interfaces and even then it would stop in the first α particle. Micrographs showing the creep deformation mechanisms for α - β Ti-V alloy are presented in Figs. 55 and 56.

4. DISCUSSION

4.1. Alpha Ti-0.4Mn Alloy

For the α Ti-Mn alloy tensile and creep deformation behavior studies were carried out for two different grain sizes.

4.1.1. Tensile Deformation Behavior

4.1.1.1. Small Grained Material

The small grained (45 μ m) α Ti-0.4Mn alloy when tensile tested at room temperature to a total strain of 3% at an initial strain rate of $3.28 \times 10^{-5} \text{ s}^{-1}$ deformed by fine slip, occasional twinning and rare grain boundary sliding as shown in Figs. 15, 17 and 27. It is to be noted that the fine slip lines are not visible on the specimen, however this conclusion was drawn by a comparison of grid lines before and after deformation. These observations are consistent with those reported earlier by Ankem and Margolin for α Ti - 0.39 wt% Mn alloy with comparable interstitial contents [6,17]. They [6] performed slip band and deformation studies during dynamic loading on α Ti-Mn alloy with grain sizes ranging from 11 to 281 μ m, reporting negligibly small effects due to grain size variation.

4.1.1.2. Large Grained Material

Yield stress of the larger grain size (500 μm) α Ti-0.4Mn alloy was slightly higher than the smaller grained material which is the opposite of what is expected. The small increase in yield stress is due to a lower initial dislocation density. Dislocations are annealed out at the higher processing temperature for the larger grained material. Another explanation for the slightly higher strength could be related to the distribution of manganese. The large grained material heat treated at a high temperature for 2 h, see section 2.1, is likely to have a more homogeneous distribution of Mn throughout its grains than the small grained material which was not raised to the high temperature during heat treatment. The homogeneous distribution of Mn could be responsible for the slightly higher strength of the large grained material.

Strain hardening in the large grained alloy may be due to an extensive increase in twinning. The twinning effectively refines the grain size, strengthening the alloy [64]. Other deformation mechanisms were found to be fine slip in agreement with previous investigators [6,9,11,59,60] and coarse slip in a few areas due to the large grain size.

4.1.2. Creep Deformation Behavior

4.1.2.1. Small Grained Material

Observation of Figs. 21 (a), (b), and (c) indicates that the α Ti-Mn alloy, with a grain size of $\sim 45 \mu\text{m}$ crept at ambient temperature at 95%

YS, deforms predominately by fine slip, occasional twinning and rare grain boundary sliding as in the case of tensile deformation. It is to be noted that the fine slip lines are not visible on the specimen, however this conclusion was drawn from a comparison of grid lines before and after deformation. In contrast, the occasional twins can be clearly seen, for example see Fig. 21 (c). The twinning in this alloy can be seen even more clearly in the optical micrographs, see Fig. 23. It is interesting to note that this α Ti-Mn alloy creeps at a higher rate in the beginning followed by creep exhaustion. Miller, Chen and Starke [25] observed similar behavior in the near α alloy Ti-6211. They call this phenomenon creep saturation or creep exhaustion and attribute it to a lack of recovery at room temperature. In low temperature creep ($T \leq 0.2T_m$, where T_m is the melting temperature of the material), deformation mechanisms with the lowest activation energy are likely to occur first upon initial loading and creep continues by mechanisms of higher activation energies [23,24,32,38,44,65]. Deformation takes place via the mechanism with the greatest ease of operation.

Transient creep [44] of the form taking place at room temperature in small grained α Ti-Mn alloy follows the form:

$$\epsilon_c = At^n \quad (1)$$

where ϵ_c is the creep strain (total strain minus elastic strain), A is a material constant dependent on microstructure and creep stress [25], t is time and n is the time exponent. The data from this investigation were

reasonably well fitted by straight lines on $\log \epsilon_c$ vs. $\log t$ plots, see Fig. 57, in contrast to ϵ_c vs. $\log t$ plots. This is usually the case for low temperature creep of titanium alloys and agrees well with many previous investigators [23-25,32].

A range of n values has been reported for ambient temperature creep for α and near α titanium alloys [23,25,44]. These n values depended on microstructure, processing conditions and alloying elements. However, it is not clearly known which microstructure gives what n value or for that matter, how the value of n depends on the deformation mechanism. In general, deformation by slip as the rate controlling mechanism has been implied irrespective of n value. Our results are consistent with this explanation because the n value we obtained for this material is 0.184, see Table 6 and Fig. 57, which falls within this range. Optical and SEM observations also indicate slip as the predominate deformation mode in this small grained material.

4.1.2.2. Large Grained Material

The creep deformation mechanisms of the large grained α Ti-0.4Mn alloy were similar to its dynamic deformation mechanisms, however the time dependent twinning observed in this alloy during creep resulted in larger creep strains and longer times to creep exhaustion than in the other alloys tested.

It is known [10,15,16] that there are four common types of deformation twins in CP titanium, $\{10\bar{1}2\}$, $\{11\bar{2}1\}$, $\{11\bar{2}2\}$, $\{10\bar{1}1\}$. In

addition, two less common $\{11\bar{2}3\}$, $\{11\bar{2}4\}$ twins have also been observed [60,67]. Out of these six possibilities, the most common twin modes during tensile deformation are $\{10\bar{1}2\}$ and $\{11\bar{2}1\}$ [15,16,60]. Observation of Figs. 33 and 34 indicates that some twins form almost instantaneously, see the location marked "A" in Fig. 33 (b), while other twins form after some time, i.e. time dependent twinning exists, see Figs. 33 (c) location "B", 33 (d) locations "B" and "C", 34 (c) location "B" and Fig. 35 (c) location "A". The instantaneously formed twins grow, compare location "A" in Fig. 33 (b) with 33 (d), while other twins nucleate as creep progresses. In general, the twins formed can be divided into two groups. The first group, such as twins seen in Fig. 33 (b) location "A", which formed either instantaneously as in Fig. 33 (b) or later as in Figs. 33 (c) and (d) location "B", grow extremely rapidly in the length direction across the grain, but grow more slowly in the thickness direction. These twins can grow to very large thicknesses, as much as 40 μm , when the creep strain is as small as 2.8%. The other group of twins, such as those in location "C" of Fig. 33 (d), location "B" of Fig. 34 (c) and location "A" of Fig. 35 (c), appear to be short, often ending inside the grains, intersecting each other at times, and being much more lenticular. This group of twins appears to grow more slowly in relation to the first group of twins. The later group of twins, because of their small size, can easily be seen in the TEM, see Fig. 13. They are identified as $\{10\bar{1}2\}$ twins following the method described by Partridge [56].

Occasionally, when a twin encountered a grain boundary it

triggered twinning in the adjacent grain, as shown in Fig. 58, i.e. twins triggering twins [68,69]. Since slip occurred in many areas prior to twinning and there is continuous slip after twinning, it was not possible to accurately determine the direct contribution of both instantaneous and time dependent twinning to the creep strain, but a comparison of the creep of this coarse grain size (500 μm) with a small grained (45 μm) α Ti-0.4Mn alloy, which has very little twinning [7], suggests the contribution of twinning and its associated slip to creep is in excess of 50% of the total creep strain.

In Fig. 13 a dislocation tangle can be seen in the lower right. These dislocations are likely accommodating the strain from twinning, also visible in the figure, and are possible sources of further twin nucleation. Fig. 59, another area of the large grained α Ti-0.4Mn alloy shown in Fig. 13, indicates long dislocations with twins nucleating near these dislocations at location "A". However, it is difficult to prove from this figure that the dislocations existed before the twins formed.

There exists some controversy as to whether slip is a prerequisite for twinning [10,11,70]. For this reason, the grid line spacing of several regions of the specimen were measured before deformation and in subsequent steps prior to nucleation of time dependent twins. For example, the grid line spacing at location "B" in Fig. 34 prior to twinning increased in the loading direction. This is true for most of the twins which are forming later and suggests fine slip prior to twinning. However, it is not clear at this time whether slip occurred prior to

formation of the instantaneous twins. At these locations of fine slip, twins are formed on further creep, compare location "B" in Fig. 34 (b) with the same location in 34 (c). Slip continues to occur while the twins are growing. Large displacements were measured in the vicinity of growing twins. It is not clear at this time why twins are nucleating after certain creep strain or time, but there are at least two possibilities. The first one is related to the development of high local stresses required to nucleate twins. High local stresses can develop if dislocations are allowed to pile-up at obstacles [71,72]. The second possibility comes from the presence of interstitial and substitutional atoms. It has been found in the past that during tensile deformation the presence of oxygen raises the stress required for the formation of twins [60,73,74]. The time delay could be related to the diffusion of these atoms so that the twin can grow.

The time exponent n obtained for this alloy, which is 0.290, is significantly higher than that found for the finer grained material which is 0.184, see Table 6 and Fig. 57. Given that here the chemistry of the alloy is the same and the final heat treatment is the same, it is reasonable to suggest that the difference in the two n values is related to the difference in the deformation mechanisms. These results suggest that when time dependent twinning is one of the major deformation mechanisms the n value increases. However, it is to be noted that the increase in n value can not be related only to twinning, but to the twinning/slip combination mechanism. As mentioned before, such a

correlation between the n value and twinning has not been reported before and further work is needed to confirm this.

Based on the observations, it can be concluded that the ambient temperature creep deformation mechanisms in this coarse grained α Ti-0.4Mn alloy are due to slip and instantaneous and time dependent twinning. In the very beginning of the creep process most of the deformation is due to fine slip and to a lesser extent, instantaneous twinning. As time progresses, slip continues to play a significant role as does twinning. The twins which formed instantaneously grow while new twins continually nucleate with time. Slip as well as the nucleation and growth of twins contribute to the creep strain. In addition, dislocations which move in the matrix can cross slip and glide in the twins under certain conditions [15] also contributing to the creep strain. However, as time progresses the resistance to further twinning and dislocation motion becomes more and more difficult resulting in eventual creep saturation. As mentioned before, the creep strain of a small grained ($45\text{ }\mu\text{m}$) α Ti-0.4Mn alloy was found to be less than one half of the creep strain observed in the coarse grained material. The twinning activity was negligibly small in the case of small grained material [7]. Therefore, any factor such as decreased grain size or increased interstitial content [60] which can reduce twinning can also reduce creep strain [75].

4.2. Beta Ti Alloys

4.2.1. Tensile and Creep Deformation Behavior of Ti-13.0Mn Alloy

In contrast to α Ti-Mn alloy, β Ti-Mn alloy deforms only by coarse planar and wavy slip, see Figs. 37 and 38. The wavy nature of slip is not too distinct in these figures, but it can be found in other areas of the specimen. Tensile deformation behavior of β phase Ti-Mn alloys has been reported earlier [4,6,8,17,76]. In their earlier work, Ankem and Margolin [6] studied the tensile deformation behavior of Ti-10.2Mn alloy annealed at 973 K followed by water quenching. The phase diagram of Fig. 7 shows that Mn content of the β phase at this temperature is about 11.5 wt %. They have taken the Selected Area Diffraction Pattern (SADP) of the β phase of the undeformed near β alloy and found diffuse streaking. Such diffuse streaking was also observed in other metastable β Ti-Mn alloys [77,78]. This streaking has been ascribed to random or uncorrelated displacement of the atoms, so that ω phase lattice is not yet generated but the periodicity of the β phase bcc lattice is reduced. Since the β phase with 11.5 wt % Mn did not result in complete ω phase formation during quenching and given the fact that the annealing temperature of the present study is 963 K so that a β phase with a composition of 13.0 wt % Mn is present, it is expected that this β Ti-Mn alloy is more stable and it is not expected to have any athermal ω phase.

Indeed, TEM analysis of the β phase in the α - β Ti-6.0Mn alloy, discussed later, did not show the presence of athermal ω phase, but did show pre ω phase streaking in the SADP as shown in Fig. 60. As stated previously, the chemical composition of the β phase in the α - β Ti-6.0Mn and β Ti-13.0Mn alloys is expected to be nearly the same.

As mentioned before, the deformation mechanisms of the β phase Ti-Mn alloys studied by Ankem and Margolin [6,17-19] and that of the present study are similar, that is, coarse planar and wavy slip but no twinning, as revealed by light microscopy and SEM observations. However, Young, Jaffee and Schwartz [76] have reported twinning in β phase of a Ti-Mn alloy which was annealed at 1023 K followed by water quenching. They have reported that Mn content of their β phase was about 10%, as can be determined from the phase diagram in Fig. 7. If it is assumed that the oxygen content of all these alloys is similar, then lower Mn content causes lower stability of the β phase and more of a tendency for the β phase to twin as in the case of other metastable β Ti alloys [78-84] as well.

In contrast to α Ti-Mn alloy, β Ti-Mn alloy exhibits no significant creep strain, see Fig. 39. It is not clear at this time why the creep strain is so low but it appears to be related to the low initial mobile dislocation density [85,86] and absence of twinning of the β phase. The investigation to understand creep deformation behavior of the β Ti-Mn alloys is currently underway [87].

4.2.2. Tensile Deformation Behavior of Ti-14.8V Alloy

In contrast to β Ti-Mn alloy, the β Ti-V alloy exhibits both coarse slip and what appears to be twinning during tensile deformation, see Figs. 43 and 44. In the past there was some controversy over the stress induced plates, whether they are martensite or twins [18,63]. Several groups of investigators have studied the deformation behavior of different β Ti-V alloys with V content ranging from 14.0 to 40.0 wt % [8,21,63,78,80,82]. For the Ti-V alloys with V content in the vicinity of 15 wt %, most of these investigators observed stress induced plates after deformation [20,21,63,80,82]. Hanada and coworkers [80,82] and Oka and Tanaguchi [63] have concluded that the plates are twins. Koul and Breedis [20], on the other hand, have reported that the plates are one variant of the ω phase. The origin of this discrepancy is not clear at this time, but it can be related to the variation in the oxygen content of the alloys for a given V content. The presence of oxygen changes the stability of the β phase [83-89]. It is to be noted that variation of the other impurities can also effect the stability of the β phase, but oxygen is more likely the most significant variant in the alloys of different investigators giving rise to differences in the stability of the β phase [8]. The deformation mechanism of the β phase in Ti-V alloys is expected to change with changes in the stability of the β phase, as was the case with Ti-Mn alloys.

The stress induced plates seen after deformation of Ti-14.8V alloy with 0.092 wt % oxygen as shown in Figs. 43 (b), 43 (d) and 48 were recently confirmed to be {332} twins by Sil et al. [8]. This observation supports the results of Oka and Tanaguchi [63], who also have reported that the stress induced plates are indeed twins. These investigators [8] have also identified athermal ω phase in the β phase of this Ti-14.8V alloy, which is also the case for the β phase of the Ti-V alloys used by the other investigators [20,21,63] with similar V contents. In addition, athermal ω phase was seen in the SADP of the β phase in the α - β Ti-8.1V alloy in this study, as seen in Fig. 61. This is expected, as noted earlier, because the β phase in the two alloys Ti-14.8V and Ti-8.1V quenched from 963 K is expected to have the same chemical composition and thus relatively similar degree of instability.

Although oxygen has a strong effect on the stability of the β phase, the absence of twinning in the β Ti-13.0Mn alloy and the occurrence of twin like stress induced plates in the β Ti-14.8V alloy, i.e., the stability of the β phase, may be related to the atomic size differences between the titanium and the solute elements. The atomic size difference between Ti and V is much smaller than the atomic size difference between Ti and Mn. Even though the β Ti-V alloy has more solute than the Ti-Mn alloy, it appears to be less stable.

The difference in the deformation behavior between the Ti-Mn and Ti-V systems can be attributed to the stability of the β phase. The β

Ti-14.8V alloy appears to be less stable than the Ti-13Mn alloy and therefore resulted in stress induced plate formation and slip rather than slip alone as in the case of the Ti-13.0Mn alloy. It will be interesting to see whether the creep deformation behavior of β Ti-V is different from that of the β Ti-Mn alloy.

4.3. Alpha-Beta Ti-6.0Mn and Ti-8.1V Alloys

4.3.1. Tensile Deformation Behavior

The tensile deformation mechanisms for the α - β Ti-6.0Mn alloy with Widmanstatten type microstructure consisting of ~46% α particles and grain boundary α in β matrix are seen in the before and after deformation SEM micrographs of Fig. 46 and the after deformation light microscopy pictures of Fig. 47. Observation of these figures indicates that the deformation mechanisms are coarse slip in the β phase occasionally penetrating, but not passing through, α particles, rare twinning in the α particles, fine slip which is not directly visible but must be deduced by measuring grid line displacements and α - β interface sliding. Similar deformation mechanisms were observed earlier by Ankem and Margolin [6].

The α - β Ti-8.1V alloy deformed by fine slip as well as coarse slip which traversed many α platelets in a given colony, see Figs. 52 through

54. The slip traversing the α - β interfaces has been reported in other titanium alloys by various investigators [90-95]. This has been attributed to the Burgers orientation relationship which exists between α and β phases. It is to be noted that the slip traversing the α - β interfaces was not observed in the α - β Ti-Mn alloy. The reason for this difference is not clear at this time, but appears to be related to the stability of the β phase as discussed later.

4.3.2. Creep Deformation Behavior

The α - β Ti-6.0Mn alloy was crept at 95 and 100% of its 0.2% YS as previously indicated. The microstructure before and after deformation is shown in Figs. 49 through 51. The creep deformation mechanisms appear to be the same as the dynamic deformation mechanisms, i.e., fine slip in the α phase, α - β interface sliding, rare coarse slip in the β phase and rare twinning in the α phase. These deformation mechanisms were seen at both creep stresses of 95% and 100% YS though the interface sliding is difficult to detect at the lower creep strains resulting at the lower creep stress of 95% YS. It is expected that the β phase will not show much deformation taking place since the ~100% single phase β Ti-13.0Mn alloy did not creep significantly. However, due to elastic interactions [96,97] in the two-phase alloy, the stress on the β phase is likely to exceed its yield strength leading to deformation by coarse planar

and wavy slip.

The α - β Ti-6.1V alloy creeps more than the α - β Ti-6.1Mn alloy at both 95% and 100% of their respective yield stresses. This difference was attributed to the differences in creep deformation mechanisms. The creep deformation mechanisms for the α - β Ti-6.1V alloy include coarse continuous slip in the α and β phases and slip across the α - β interface, see Figs. 55 and 56. This difference in the mechanisms could be related to the difference in the strengths of the α and β phases in the two systems, the relative stability of their β phases and a difference in the nature of the α - β interfaces.

The α and β phases in the Ti-Mn system have a much higher strength difference than the α and β phases in the Ti-V system. This can be seen by comparing Figs. 16 and 36 with Figs. 42 and 62 [98]. Since elastic interactions play a role in the deformation of two-phase alloys [96,97], and the lower strength α phase is deforming first, in the manganese system the stress concentration at the α - β interface due to plastic deformation in the α phase has to be much higher than in the vanadium system, before slip can be initiated in the neighboring β phase.

Another and probably the most important difference in the α - β alloys of the Ti-Mn and Ti-V systems is related to the stability of the β phase. The β phase in the two-phase alloy of the vanadium system is

much more unstable than the β phase in the alloy of the manganese system, therefore it may tend to deform easily once stress is built up or concentrated from deformation of the α phase. The sequence leading to plastic deformation begins with fine slip in the α phase because it is softer, the β phase resists this deformation until the stress level becomes high enough to initiate deformation in the β phase. In the case of Ti-8.1V alloy the β phase simply deforms coarsely and suddenly because it is highly unstable. In the Ti-Mn system the β phase is more stable and able to dissipate the stress applied by the α phase resulting in finer, discontinuous slip and greater resistance to deformation.

The third possible explanation for the difference in the creep deformation modes between the α - β alloys of the Ti-Mn and Ti-V systems is related to the nature of the α - β interfaces. The nature of the α - β interface was studied in the TEM. By measurement of the r spacing, where r is a function of the interplanar spacing, d , and the camera constant, in the diffraction patterns of the α and β phases, δ , the degree of misfit could be calculated. The Burgers orientation relationships are known to describe planes in the two-phase alloys where slip can easily occur across the interfaces [96,97]. The Burgers orientation relationships are

$$\langle 1210 \rangle_{\alpha} // \langle 111 \rangle_{\beta} \quad (2)$$

from which it follows [96]

$$\langle 1120 \rangle_{\alpha} // \langle 111 \rangle_{\beta} \quad (3)$$

and

$$\langle 1120 \rangle (0111)_{\alpha} // \langle 111 \rangle (011)_{\beta} \quad (4)$$

where the interface plane has been found to be $(5140)_{\alpha} // (334)_{\beta}$ [99-101], see Fig. 63. The degree of misfit can be expressed as δ [102] where

$$\delta = (d_{\alpha} - d_{\beta}) / d_{\beta} \quad (5)$$

where d_{α} is the unstressed interplanar spacing for the plane in the α phase and d_{β} is the unstressed interplanar spacing for the plane in the β phase. Preliminary results indicated the difference in δ between the Ti-V and Ti-Mn systems is small, but more work involving High Resolution Electron Microscopy (HREM) needs to be performed to accurately predict these differences and to study the α - β interface structure. However, it is reasonable to suggest at this point, such a difference in the α - β interface structure in the two systems is not the primary reason why the Ti-V system has a different creep deformation mechanism and higher creep strain.

The values for n obtained for the two-phase α - β titanium alloys from the $\ln \epsilon_c$ vs. $\ln t$ curve of Fig. 57, see Table 6, are similar to those reported by Imam and Gilmore [24] for the α - β alloy Ti-64. They [24] ascribed the creep to be occurring by thermally activated overcoming of interstitial obstacles to glide as first proposed by Odegard and Thompson [32]. The longer slip lengths observed in the α - β Ti-6.1V alloy resulting from continuous slip across many α platelets in a given colony seem to

be responsible for the higher creep rate. Long slip lengths also resulted in higher creep rates in a near α titanium alloy, Ti-6211, as reported by Miller et al. [25]. However, it appears that the reasons leading to slip lengths are different in the present Ti-V system than in the Ti-6211 alloy. In the present case the longer slip lengths appear to be related to the nature of the unstable β phase with athermal ω phase in the α - β Ti-V alloy.

5. SUGGESTIONS FOR FUTURE STUDIES

Work is already underway in a number of complimentary studies [87,98]. These areas will be briefly mentioned before suggesting future studies.

1. The grain size effect on the room temperature creep of α Ti-0.4Mn alloy is being systematically studied by Singh and Ankem [98].
2. TEM studies of β Ti-13.0Mn alloy to determine why it does not creep and creep studies of β Ti-14.8V alloy to compare with β Ti-13.0Mn alloy are carefully being investigated by Sil and Ankem [87].
3. In regard to the α - β titanium alloys, the equiaxed microstructure is being studied [98] and a systematic investigation to determine the effect of particle size in the Widmanstatten type microstructure is underway [87].

Future studies indicated by questions arising from this work in addition to the complimentary studies listed above include:

1. In-situ TEM studies using a tensile stage currently available to investigate the nucleation of twins in α Ti-0.4Mn alloy under constant stress.

2. Study the deformation mechanisms of the α - β titanium alloys as a function of β phase stability.
3. Perform interface studies of α - β titanium alloys to determine the degree of coherency depending on the alloying elements and the type of barrier these interfaces present to dislocations and twinning.

6. CONCLUSIONS

1. When the 45 μm grain size α Ti-0.4Mn alloy was crept at 95% yield stress at room temperature (298 K), significant creep strain was observed in the beginning and this was followed by creep exhaustion. The creep deformation mechanisms appear to be similar to those in tensile deformation, i.e. fine slip, occasional twinning and rare grain boundary sliding.
2. A coarse grained (500 μm) α Ti-0.4Mn alloy, when creep tested at 298 K and at a constant stress of 95% YS, exhibited significantly more creep strain than the smaller grained α alloy. The creep mechanisms were found to be slip, instantaneous twinning and *time dependent twinning*.
3. In the coarse grained α Ti-0.4Mn alloy, the twins which formed instantaneously and those twins which formed after some time grew in the length direction and thickness direction with time. Growth in the length direction was found to be much faster.
4. Significant slip/twin interactions were observed in the coarse grained α Ti-0.4Mn alloy. The regions where twins form after some time deformed by fine slip prior to twinning. Twin-twin interactions where twins nucleate other twins in the same grain and

in the neighboring grains were also observed.

5. Since slip occurred in many areas prior to twinning and there is continuous slip after twinning in the coarse grained α Ti-0.4Mn alloy, it was not possible to accurately determine the direct contribution of both instantaneous and time dependent twinning to the creep strain, but a comparison of the creep of this coarse grain size (500 μm) with the small grained (45 μm) α Ti-0.4Mn alloy, which has very little twinning, suggests the contribution of twinning and its associated slip to creep is in excess of 50% of the total creep strain.
6. When the β Ti-13.0Mn alloy was crept at 95% yield stress at room temperature no significant creep strain was observed. This is in contrast to α Ti-Mn alloy where significant creep strain was observed. The creep resistance of this alloy was attributed to the low initial mobile dislocation density.
7. In β Ti-14.8V, the tensile deformation occurs by coarse planar and wavy slip and stress induced plate formation. This is in contrast to the tensile deformation of β Ti-Mn alloy which deforms by coarse planar and wavy slip. This difference appears to be related to the relative stability of the β phase.

8. It was found that the tensile deformation mechanisms of the α - β titanium alloys for a given morphology and volume percent of phases, depended on the alloying elements. Fine slip in α phase of both these systems occurs, however, coarse slip traversing many α - β interfaces was found only in the Ti-V system and not the Ti-Mn system. On the other hand, occasional α - β interface sliding was observed only in the Ti-Mn system. The difference in the slip behavior was attributed to the difference in the stability of the β phases in the two systems.
9. It was found that, for two-phase α - β Ti-6.0Mn and Ti-8.1V alloys with similar morphology of phases and volume percent of phases, that the creep strain and creep mechanisms are also different.
10. The α - β Ti-6.0Mn alloy deforms by two-phase interface sliding, fine slip in the α phase, and occasional coarse, dispersed slip in the β phase. The Ti-8.1V alloy, on the other hand, deforms by continuous slip in both α and β phases and across the α - β interface in addition to fine slip in the α and β phases, however, no interface sliding was observed in the Ti-8.1V alloy.
11. The difference in the creep behavior between the α - β Ti-6.0Mn and Ti-8.1V alloys appears to be predominately related to the difference

in the relative stability of their β phases.

12. At both 95% and 100% yield stress at room temperature the α - β Ti-8.1V alloy was found to exhibit more creep strain than the Ti-6.0Mn alloy. This appears to be due to the difference in deformation mechanisms of the two systems.

7. APPENDICES

A. Typical Tensile Test Data

Table A.1: Tensile Test Data for Ti-0.4(wt%)Mn Alloy Tested at 298 K and an Initial Strain Rate of $3.28 \times 10^{-5} \text{ s}^{-1}$

True Strain (%)	True Stress (MPa)	True Strain (%)	True Stress (MPa)	True Strain (%)	True Stress (MPa)	True Strain (%)	True Stress (MPa)
0.00	-5.20	0.01	1.90	0.02	14.79	0.04	28.88
0.01	-5.37	0.02	2.90	0.04	15.57	0.03	28.30
0.01	-5.07	0.03	3.60	0.02	15.98	0.05	29.72
0.01	-4.67	0.03	4.35	0.04	15.39	0.03	29.63
0.01	-4.32	0.02	4.53	0.03	16.21	0.03	30.72
0.01	-3.90	0.01	4.29	0.03	16.17	0.04	31.84
0.01	-4.30	0.02	5.48	0.04	17.71	0.04	31.73
0.01	-4.43	0.03	5.61	0.03	18.10	0.04	33.23
0.01	-4.21	0.03	6.05	0.04	18.90	0.04	31.81
0.01	-4.32	0.03	6.36	0.03	18.12	0.06	33.34
0.01	-3.96	0.01	7.14	0.04	19.61	0.04	33.06
0.01	-3.31	0.02	7.07	0.03	19.49	0.06	34.99
0.01	-2.95	0.03	7.91	0.04	21.06	0.04	34.75
0.01	-2.78	0.02	7.65	0.03	20.69	0.06	35.36
0.01	-2.75	0.03	8.93	0.04	20.86	0.04	35.41
0.02	-1.98	0.03	8.81	0.03	21.24	0.06	35.83
0.02	-1.80	0.02	9.34	0.03	21.23	0.06	36.51
0.02	-1.65	0.02	10.32	0.04	22.89	0.05	37.24
0.02	-1.32	0.02	10.35	0.03	22.94	0.06	38.72
0.02	-0.57	0.03	10.94	0.05	24.14	0.04	38.58
0.02	-0.19	0.02	10.85	0.03	24.81	0.06	39.52
0.02	0.30	0.03	11.59	0.03	24.84	0.04	39.11
0.01	0.47	0.03	11.99	0.04	24.85	0.06	40.25
0.02	0.74	0.02	12.03	0.04	25.66	0.05	40.00
0.03	1.80	0.03	13.74	0.04	25.78	0.06	41.03
0.02	1.60	0.03	13.58	0.05	27.06	0.05	40.98
0.01	1.72	0.04	13.90	0.03	27.84	0.06	42.00
0.00	2.43	0.04	13.57	0.04	27.73	0.04	42.17

(Continued on next page)

Table A.1: (Continued)

True Strain (%)	True Stress (MPa)	True Strain (%)	True Stress (MPa)	True Strain (%)	True Stress (MPa)	True Strain (%)	True Stress (MPa)
0.06	43.82	0.07	63.76	0.11	84.99	0.11	108.16
0.05	43.74	0.07	63.54	0.10	86.15	0.11	108.64
0.07	44.26	0.07	65.07	0.10	87.18	0.12	109.30
0.05	44.56	0.06	64.87	0.10	87.46	0.12	110.74
0.06	45.07	0.07	65.42	0.09	87.97	0.12	111.68
0.05	45.44	0.08	66.24	0.09	88.05	0.11	111.79
0.06	45.81	0.08	66.79	0.11	88.71	0.11	112.25
0.06	47.30	0.08	67.40	0.11	89.65	0.11	112.94
0.06	46.94	0.07	68.06	0.11	90.76	0.11	113.31
0.06	48.42	0.08	67.73	0.11	91.42	0.12	114.03
0.06	48.05	0.08	68.75	0.10	92.62	0.12	114.22
0.06	49.32	0.09	69.55	0.10	93.25	0.12	115.53
0.05	48.62	0.09	70.45	0.10	93.21	0.12	116.01
0.07	50.10	0.09	71.65	0.10	93.90	0.12	116.52
0.06	50.41	0.09	72.71	0.10	94.04	0.14	117.47
0.08	51.69	0.08	72.78	0.09	94.02	0.13	117.93
0.06	52.46	0.07	72.85	0.10	95.04	0.12	118.69
0.06	51.89	0.07	73.08	0.10	95.92	0.12	119.02
0.07	53.15	0.08	74.05	0.10	96.73	0.12	119.70
0.06	52.68	0.08	74.85	0.10	97.55	0.12	120.41
0.07	54.50	0.08	75.97	0.10	98.05	0.13	120.77
0.06	54.24	0.08	76.10	0.10	97.63	0.13	121.65
0.05	55.87	0.08	76.55	0.11	98.30	0.14	121.94
0.08	56.95	0.09	75.91	0.12	99.37	0.15	122.59
0.06	56.54	0.10	77.17	0.12	100.42	0.14	123.63
0.08	56.78	0.10	77.29	0.12	100.88	0.13	123.51
0.06	57.11	0.09	78.81	0.12	102.11	0.14	124.63
0.08	57.09	0.09	79.73	0.11	103.21	0.14	126.52
0.06	58.99	0.09	80.36	0.12	102.82	0.13	126.99
0.07	58.84	0.09	80.88	0.13	103.37	0.13	128.06
0.08	60.54	0.09	80.48	0.13	104.40	0.13	128.13
0.07	59.75	0.10	82.37	0.12	104.86	0.13	127.93
0.08	60.63	0.08	82.76	0.12	105.48	0.13	128.93
0.09	61.12	0.09	82.85	0.12	106.36	0.14	128.88
0.07	62.12	0.09	82.77	0.12	107.16	0.14	129.63
0.08	62.12	0.11	83.44	0.11	107.54	0.15	130.28

(Continued on next page)

Table A.1: (Continued)

True Strain (%)	True Stress (MPa)	True Strain (%)	True Stress (MPa)	True Strain (%)	True Stress (MPa)	True Strain (%)	True Stress (MPa)
0.15	131.73	0.18	156.98	0.19	180.16	0.25	200.28
0.13	133.02	0.17	158.06	0.20	180.09	0.25	201.50
0.14	133.60	0.17	157.79	0.22	181.80	0.25	202.03
0.14	133.72	0.16	158.31	0.20	183.14	0.25	201.90
0.14	134.12	0.17	158.26	0.19	182.86	0.25	202.98
0.15	134.86	0.19	159.66	0.21	183.19	0.26	203.15
0.15	135.37	0.18	160.97	0.21	184.76	0.26	204.19
0.16	136.43	0.17	162.10	0.20	185.04	0.25	204.63
0.16	136.91	0.17	162.33	0.21	185.01	0.26	204.03
0.15	138.81	0.18	163.18	0.21	186.67	0.26	205.57
0.15	139.76	0.17	163.69	0.21	186.46	0.26	205.03
0.14	139.76	0.17	162.92	0.21	186.12	0.27	205.51
0.16	140.14	0.19	163.71	0.23	186.79	0.27	207.20
0.15	140.47	0.19	165.24	0.22	189.11	0.27	207.18
0.15	141.12	0.19	166.07	0.21	189.27	0.27	207.55
0.14	141.52	0.18	167.42	0.22	189.08	0.28	208.97
0.15	141.26	0.17	167.37	0.23	190.70	0.27	208.76
0.15	142.53	0.18	167.79	0.22	190.71	0.27	208.51
0.15	143.78	0.20	168.26	0.23	190.81	0.29	209.14
0.16	144.62	0.19	169.41	0.23	191.75	0.28	209.67
0.17	145.50	0.18	169.36	0.22	191.76	0.28	209.68
0.16	146.16	0.19	169.43	0.24	192.67	0.29	210.45
0.16	147.12	0.19	171.13	0.24	193.48	0.29	212.41
0.17	147.56	0.20	172.00	0.22	193.96	0.28	212.43
0.16	148.50	0.19	173.38	0.24	193.68	0.30	212.33
0.15	148.89	0.19	173.21	0.24	195.32	0.29	213.33
0.15	149.60	0.19	173.13	0.23	196.53	0.29	212.16
0.16	150.52	0.21	174.30	0.24	195.88	0.30	212.91
0.17	151.37	0.20	175.06	0.24	196.43	0.30	213.61
0.17	152.20	0.19	176.23	0.24	196.88	0.29	213.55
0.16	153.16	0.19	175.78	0.24	197.53	0.30	213.69
0.16	153.22	0.20	176.89	0.25	198.21	0.31	214.40
0.16	153.75	0.19	177.51	0.24	199.02	0.31	215.73
0.16	153.98	0.19	178.09	0.24	199.28	0.30	216.56
0.17	154.71	0.21	179.90	0.25	200.78	0.30	216.21
0.18	155.75	0.19	180.77	0.24	200.52	0.30	216.06

(Continued on next page)

Table A.1: (Continued)

True Strain (%)	True Stress (MPa)	True Strain (%)	True Stress (MPa)	True Strain (%)	True Stress (MPa)	True Strain (%)	True Stress (MPa)
0.31	215.88	0.38	229.08	0.46	239.03	0.54	248.24
0.32	216.42	0.39	229.01	0.47	239.30	0.54	248.40
0.32	217.54	0.39	229.72	0.47	240.42	0.55	249.09
0.31	217.71	0.39	230.43	0.46	241.32	0.55	249.04
0.32	217.74	0.39	230.36	0.47	241.49	0.55	249.30
0.33	219.10	0.39	230.77	0.47	240.74	0.56	248.86
0.32	219.71	0.40	231.04	0.49	240.99	0.57	249.64
0.32	219.71	0.40	231.61	0.48	240.97	0.57	250.59
0.32	219.87	0.40	231.29	0.48	241.80	0.57	250.59
0.33	219.47	0.40	232.02	0.48	241.99	0.57	250.52
0.33	219.83	0.41	232.58	0.48	242.43	0.57	251.25
0.32	220.81	0.40	233.28	0.49	241.73	0.57	251.02
0.33	220.45	0.40	233.37	0.50	242.12	0.57	250.17
0.34	221.18	0.42	233.47	0.49	242.65	0.58	250.72
0.35	222.23	0.42	232.99	0.49	243.81	0.58	251.78
0.33	222.08	0.42	234.03	0.49	243.86	0.58	251.61
0.33	221.67	0.41	233.78	0.50	242.29	0.60	251.11
0.34	221.71	0.42	233.20	0.51	243.73	0.59	251.76
0.36	222.70	0.43	234.19	0.50	243.13	0.58	251.37
0.35	223.42	0.42	235.41	0.52	243.99	0.59	251.88
0.34	224.05	0.42	235.34	0.51	244.73	0.60	252.82
0.35	224.37	0.44	235.63	0.51	245.69	0.60	254.04
0.36	224.80	0.43	235.75	0.51	245.31	0.59	253.27
0.35	225.30	0.43	235.07	0.51	245.36	0.60	252.72
0.35	224.20	0.44	234.88	0.52	244.90	0.61	253.37
0.37	225.01	0.44	236.37	0.53	245.21	0.60	254.03
0.36	226.52	0.43	236.87	0.53	245.26	0.60	254.34
0.36	226.62	0.44	236.44	0.52	246.43	0.61	254.18
0.37	226.61	0.45	237.41	0.52	246.30	0.62	254.65
0.38	226.98	0.44	237.29	0.53	247.10	0.62	254.92
0.37	228.27	0.45	236.73	0.53	246.69	0.61	254.41
0.37	227.12	0.46	237.43	0.53	246.11	0.63	254.73
0.37	227.64	0.45	237.78	0.55	247.13	0.62	256.43
0.39	227.91	0.46	238.24	0.55	247.45	0.62	255.97
0.38	228.66	0.46	239.84	0.54	248.13	0.63	255.44
0.38	229.51	0.45	239.96	0.54	248.28	0.64	256.48

(Continued on next page)

Table A.1: (Continued)

True Strain (%)	True Stress (MPa)	True Strain (%)	True Stress (MPa)	True Strain (%)	True Stress (MPa)	True Strain (%)	True Stress (MPa)
0.63	256.57	0.72	262.35	0.81	267.23	0.92	272.55
0.63	255.69	0.73	262.35	0.82	266.77	0.91	273.80
0.63	256.41	0.73	263.33	0.82	268.45	0.91	274.34
0.65	257.08	0.73	262.83	0.81	268.26	0.91	273.27
0.64	257.36	0.73	262.67	0.83	268.53	0.93	273.31
0.64	257.47	0.75	263.49	0.84	268.69	0.91	272.93
0.65	256.39	0.73	263.97	0.82	268.78	0.93	272.88
0.66	257.12	0.73	263.17	0.83	267.66	0.93	274.33
0.65	258.14	0.75	263.70	0.84	268.23	0.92	274.43
0.65	257.44	0.75	264.34	0.85	268.67	0.95	274.18
0.67	258.70	0.75	264.00	0.83	269.12	0.94	274.67
0.66	258.62	0.75	264.29	0.84	268.75	0.93	275.03
0.66	257.68	0.76	264.48	0.86	270.12	0.95	274.01
0.67	258.38	0.76	265.16	0.85	270.94	0.95	274.47
0.66	258.03	0.75	264.94	0.85	269.83	0.94	274.39
0.68	258.30	0.77	264.09	0.85	269.31	0.95	273.85
0.68	259.71	0.77	265.29	0.86	270.14	0.96	275.10
0.67	259.87	0.76	265.49	0.85	270.33	0.95	275.58
0.68	259.11	0.77	264.64	0.86	270.30	0.96	275.17
0.69	259.05	0.78	265.77	0.87	271.12	0.97	275.28
0.68	259.56	0.77	265.92	0.86	271.38	0.96	275.61
0.69	258.93	0.77	265.14	0.87	270.96	0.96	274.81
0.70	259.97	0.78	264.36	0.88	271.32	0.98	275.30
0.69	261.09	0.78	265.52	0.87	271.69	0.97	275.73
0.69	259.28	0.78	266.14	0.87	271.32	0.97	275.00
0.70	260.46	0.79	265.54	0.89	271.21	0.98	276.54
0.69	260.64	0.80	266.59	0.88	271.60	0.98	276.89
0.70	260.30	0.79	266.79	0.88	271.49	0.99	276.73
0.71	261.47	0.79	266.62	0.90	271.70	0.98	277.85
0.71	262.18	0.81	266.17	0.88	272.83	0.98	276.99
0.70	261.94	0.80	267.35	0.90	272.79	0.99	276.12
0.71	260.91	0.79	267.32	0.89	272.68	0.99	277.19
0.72	261.30	0.81	267.19	0.90	271.55	0.99	276.64
0.72	261.96	0.81	267.21	0.91	271.96	0.99	276.20
0.71	261.97	0.81	268.03	0.90	272.72	1.01	276.72
0.72	263.04	0.81	267.82	0.90	272.80	0.99	276.65

(Continued on next page)

Table A.1: (Continued)

True Strain (%)	True Stress (MPa)	True Strain (%)	True Stress (MPa)	True Strain (%)	True Stress (MPa)	True Strain (%)	True Stress (MPa)
1.01	276.59	1.10	280.70	1.19	284.14	1.30	286.81
1.01	277.35	1.11	281.39	1.20	283.16	1.29	285.99
1.00	277.43	1.10	281.43	1.21	284.03	1.31	286.40
1.01	277.57	1.10	280.81	1.20	284.40	1.31	287.49
1.03	277.20	1.12	280.86	1.21	284.02	1.30	287.65
1.01	278.57	1.11	281.82	1.21	285.10	1.31	287.11
1.01	277.44	1.11	281.04	1.21	284.14	1.31	287.21
1.03	277.27	1.12	280.65	1.22	283.22	1.33	287.15
1.02	278.36	1.13	280.93	1.22	284.39	1.32	287.93
1.02	278.22	1.12	281.55	1.22	284.76	1.32	287.44
1.04	277.90	1.13	280.68	1.22	284.66	1.34	287.37
1.04	279.34	1.14	281.27	1.23	284.67	1.33	289.01
1.03	279.38	1.13	281.99	1.23	285.96	1.32	288.72
1.05	278.78	1.13	282.22	1.23	283.91	1.33	287.83
1.04	279.31	1.14	281.95	1.24	284.09	1.34	288.05
1.06	279.64	1.15	282.16	1.24	285.00	1.33	288.22
1.05	279.95	1.14	282.95	1.23	285.01	1.34	287.74
1.05	278.74	1.14	282.49	1.26	285.11	1.35	288.91
1.06	279.15	1.16	282.12	1.24	285.99	1.35	288.83
1.05	279.42	1.16	282.44	1.25	285.14	1.36	288.51
1.07	278.74	1.15	282.46	1.26	284.81	1.35	289.48
1.06	280.00	1.16	281.49	1.25	285.26	1.35	288.20
1.06	279.12	1.16	281.53	1.25	285.64	1.37	288.35
1.08	280.05	1.17	282.39	1.26	285.64	1.36	288.90
1.06	280.38	1.16	282.52	1.26	285.78	1.37	288.42
1.06	280.60	1.17	281.79	1.27	286.00	1.37	288.85
1.07	279.64	1.18	282.46	1.27	286.37	1.36	288.86
1.08	280.51	1.17	283.76	1.27	286.13	1.38	288.81
1.07	279.65	1.17	283.51	1.28	284.75	1.37	288.50
1.09	279.42	1.18	283.35	1.28	285.21	1.39	288.71
1.08	280.70	1.19	283.69	1.28	286.84	1.38	289.08
1.09	279.27	1.18	283.72	1.29	285.74	1.38	288.68
1.10	280.11	1.18	283.02	1.29	287.01	1.39	289.49
1.08	281.26	1.18	283.44	1.28	286.18	1.38	290.25
1.09	280.31	1.19	282.68	1.30	286.38	1.39	289.60
1.10	281.27	1.21	283.03	1.30	286.64	1.40	290.31

(Continued on next page)

Table A.1: (Continued)

True Strain (%)	True Stress (MPa)	True Strain (%)	True Stress (MPa)	True Strain (%)	True Stress (MPa)	True Strain (%)	True Stress (MPa)
1.39	289.50	1.51	291.60	1.59	293.88	1.70	295.84
1.40	289.26	1.50	291.38	1.62	292.98	1.70	295.80
1.41	289.82	1.51	290.97	1.61	294.45	1.71	296.99
1.41	289.89	1.51	291.86	1.60	293.86	1.71	296.22
1.40	290.49	1.50	291.49	1.63	294.50	1.72	296.08
1.41	290.03	1.51	291.10	1.62	294.35	1.71	296.28
1.42	290.85	1.52	291.60	1.61	294.15	1.73	296.78
1.41	290.84	1.51	292.79	1.63	293.98	1.73	296.40
1.42	289.69	1.52	291.87	1.63	295.18	1.73	296.91
1.43	290.71	1.53	292.97	1.62	294.92	1.73	296.20
1.42	291.26	1.52	293.58	1.63	293.53	1.74	296.38
1.42	290.21	1.52	292.55	1.64	294.61	1.73	297.56
1.44	290.33	1.53	292.16	1.64	295.72	1.74	296.88
1.44	291.12	1.55	291.89	1.64	294.69	1.74	296.74
1.45	290.93	1.54	293.33	1.65	294.68	1.74	296.28
1.43	290.56	1.53	293.51	1.64	294.47	1.76	297.04
1.44	289.87	1.55	293.14	1.65	293.79	1.74	297.46
1.45	291.61	1.55	293.27	1.65	295.37	1.75	296.37
1.44	291.24	1.55	291.94	1.65	294.94	1.76	296.44
1.45	290.62	1.56	292.76	1.66	294.83	1.76	298.01
1.46	291.08	1.56	294.03	1.67	295.08	1.75	297.66
1.45	291.90	1.56	293.27	1.65	295.94	1.77	298.02
1.47	291.79	1.56	293.71	1.67	295.40	1.76	297.29
1.46	291.47	1.57	293.34	1.67	296.79	1.78	296.38
1.46	291.07	1.56	293.80	1.67	295.64	1.77	297.93
1.48	291.07	1.57	293.12	1.68	295.04	1.77	297.63
1.47	290.58	1.58	294.37	1.67	295.43	1.79	297.63
1.48	291.01	1.57	293.87	1.68	295.77	1.77	297.81
1.47	291.26	1.59	293.12	1.69	296.15	1.78	296.58
1.48	289.87	1.58	294.05	1.67	296.20	1.80	297.23
1.49	291.10	1.58	293.83	1.69	294.78	1.79	298.51
1.48	291.34	1.60	293.94	1.70	295.51	1.79	297.78
1.49	291.08	1.59	294.13	1.70	296.31	1.80	298.06
1.50	291.93	1.59	293.52	1.69	296.61	1.79	297.38
1.49	291.73	1.61	294.23	1.70	295.28	1.80	296.84
1.49	291.72	1.60	294.75	1.71	295.88	1.81	297.70

(Continued on next page)

Table A.1: (Continued)

True Strain (%)	True Stress (MPa)	True Strain (%)	True Stress (MPa)	True Strain (%)	True Stress (MPa)	True Strain (%)	True Stress (MPa)
1.80	298.17	1.91	300.30	2.00	302.09	2.13	303.62
1.81	297.42	1.91	300.33	2.02	300.89	2.11	303.71
1.82	298.09	1.91	300.36	2.04	301.65	2.13	302.73
1.81	298.27	1.92	300.71	2.02	301.72	2.13	304.23
1.81	298.82	1.91	300.36	2.02	301.24	2.12	303.91
1.82	297.90	1.92	299.19	2.05	301.75	2.13	303.66
1.82	299.22	1.92	301.07	2.03	303.07	2.14	304.69
1.82	298.36	1.92	299.35	2.02	302.45	2.14	304.53
1.84	297.89	1.94	300.23	2.06	302.54	2.13	303.76
1.83	298.68	1.93	301.81	2.04	303.30	2.15	303.10
1.83	298.29	1.94	299.88	2.03	302.73	2.15	304.41
1.85	298.53	1.95	300.14	2.06	301.82	2.14	304.10
1.84	299.54	1.94	300.34	2.07	302.14	2.17	304.27
1.84	298.19	1.95	301.27	2.04	302.32	2.14	304.53
1.86	298.34	1.94	301.01	2.06	301.31	2.16	304.53
1.86	298.23	1.96	300.80	2.07	301.87	2.16	305.13
1.85	299.19	1.95	301.42	2.05	302.35	2.15	304.96
1.86	298.21	1.96	300.18	2.06	302.57	2.19	304.97
1.86	299.13	1.97	301.01	2.08	303.05	2.19	305.27
1.85	299.43	1.96	300.88	2.05	303.23	2.16	304.87
1.87	298.67	1.97	300.22	2.07	302.07	2.17	303.39
1.87	298.70	1.97	301.14	2.06	303.23	2.20	304.37
1.86	298.58	1.96	301.31	2.07	302.23	2.18	304.73
1.88	298.11	1.98	301.31	2.10	302.82	2.18	303.87
1.88	299.19	1.98	301.69	2.08	303.13	2.20	304.45
1.87	299.59	1.97	301.15	2.07	302.04	2.21	304.74
1.88	299.57	1.98	300.49	2.11	302.21	2.21	305.09
1.89	299.89	1.99	301.39	2.08	302.80	2.21	304.89
1.88	299.95	1.98	301.90	2.08	302.23	2.22	304.65
1.89	298.64	1.99	301.50	2.12	303.09	2.22	304.08
1.90	300.06	2.00	301.47	2.09	304.04	2.19	304.19
1.89	300.25	1.99	301.24	2.09	303.54	2.21	303.89
1.90	299.70	2.01	301.43	2.10	303.86	2.21	304.42
1.90	300.44	2.00	301.51	2.13	303.83	2.21	304.36
1.90	300.02	2.01	300.74	2.10	303.97	2.23	305.34
1.91	299.55	2.03	301.86	2.11	303.01	2.20	305.63

(Continued on next page)

Table A.1: (Continued)

True Strain (%)	True Stress (MPa)	True Strain (%)	True Stress (MPa)	True Strain (%)	True Stress (MPa)	True Strain (%)	True Stress (MPa)
2.22	304.78	2.32	306.52	2.43	307.83	2.51	310.33
2.24	305.13	2.34	307.74	2.43	309.25	2.54	309.91
2.21	305.79	2.32	308.12	2.42	309.03	2.54	311.14
2.23	305.24	2.33	307.08	2.45	309.04	2.52	311.01
2.25	305.57	2.36	307.08	2.42	309.33	2.56	311.12
2.23	306.51	2.32	307.96	2.45	309.56	2.54	311.30
2.22	304.87	2.33	307.05	2.43	309.35	2.55	309.80
2.26	305.27	2.37	307.53	2.46	308.66	2.57	310.26
2.25	306.53	2.35	308.56	2.43	309.13	2.55	310.01
2.23	306.37	2.34	307.76	2.45	309.05	2.57	310.64
2.26	306.00	2.37	307.88	2.47	310.27	2.54	311.26
2.26	306.42	2.35	309.22	2.44	310.22	2.57	310.42
2.24	306.30	2.35	307.95	2.47	309.32	2.58	311.62
2.25	305.84	2.37	307.23	2.46	310.50	2.55	311.82
2.28	305.89	2.36	308.27	2.45	309.50	2.57	311.10
2.25	305.88	2.35	307.91	2.48	309.67	2.57	311.77
2.27	306.60	2.37	307.33	2.46	310.39	2.56	311.58
2.25	306.42	2.38	308.33	2.49	309.42	2.59	310.86
2.29	306.30	2.36	307.89	2.48	310.80	2.58	311.85
2.26	307.29	2.38	307.43	2.48	309.71	2.58	311.62
2.26	306.80	2.38	308.64	2.50	310.25	2.59	310.79
2.30	306.53	2.37	307.67	2.47	310.42	2.59	311.95
2.27	307.49	2.39	307.19	2.49	311.25	2.58	311.70
2.27	306.18	2.39	308.20	2.52	310.41	2.59	310.67
2.30	306.18	2.38	307.62	2.49	311.16	2.61	312.02
2.29	307.42	2.41	308.36	2.51	310.15	2.59	311.81
2.28	306.84	2.39	309.18	2.50	310.45	2.59	310.81
2.29	307.26	2.40	308.26	2.50	309.25	2.62	311.40
2.31	307.48	2.41	308.68	2.52	310.10	2.61	312.11
2.30	307.36	2.39	308.59	2.49	309.90	2.60	311.18
2.29	306.89	2.42	307.85	2.52	309.97	2.63	310.96
2.33	306.46	2.41	309.40	2.50	310.94	2.63	311.71
2.31	307.06	2.41	308.45	2.53	310.33	2.60	311.70
2.30	306.53	2.43	309.51	2.53	310.60	2.62	310.68
2.32	307.18	2.40	308.92	2.52	310.35	2.63	312.28
2.30	307.40	2.41	309.35	2.54	310.14	2.62	312.32

(Continued on next page)

Table A.1: (Continued)

True Strain (%)	True Stress (MPa)	True Strain (%)	True Stress (MPa)	True Strain (%)	True Stress (MPa)	True Strain (%)	True Stress (MPa)
2.62	311.70	2.73	313.15	2.84	315.81	2.94	316.60
2.65	312.27	2.75	313.64	2.82	314.40	2.92	316.26
2.64	312.66	2.74	314.04	2.84	314.67	2.96	316.64
2.62	312.71	2.76	313.21	2.86	316.12	2.95	317.19
2.67	312.22	2.73	314.06	2.85	316.32	2.94	316.35
2.63	312.42	2.75	312.84	2.84	315.05	2.96	315.14
2.64	311.61	2.78	312.86	2.88	315.26	2.98	316.81
2.67	311.96	2.74	313.69	2.85	315.87	2.95	316.94
2.65	313.30	2.76	312.82	2.85	316.05	2.96	316.30
2.64	312.84	2.77	314.38	2.88	315.86	2.97	316.02
2.67	312.63	2.76	315.36	2.85	316.04	2.98	316.96
2.66	313.62	2.76	314.23	2.88	315.43	2.97	316.48
2.65	313.21	2.78	313.50	2.87	316.84	2.96	315.55
2.67	312.19	2.77	314.55	2.86	316.68	2.98	314.66
2.69	312.34	2.78	314.36	2.88	315.85	2.98	314.57
2.67	313.85	2.76	314.24	2.88	316.24	2.96	313.70
2.67	312.34	2.78	313.97	2.88	316.03	2.98	311.57
2.67	313.58	2.79	314.21	2.88	315.65	2.99	311.00
2.68	312.82	2.77	314.58	2.91	316.27	2.95	310.08
2.70	312.65	2.77	313.22	2.89	316.70	2.98	307.51
2.69	312.98	2.81	313.99	2.88	315.86	2.97	305.88
2.68	312.58	2.78	314.49	2.91	315.43	2.99	304.91
2.71	312.81	2.79	314.11	2.91	315.53	2.96	303.76
2.70	313.62	2.82	314.40	2.90	316.13	2.99	301.77
2.69	313.83	2.80	315.07	2.90	316.38	2.97	300.64
2.72	313.19	2.79	313.81	2.92	315.47	2.95	298.12
2.72	312.76	2.82	314.06	2.91	316.51	2.97	295.99
2.70	313.09	2.81	315.34	2.90	316.90	2.97	295.54
2.70	313.25	2.80	315.16	2.92	316.41	2.95	294.12
2.71	312.25	2.82	314.40	2.92	316.41	2.97	292.39
2.74	314.03	2.82	315.36	2.91	316.46	2.97	292.21
2.72	314.70	2.80	315.03	2.92	315.78	2.98	290.37
2.71	313.66	2.84	314.70	2.94	316.54	2.95	289.37
2.73	313.19	2.81	314.97	2.92	316.64	2.95	286.42
2.75	313.43	2.82	315.06	2.92	315.74	2.98	285.50
2.72	313.42	2.86	315.02	2.96	315.41	2.94	284.40

(Continued on next page)

Table A.1: (Continued)

True Strain (%)	True Stress (MPa)	True Strain (%)	True Stress (MPa)	True Strain (%)	True Stress (MPa)	True Strain (%)	True Stress (MPa)
2.96	281.20	2.90	236.21	2.87	193.97	2.82	156.85
2.97	281.55	2.92	234.73	2.87	192.86	2.82	155.82
2.94	279.95	2.91	234.27	2.86	189.97	2.85	155.34
2.96	278.66	2.90	232.01	2.88	190.08	2.83	154.42
2.95	278.55	2.92	230.57	2.85	188.82	2.80	153.50
2.93	276.60	2.89	230.08	2.87	187.90	2.83	152.48
2.96	275.51	2.90	227.89	2.87	188.22	2.84	152.08
2.93	273.54	2.92	226.89	2.85	185.73	2.82	151.67
2.95	271.78	2.89	226.23	2.87	184.70	2.81	150.20
2.95	271.15	2.89	223.69	2.86	184.32	2.81	149.07
2.93	269.12	2.91	223.24	2.83	183.09	2.82	147.56
2.95	266.64	2.88	222.62	2.87	181.69	2.84	147.25
2.95	266.52	2.90	219.91	2.86	180.46	2.81	146.01
2.93	265.85	2.90	220.04	2.88	180.36	2.81	146.00
2.96	264.10	2.88	218.57	2.84	179.35	2.84	144.51
2.92	262.60	2.88	217.06	2.85	176.70	2.82	144.84
2.93	261.52	2.91	215.90	2.87	175.76	2.81	144.03
2.91	260.63	2.89	216.08	2.85	175.69	2.83	142.50
2.94	258.95	2.88	213.73	2.84	173.82	2.83	141.49
2.94	258.41	2.90	213.15	2.86	172.39	2.82	141.52
2.92	256.91	2.89	212.61	2.85	171.81	2.81	140.18
2.93	255.51	2.87	210.37	2.83	171.13	2.81	139.67
2.94	254.47	2.90	209.49	2.85	169.74	2.80	138.45
2.93	253.18	2.87	209.00	2.84	169.78	2.81	136.44
2.91	251.28	2.88	206.72	2.84	168.09	2.83	136.27
2.93	249.71	2.89	205.66	2.84	166.92	2.83	136.79
2.93	249.01	2.87	204.85	2.86	165.91	2.81	135.89
2.91	248.04	2.87	203.20	2.83	165.79	2.80	134.45
2.93	246.07	2.90	202.51	2.83	164.16	2.81	133.29
2.92	245.74	2.86	202.05	2.84	162.52	2.82	133.07
2.90	243.78	2.86	200.63	2.85	162.44	2.82	132.01
2.93	242.23	2.88	199.45	2.82	161.48	2.79	131.23
2.91	242.15	2.87	199.14	2.82	159.66	2.80	130.29
2.91	239.26	2.86	196.94	2.84	158.64	2.79	129.34
2.93	238.16	2.87	195.10	2.85	158.09	2.80	128.26
2.91	237.95	2.89	194.85	2.84	157.91	2.81	127.44

(Continued on next page)

Table A.1: (Continued)

True Strain (%)	True Stress (MPa)	True Strain (%)	True Stress (MPa)	True Strain (%)	True Stress (MPa)	True Strain (%)	True Stress (MPa)
2.82	127.14	2.76	99.93	2.74	76.61	2.73	57.01
2.81	126.48	2.80	99.68	2.76	75.85	2.71	56.58
2.79	125.45	2.78	98.64	2.75	75.13	2.75	56.73
2.79	124.53	2.77	97.56	2.77	75.15	2.70	55.41
2.80	123.89	2.78	96.74	2.76	75.33	2.75	55.09
2.81	122.45	2.76	96.67	2.74	75.10	2.71	53.78
2.81	122.00	2.76	95.62	2.73	74.23	2.74	54.66
2.80	121.42	2.75	95.28	2.73	72.61	2.70	53.40
2.78	119.90	2.77	93.40	2.75	72.02	2.74	53.23
2.78	118.80	2.78	93.29	2.77	72.31	2.71	51.64
2.79	117.89	2.78	92.51	2.76	71.90	2.74	52.44
2.79	117.66	2.77	91.53	2.74	71.40	2.72	51.80
2.81	117.47	2.75	92.16	2.71	70.37	2.70	51.24
2.80	117.51	2.74	91.68	2.73	69.33	2.74	50.13
2.79	117.34	2.75	90.41	2.74	68.84	2.69	49.55
2.76	115.76	2.76	89.41	2.76	68.87	2.74	50.12
2.77	114.41	2.78	88.91	2.76	67.79	2.70	48.95
2.78	112.52	2.77	88.43	2.74	67.69	2.74	48.82
2.79	111.93	2.76	88.46	2.72	66.98	2.71	47.15
2.81	111.61	2.73	87.74	2.72	66.70	2.72	47.67
2.79	111.79	2.75	86.67	2.72	66.21	2.71	47.11
2.78	111.33	2.78	85.75	2.76	65.21	2.71	46.61
2.77	110.48	2.76	85.69	2.72	64.52	2.70	45.55
2.77	108.61	2.76	85.01	2.75	63.82	2.74	45.37
2.81	108.19	2.75	83.99	2.75	63.45	2.72	44.69
2.80	107.42	2.76	82.90	2.73	62.60	2.69	44.73
2.79	107.16	2.75	82.67	2.72	62.47	2.73	44.32
2.77	106.30	2.77	82.35	2.75	61.75	2.70	43.26
2.77	105.02	2.76	82.29	2.72	61.47	2.72	43.32
2.75	105.21	2.74	81.89	2.74	60.97	2.71	42.17
2.78	103.90	2.74	80.04	2.72	60.54	2.71	42.47
2.79	103.73	2.75	78.68	2.75	59.83	2.72	41.75
2.80	102.64	2.77	78.74	2.71	58.53	2.69	41.07
2.78	101.98	2.77	79.38	2.75	59.54	2.72	40.32
2.77	101.36	2.74	79.17	2.72	58.39	2.70	39.82
2.76	100.76	2.74	77.90	2.71	57.59	2.71	40.51

(Continued on next page)

Table A.1: (Continued)

True Strain (%)	True Stress (MPa)	True Strain (%)	True Stress (MPa)	True Strain (%)	True Stress (MPa)	True Strain (%)	True Stress (MPa)
2.69	39.52	2.70	23.74	2.66	10.22	2.67	-1.67
2.70	40.78	2.68	23.92	2.65	10.08	2.67	-1.52
2.72	39.34	2.70	23.37	2.69	9.44	2.67	-1.47
2.70	37.45	2.67	21.89	2.67	9.00		
2.69	37.93	2.70	22.17	2.67	8.30		
2.71	36.97	2.66	21.88	2.66	7.91		
2.69	36.99	2.70	22.14	2.68	7.96		
2.72	37.01	2.67	21.34	2.66	7.24		
2.69	35.59	2.71	21.37	2.66	7.64		
2.69	35.14	2.67	20.67	2.66	6.60		
2.70	35.26	2.69	19.52	2.68	6.61		
2.72	34.66	2.68	19.46	2.68	6.64		
2.68	33.99	2.69	18.43	2.66	6.23		
2.71	33.99	2.68	19.23	2.66	6.06		
2.71	34.17	2.69	17.90	2.66	5.27		
2.68	33.23	2.68	18.87	2.66	5.60		
2.70	31.96	2.70	17.92	2.66	4.64		
2.71	32.06	2.66	17.18	2.66	4.42		
2.68	31.26	2.69	16.65	2.66	4.12		
2.69	31.08	2.66	15.06	2.66	3.81		
2.69	31.00	2.70	15.92	2.66	3.91		
2.71	31.36	2.66	14.62	2.67	3.18		
2.69	30.81	2.69	15.57	2.67	2.93		
2.68	29.77	2.67	14.30	2.68	2.45		
2.71	28.58	2.68	15.09	2.67	1.73		
2.68	29.01	2.67	14.01	2.66	2.27		
2.71	28.77	2.65	13.83	2.66	1.64		
2.67	28.49	2.69	13.28	2.66	1.37		
2.71	27.95	2.67	12.30	2.67	1.37		
2.68	27.08	2.69	12.39	2.66	0.72		
2.71	26.87	2.69	12.09	2.67	0.96		
2.69	26.63	2.66	10.82	2.68	0.84		
2.69	25.77	2.67	11.81	2.67	0.53		
2.70	24.40	2.67	11.42	2.67	0.43		
2.69	25.30	2.67	10.56	2.67	-0.56		
2.69	24.35	2.66	11.30	2.67	-0.73		
2.69	24.38	2.69	10.94	2.66	-1.00		

B. Typical Creep Test Data

Table B.1: Creep Test Data for Ti-0.4(wt%)Mn Alloy Tested at 298 K and 95% of Its 0.2% Yield Stress

Time (h)	Creep Strain (%)	Time (h)	Creep Strain (%)	Time (h)	Creep Strain (%)	Time (h)	Creep Strain (%)
0.0000	-0.048	0.0089	0.137	0.0178	0.154	0.0267	0.166
0.0003	0.008	0.0092	0.138	0.0181	0.155	0.0269	0.166
0.0006	0.065	0.0094	0.138	0.0183	0.155	0.0272	0.167
0.0008	0.086	0.0097	0.139	0.0186	0.155	0.0275	0.167
0.0011	0.094	0.0100	0.140	0.0189	0.156	0.0278	0.167
0.0014	0.099	0.0103	0.140	0.0192	0.156	0.0281	0.167
0.0017	0.103	0.0106	0.141	0.0194	0.157	0.0283	0.168
0.0019	0.106	0.0108	0.142	0.0197	0.157	0.0286	0.168
0.0022	0.108	0.0111	0.142	0.0200	0.157	0.0289	0.168
0.0025	0.111	0.0114	0.143	0.0203	0.158	0.0292	0.168
0.0028	0.113	0.0117	0.144	0.0206	0.158	0.0294	0.169
0.0031	0.115	0.0119	0.144	0.0208	0.159	0.0297	0.169
0.0033	0.117	0.0122	0.145	0.0211	0.159	0.0300	0.169
0.0036	0.118	0.0125	0.145	0.0214	0.159	0.0303	0.170
0.0039	0.120	0.0128	0.147	0.0217	0.160	0.0306	0.170
0.0042	0.121	0.0131	0.146	0.0219	0.160	0.0308	0.170
0.0044	0.122	0.0133	0.147	0.0222	0.161	0.0311	0.171
0.0047	0.124	0.0136	0.148	0.0225	0.161	0.0314	0.171
0.0050	0.125	0.0139	0.148	0.0228	0.161	0.0317	0.171
0.0053	0.126	0.0142	0.149	0.0231	0.162	0.0319	0.171
0.0056	0.127	0.0144	0.149	0.0233	0.162	0.0322	0.172
0.0058	0.128	0.0147	0.150	0.0236	0.163	0.0325	0.172
0.0061	0.129	0.0150	0.150	0.0239	0.163	0.0328	0.172
0.0064	0.130	0.0153	0.150	0.0242	0.163	0.0331	0.172
0.0067	0.131	0.0156	0.151	0.0244	0.163	0.0333	0.173
0.0069	0.132	0.0158	0.152	0.0247	0.164	0.0336	0.173
0.0072	0.132	0.0161	0.152	0.0250	0.164	0.0339	0.173
0.0075	0.133	0.0164	0.152	0.0253	0.165	0.0342	0.174
0.0078	0.134	0.0167	0.153	0.0256	0.165	0.0344	0.174
0.0081	0.135	0.0169	0.153	0.0258	0.165	0.0347	0.174
0.0083	0.135	0.0172	0.154	0.0261	0.166	0.0350	0.174
0.0086	0.136	0.0175	0.154	0.0264	0.166	0.0353	0.175

(Continued on next page)

Table B.1: (Continued)

Time (h)	Creep Strain (%)	Time (h)	Creep Strain (%)	Time (h)	Creep Strain (%)	Time (h)	Creep Strain (%)
0.0356	0.175	0.0461	0.183	0.0914	0.208	0.1414	0.226
0.0358	0.175	0.0464	0.183	0.0928	0.209	0.1428	0.226
0.0361	0.175	0.0467	0.183	0.0942	0.209	0.1442	0.226
0.0364	0.176	0.0469	0.184	0.0956	0.209	0.1456	0.227
0.0367	0.176	0.0481	0.184	0.0969	0.210	0.1469	0.227
0.0369	0.176	0.0483	0.185	0.0983	0.211	0.1483	0.228
0.0372	0.176	0.0497	0.186	0.0997	0.211	0.1497	0.228
0.0375	0.176	0.0511	0.187	0.1011	0.212	0.1511	0.229
0.0378	0.176	0.0525	0.188	0.1025	0.212	0.1525	0.229
0.0381	0.177	0.0539	0.188	0.1039	0.213	0.1539	0.229
0.0383	0.176	0.0553	0.190	0.1053	0.213	0.1553	0.230
0.0386	0.177	0.0567	0.190	0.1067	0.214	0.1567	0.230
0.0389	0.177	0.0581	0.191	0.1081	0.214	0.1581	0.231
0.0392	0.177	0.0594	0.192	0.1094	0.215	0.1594	0.231
0.0394	0.178	0.0608	0.193	0.1108	0.216	0.1608	0.231
0.0397	0.178	0.0622	0.194	0.1122	0.216	0.1622	0.232
0.0400	0.178	0.0636	0.195	0.1136	0.217	0.1636	0.232
0.0403	0.178	0.0650	0.195	0.1150	0.217	0.1650	0.233
0.0406	0.178	0.0664	0.196	0.1164	0.218	0.1664	0.233
0.0408	0.179	0.0678	0.196	0.1178	0.218	0.1678	0.233
0.0411	0.179	0.0692	0.197	0.1192	0.219	0.1692	0.234
0.0414	0.179	0.0706	0.198	0.1206	0.219	0.1706	0.234
0.0417	0.180	0.0719	0.199	0.1219	0.219	0.1719	0.234
0.0419	0.180	0.0733	0.200	0.1233	0.220	0.1731	0.235
0.0422	0.180	0.0747	0.200	0.1247	0.220	0.1750	0.236
0.0425	0.181	0.0761	0.201	0.1261	0.220	0.1778	0.236
0.0428	0.181	0.0775	0.201	0.1275	0.221	0.1808	0.237
0.0433	0.181	0.0789	0.202	0.1289	0.222	0.1833	0.237
0.0436	0.182	0.0803	0.203	0.1303	0.223	0.1861	0.238
0.0439	0.181	0.0817	0.204	0.1317	0.223	0.1892	0.239
0.0444	0.182	0.0831	0.204	0.1331	0.223	0.1919	0.240
0.0447	0.182	0.0844	0.205	0.1344	0.224	0.1947	0.241
0.0453	0.182	0.0858	0.205	0.1358	0.224	0.1972	0.241
0.0453	0.182	0.0872	0.206	0.1372	0.224	0.2003	0.242
0.0456	0.182	0.0886	0.207	0.1386	0.225	0.2031	0.242
0.0458	0.183	0.0900	0.207	0.1400	0.225	0.2056	0.243

(Continued on next page)

Table B.1: (Continued)

Time (h)	Creep Strain (%)	Time (h)	Creep Strain (%)	Time (h)	Creep Strain (%)	Time (h)	Creep Strain (%)
0.2083	0.243	0.3086	0.263	0.4083	0.279	0.5283	0.293
0.2111	0.244	0.3111	0.264	0.4111	0.279	0.5339	0.294
0.2142	0.245	0.3139	0.264	0.4139	0.279	0.5394	0.294
0.2167	0.245	0.3169	0.265	0.4167	0.280	0.5450	0.295
0.2194	0.246	0.3194	0.265	0.4197	0.280	0.5506	0.296
0.2222	0.246	0.3225	0.266	0.4222	0.280	0.5561	0.296
0.2250	0.247	0.3250	0.266	0.4253	0.281	0.5617	0.297
0.2281	0.248	0.3281	0.266	0.4278	0.281	0.5672	0.297
0.2306	0.248	0.3306	0.267	0.4308	0.281	0.5728	0.298
0.2336	0.249	0.3336	0.268	0.4336	0.282	0.5783	0.299
0.2364	0.249	0.3364	0.268	0.4364	0.282	0.5839	0.299
0.2389	0.250	0.3389	0.268	0.4389	0.282	0.5894	0.300
0.2417	0.251	0.3417	0.269	0.4419	0.283	0.5950	0.300
0.2447	0.251	0.3447	0.270	0.4444	0.283	0.6006	0.301
0.2472	0.252	0.3472	0.270	0.4472	0.284	0.6061	0.301
0.2503	0.252	0.3503	0.270	0.4503	0.284	0.6117	0.302
0.2531	0.253	0.3528	0.270	0.4528	0.284	0.6172	0.303
0.2558	0.253	0.3556	0.271	0.4558	0.285	0.6228	0.303
0.2583	0.254	0.3586	0.271	0.4586	0.285	0.6283	0.304
0.2614	0.255	0.3611	0.272	0.4611	0.285	0.6339	0.304
0.2642	0.255	0.3639	0.272	0.4639	0.286	0.6394	0.305
0.2667	0.256	0.3667	0.273	0.4667	0.286	0.6450	0.306
0.2694	0.257	0.3697	0.273	0.4694	0.286	0.6506	0.306
0.2722	0.257	0.3725	0.274	0.4722	0.286	0.6561	0.307
0.2753	0.257	0.3750	0.274	0.4753	0.287	0.6594	0.307
0.2781	0.258	0.3778	0.275	0.4778	0.287	0.6753	0.308
0.2808	0.259	0.3806	0.275	0.4806	0.287	0.6919	0.310
0.2836	0.259	0.3833	0.275	0.4836	0.288	0.7086	0.312
0.2864	0.259	0.3861	0.276	0.4847	0.288	0.7253	0.313
0.2892	0.260	0.3892	0.276	0.4894	0.289	0.7419	0.314
0.2917	0.260	0.3919	0.276	0.4950	0.289	0.7586	0.316
0.2947	0.261	0.3944	0.277	0.5006	0.290	0.7753	0.317
0.2972	0.261	0.3972	0.277	0.5061	0.291	0.7919	0.319
0.3000	0.262	0.4003	0.277	0.5117	0.292	0.8086	0.321
0.3028	0.263	0.4028	0.277	0.5172	0.292	0.8253	0.321
0.3058	0.263	0.4058	0.278	0.5228	0.292	0.8419	0.323

(Continued on next page)

Table B.1: (Continued)

Time (h)	Creep Strain (%)	Time (h)	Creep Strain (%)	Time (h)	Creep Strain (%)	Time (h)	Creep Strain (%)
0.8586	0.324	1.4586	0.361	4.1175	0.445	7.1175	0.498
0.8753	0.326	1.4753	0.361	4.2008	0.448	7.2008	0.498
0.8919	0.327	1.4919	0.362	4.2842	0.449	7.2842	0.500
0.9086	0.328	1.5086	0.363	4.3675	0.451	7.3675	0.501
0.9253	0.329	1.5253	0.364	4.4508	0.453	7.4508	0.502
0.9419	0.330	1.5350	0.364	4.5342	0.454	7.5342	0.503
0.9586	0.332	1.6175	0.368	4.6175	0.457	7.6175	0.504
0.9753	0.333	1.7008	0.372	4.7008	0.458	7.7008	0.505
0.9919	0.334	1.7842	0.375	4.7842	0.459	7.7842	0.506
1.0086	0.335	1.8675	0.379	4.8675	0.461	7.8675	0.507
1.0253	0.336	1.9508	0.382	4.9508	0.463	7.9508	0.508
1.0419	0.337	2.0342	0.385	5.0342	0.465	8.0342	0.509
1.0586	0.338	2.1175	0.388	5.1175	0.466	8.1175	0.510
1.0753	0.339	2.2008	0.392	5.2008	0.467	8.2008	0.512
1.0919	0.340	2.2842	0.394	5.2842	0.469	8.2842	0.512
1.1086	0.341	2.3675	0.397	5.3675	0.470	8.3675	0.514
1.1253	0.342	2.4508	0.400	5.4508	0.471	8.4508	0.514
1.1419	0.343	2.5342	0.403	5.5342	0.473	8.5342	0.516
1.1586	0.344	2.6175	0.405	5.6175	0.475	8.6175	0.516
1.1753	0.345	2.7008	0.407	5.7008	0.476	8.7008	0.517
1.1919	0.346	2.7842	0.411	5.7842	0.477	8.7842	0.519
1.2086	0.347	2.8675	0.413	5.8675	0.479	8.8675	0.520
1.2253	0.348	2.9508	0.416	5.9508	0.480	8.9508	0.520
1.2419	0.349	3.0342	0.418	6.0342	0.482	9.0342	0.521
1.2586	0.350	3.1175	0.420	6.1175	0.482	9.1175	0.522
1.2753	0.351	3.2008	0.423	6.2008	0.484	9.2008	0.523
1.2919	0.352	3.2842	0.425	6.2842	0.485	9.2842	0.524
1.3086	0.353	3.3675	0.427	6.3675	0.486	9.3675	0.524
1.3253	0.353	3.4508	0.430	6.4508	0.488	9.4508	0.525
1.3419	0.354	3.5342	0.432	6.5342	0.489	9.5342	0.527
1.3586	0.355	3.6175	0.433	6.6175	0.491	9.6175	0.527
1.3753	0.357	3.7008	0.436	6.7008	0.491	9.7008	0.529
1.3919	0.357	3.7842	0.438	6.7842	0.493	9.7842	0.529
1.4086	0.358	3.8675	0.440	6.8675	0.494	9.8675	0.530
1.4253	0.359	3.9508	0.442	6.9508	0.494	9.9508	0.531
1.4419	0.359	4.0342	0.444	7.0342	0.496	10.034	0.531

(Continued on next page)

Table B.1: (Continued)

Time (h)	Creep Strain (%)	Time (h)	Creep Strain (%)	Time (h)	Creep Strain (%)	Time (h)	Creep Strain (%)
10.118	0.532	13.118	0.559	16.118	0.581	19.118	0.599
10.201	0.533	13.201	0.560	16.201	0.581	19.201	0.599
10.284	0.534	13.284	0.560	16.284	0.582	19.284	0.599
10.368	0.535	13.368	0.561	16.368	0.582	19.368	0.600
10.451	0.535	13.451	0.562	16.451	0.583	19.451	0.601
10.534	0.537	13.534	0.563	16.534	0.583	19.534	0.601
10.618	0.537	13.618	0.563	16.618	0.584	19.618	0.602
10.701	0.538	13.701	0.564	16.701	0.584	19.701	0.602
10.784	0.539	13.784	0.564	16.784	0.584	19.784	0.603
10.868	0.540	13.868	0.565	16.868	0.585	19.868	0.603
10.951	0.540	13.951	0.566	16.951	0.586	19.951	0.603
11.034	0.541	14.034	0.565	17.034	0.587	20.034	0.605
11.118	0.542	14.118	0.566	17.118	0.587	20.118	0.605
11.201	0.543	14.201	0.567	17.201	0.587	20.201	0.605
11.284	0.544	14.284	0.568	17.284	0.587	20.284	0.606
11.368	0.544	14.368	0.568	17.368	0.589	20.368	0.607
11.451	0.545	14.451	0.569	17.451	0.589	20.451	0.607
11.534	0.546	14.534	0.569	17.534	0.589	20.534	0.607
11.618	0.546	14.618	0.570	17.618	0.590	20.618	0.608
11.701	0.547	14.701	0.570	17.701	0.591	20.701	0.608
11.784	0.548	14.784	0.572	17.784	0.591	20.784	0.609
11.868	0.549	14.868	0.572	17.868	0.591	20.868	0.609
11.951	0.549	14.951	0.573	17.951	0.592	20.869	0.609
12.034	0.550	15.034	0.573	18.034	0.592	21.202	0.610
12.118	0.551	15.118	0.573	18.118	0.593	21.535	0.612
12.201	0.552	15.201	0.574	18.201	0.593	21.869	0.613
12.284	0.552	15.284	0.575	18.284	0.594	22.202	0.615
12.368	0.553	15.368	0.575	18.368	0.594	22.535	0.617
12.451	0.554	15.451	0.576	18.451	0.595	22.869	0.618
12.534	0.554	15.534	0.576	18.534	0.595	23.202	0.620
12.618	0.555	15.618	0.577	18.618	0.596	23.535	0.621
12.701	0.555	15.701	0.578	18.701	0.597	23.869	0.623
12.784	0.556	15.784	0.578	18.784	0.596	24.202	0.625
12.868	0.557	15.868	0.579	18.868	0.597	24.535	0.626
12.951	0.558	15.951	0.579	18.951	0.597	24.869	0.628
13.034	0.558	16.034	0.580	19.034	0.598	25.202	0.629

(Continued on next page)

Table B.1: (Continued)

Time (h)	Creep Strain (%)	Time (h)	Creep Strain (%)	Time (h)	Creep Strain (%)	Time (h)	Creep Strain (%)
25.535	0.631	37.535	0.674	62.623	0.745	98.623	0.801
25.869	0.632	37.869	0.675	63.623	0.747	99.623	0.802
26.202	0.634	38.202	0.676	64.623	0.749	100.62	0.803
26.535	0.636	38.535	0.677	65.623	0.751	101.62	0.805
26.869	0.636	38.869	0.678	66.623	0.753	102.62	0.806
27.202	0.638	39.202	0.679	67.623	0.755	103.62	0.807
27.535	0.639	39.535	0.680	68.623	0.757	104.62	0.808
27.869	0.640	39.869	0.681	69.623	0.758	105.62	0.810
28.202	0.641	40.202	0.682	70.623	0.760	106.62	0.811
28.535	0.642	40.535	0.683	71.623	0.762	107.62	0.813
28.869	0.644	40.869	0.683	72.623	0.763	108.62	0.814
29.202	0.645	41.202	0.684	73.623	0.765	109.62	0.815
29.535	0.646	41.535	0.686	74.623	0.767	110.62	0.817
29.869	0.648	41.869	0.686	75.623	0.768	111.62	0.818
30.202	0.649	42.202	0.687	76.623	0.770	112.62	0.820
30.535	0.650	42.535	0.688	77.623	0.771	113.62	0.821
30.869	0.651	42.624	0.689	78.623	0.773	114.62	0.823
31.202	0.652	43.623	0.692	79.623	0.775	115.62	0.823
31.535	0.654	44.623	0.695	80.623	0.777	116.62	0.825
31.869	0.655	45.623	0.698	81.623	0.779	117.62	0.827
32.202	0.657	46.623	0.701	82.623	0.781	118.62	0.828
32.535	0.657	47.623	0.703	83.623	0.782	119.62	0.829
32.869	0.659	48.623	0.705	84.623	0.783	120.62	0.830
33.202	0.660	49.623	0.707	85.623	0.785	121.62	0.833
33.535	0.661	50.623	0.707	86.623	0.786	122.62	0.834
33.869	0.662	51.623	0.710	87.623	0.787	123.62	0.836
34.202	0.663	52.623	0.714	88.623	0.788	124.62	0.838
34.535	0.664	53.623	0.717	89.623	0.790	125.62	0.840
34.869	0.666	54.623	0.722	90.623	0.792	126.62	0.841
35.202	0.667	55.623	0.726	91.623	0.793	127.62	0.842
35.535	0.667	56.623	0.729	92.623	0.794	127.69	0.842
35.869	0.669	57.623	0.732	93.623	0.795	128.69	0.842
36.202	0.670	58.623	0.734	94.623	0.796	129.69	0.844
36.535	0.671	59.623	0.737	95.623	0.797	130.69	0.845
36.869	0.672	60.623	0.740	96.623	0.799	131.69	0.845
37.202	0.673	61.623	0.743	97.623	0.800	132.69	0.847

(Continued on next page)

Table B.1: (Continued)

Time (h)	Creep Strain (%)	Time (h)	Creep Strain (%)	Time (h)	Creep Strain (%)	Time (h)	Creep Strain (%)
133.69	0.847	170.69	0.888	214.88	0.921	289.02	0.961
134.69	0.848	171.69	0.888	216.88	0.922	291.02	0.962
135.69	0.850	172.69	0.888	218.88	0.920	293.02	0.963
136.69	0.851	173.69	0.889	220.88	0.923	295.02	0.964
137.69	0.851	174.69	0.889	222.88	0.924	297.02	0.965
138.69	0.852	175.69	0.890	224.88	0.925	299.02	0.965
139.69	0.853	176.69	0.891	226.88	0.927	301.02	0.966
140.69	0.854	177.69	0.891	228.88	0.928		
141.69	0.855	178.69	0.892	230.88	0.930		
142.69	0.856	179.69	0.893	232.88	0.931		
143.69	0.858	180.69	0.893	234.88	0.932		
144.69	0.859	181.69	0.893	236.88	0.930		
145.69	0.859	182.69	0.893	238.88	0.926		
146.69	0.861	183.69	0.894	240.88	0.926		
147.69	0.862	184.69	0.895	242.77	0.927		
148.69	0.862	185.69	0.896	245.02	0.931		
149.69	0.863	186.69	0.896	247.02	0.932		
150.69	0.864	187.69	0.898	249.02	0.932		
151.69	0.865	188.69	0.899	251.02	0.932		
152.69	0.866	189.69	0.901	253.02	0.933		
153.69	0.867	190.69	0.902	255.02	0.934		
154.69	0.869	191.69	0.903	257.02	0.936		
155.69	0.870	192.69	0.904	259.02	0.937		
156.69	0.872	193.69	0.905	261.02	0.939		
157.69	0.873	194.69	0.905	263.02	0.941		
158.69	0.874	195.69	0.907	265.02	0.943		
159.69	0.876	196.69	0.908	267.02	0.943		
160.69	0.877	197.69	0.908	269.02	0.943		
161.69	0.878	198.69	0.909	271.02	0.944		
162.69	0.879	199.69	0.910	273.02	0.945		
163.69	0.882	200.43	0.910	275.02	0.946		
164.69	0.882	202.88	0.910	277.02	0.948		
165.69	0.883	204.88	0.911	279.02	0.949		
166.69	0.884	206.88	0.913	281.02	0.952		
167.69	0.885	208.88	0.914	283.02	0.954		
168.69	0.887	210.88	0.915	285.02	0.957		
169.69	0.888	212.88	0.919	287.02	0.960		

8. TABLES

This section contains Tables 1 through 6 on pages 78 through 82 beginning with Table 1 on the following page.

Table 1: Chemical Compositions of Titanium Alloys Used In This Investigation

System	Alloy Number	Microstructure (200 hrs. @ 690°C, W.Q.)	Major Alloying Elements, Wt. %	Other Elements, Wt %			
Ti-Mn	1	~100% α	0.4 Mn	Fe	O	N	C
	2	~46% α - 54% β	6.0 Mn	0.02	0.071	0.01	0.02
	3	~100% β	13.0 Mn	0.01	0.083	0.008	0.01
Ti-V	--	~100% α [98]	1.5 V	0.01	0.116	0.012	0.02
	4	~51% α - 49% β	8.1 V	--	--	--	--
	5	~100% β	14.8 V	0.01	0.082	0.16	0.02
				0.01	0.092	0.021	0.02

Table 2: Electropolish and Etching Solutions

Electropolish Solution	
560 (mL)	Methanol (CH_3OH)
30	Sulfuric Acid Conc (H_2SO_4)
15	Hydrofluoric Acid (HF 50%)
Etching Solutions [49]	
<u>A-Etch</u>	
25 (mL)	Hydrofluoric Acid (HF 50%)
25	Nitric Acid Conc (HNO_3)
50	Glycerine
<u>R-Etch</u>	
18.5 gm (17 mL)	Benzalkonium Chloride
35 (mL)	Ethanol ($\text{CH}_3\text{CH}_2\text{OH}$)
40	Glycerine
25	Hydrofluoric Acid (HF 50%)

Table 3: Example of Point Table for 20 μm Line Spacing

20 μm Spacing					
Point No.	y-coordinate (mm)	Point No.	y-coord. (mm)	Point No.	y-coord. (mm)
1	35.000 (center)	36	35.320	71	34.620
2	36.000	37	35.300	72	34.600
3	35.980	38	35.280	73	34.580
4	35.960	39	35.260	74	34.560
5	35.940	40	35.240	75	34.540
6	35.920	41	35.220	76	34.520
7	35.900	42	35.200	77	34.500
8	35.880	43	35.180	78	34.480
9	35.860	44	35.160	79	34.460
10	35.840	45	35.140	80	34.440
11	35.820	46	35.120	81	34.420
12	35.800	47	35.100	82	34.400
13	35.780	48	35.080	83	34.380
14	35.760	49	35.060	84	34.360
15	35.740	50	35.040	85	34.340
16	35.720	51	35.020	86	34.320
17	35.700	52	35.000	87	34.300
18	35.680	53	34.980	88	34.280
19	35.660	54	34.960	89	34.260
20	35.640	55	34.940	90	34.240
21	35.620	56	34.920	91	34.220
22	35.600	57	34.900	92	34.200
23	35.580	58	34.880	93	34.180
24	35.560	59	34.860	94	34.160
25	35.540	60	34.840	95	34.140
26	35.520	61	34.820	96	34.120
27	35.500	62	34.800	97	34.100
28	35.480	63	34.780	98	34.080
29	35.460	64	34.760	99	34.060
30	35.440	65	34.740		
31	35.420	66	34.720		
32	35.400	67	34.700		
33	35.380	68	34.680		
34	35.360	69	34.660		
35	35.340	70	34.640		

Table 4: Dilute Titanium Etchant

194 (mL)	Water (H_2O)
4	Nitric Acid Conc (HNO_3)
2	Hydrofluoric Acid (HF 50%)

Table 5: Twinning Rotation Angle and Rotation Axis [56]

Twin Plane, K_1	Rotation Axis	Angle of Rotation
$\{10\bar{1}2\}$	$\langle\bar{1}2\bar{1}0\rangle$	$94^\circ 52'$
$\{\bar{1}\bar{1}22\}$	$\langle\bar{1}100\rangle$	$63^\circ 58'$
$\{\bar{1}\bar{1}21\}$	$\langle\bar{1}100\rangle$	$34^\circ 54'$

Table 6: Creep Curve Parameter n , Time Exponent, and Material Constant A

Material	Stress, % YS	n	A
Ti-0.4Mn Alloy (500 μm grain size)	95	0.290	8.60×10^{-3}
Ti-0.4Mn Alloy (45 μm grain size)	95	0.184	3.39×10^{-3}
Ti-8.1V Alloy	100	0.144	3.48×10^{-3}
Ti-6.0Mn Alloy	100	0.136	3.12×10^{-3}
Ti-8.1V Alloy	95	0.165	2.28×10^{-3}
Ti-6.0Mn Alloy	95	0.146	2.35×10^{-3}
Ti-13.0Mn Alloy	95	0.032	5.52×10^{-4}

9. FIGURES

This section contains Figures 1 through 63 on pages 84 through 188 beginning with Figure 1 on the following page.

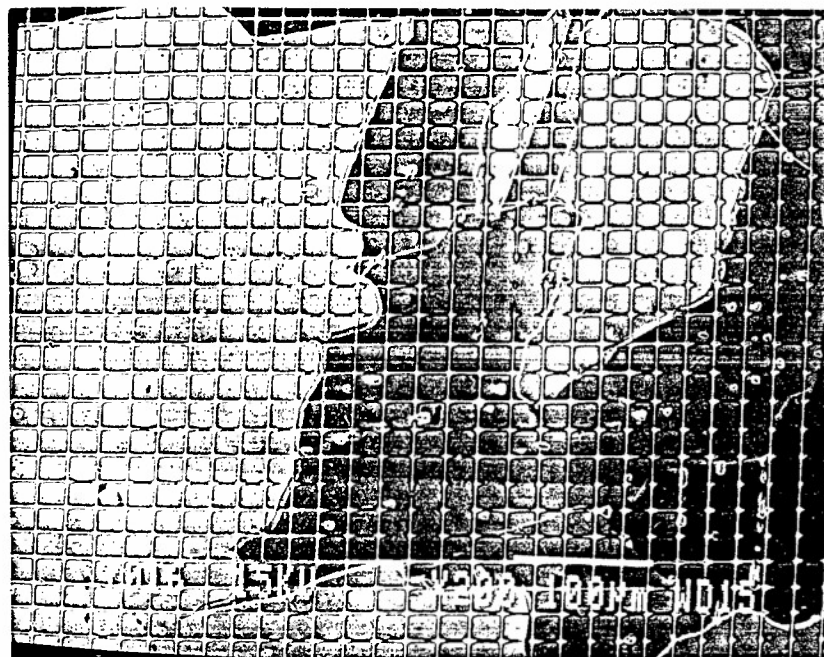


Fig. 1 Typical microstructure of Ti-0.4 wt % Mn ($\sim 100\%$ α) alloy. The alloy was heat treated for 2 hours at 1173 K, furnace cooled (FC) to 963 K, annealed for 200 hours and water quenched. Grain size is $\sim 500\ \mu\text{m}$.

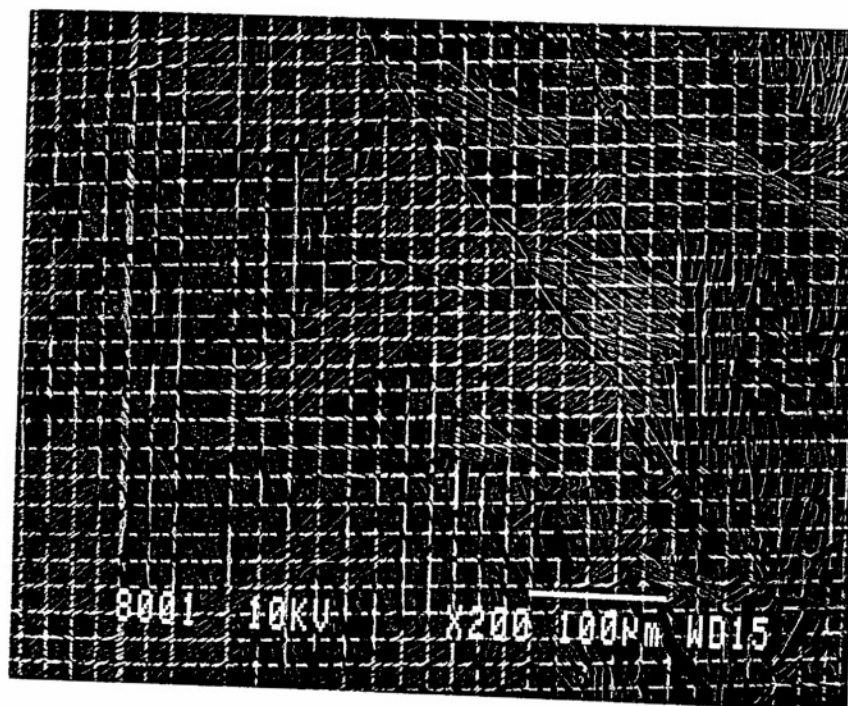


Fig. 2 Typical Widmanstätten type microstructure of Ti-6.0Mn (~46% α - 54% β) alloy. The alloy was heat treated for 2 h at 1173 K, FC to 963 K, annealed for 200 h and water quenched.

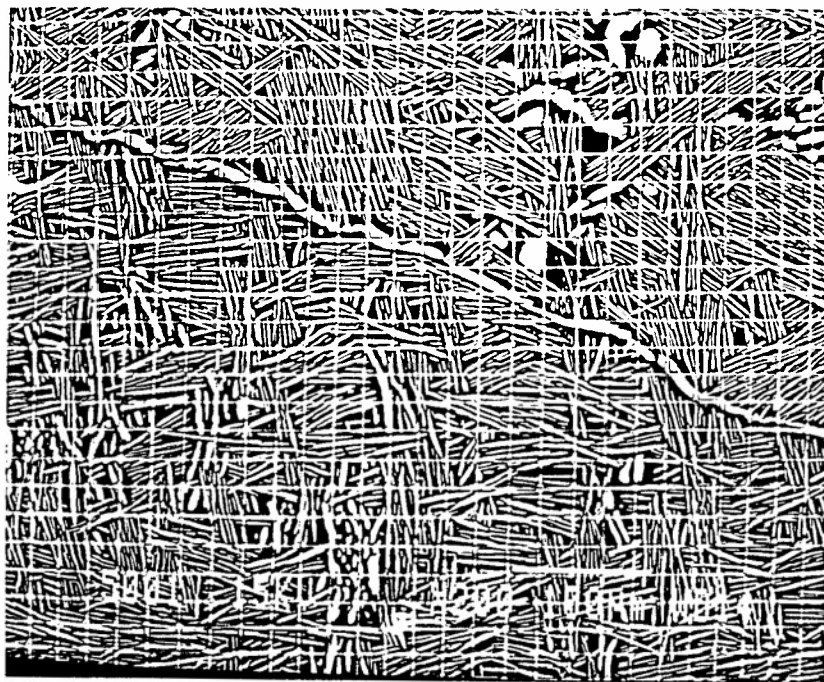


Fig. 3 Typical Widmanstätten type microstructure of Ti-8.1V (~51% α - 49% β) alloy. The alloy was heat treated for 2 h at 1173 K, FC to 963 K, annealed for 200 h and water quenched.

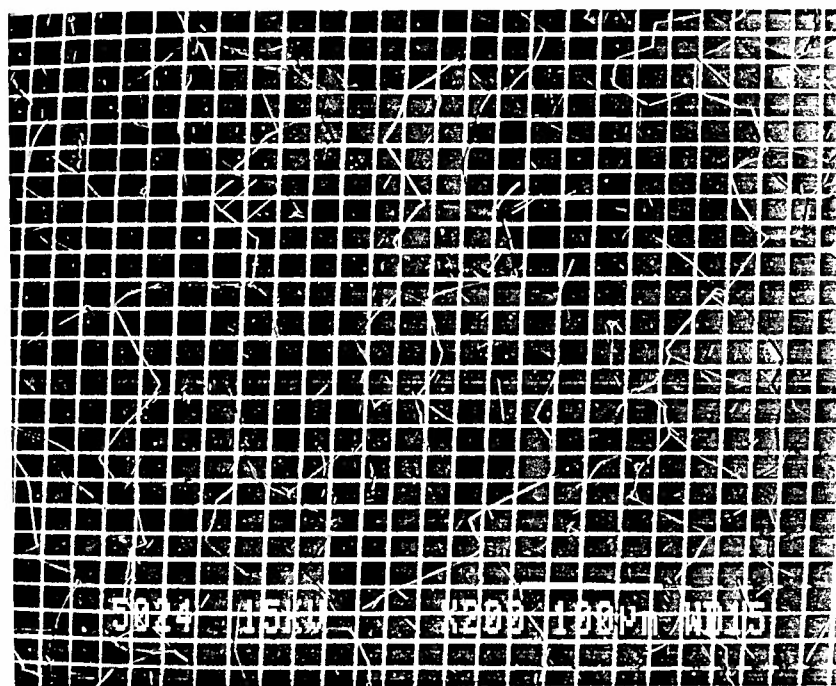


Fig. 4 Typical microstructure of small grained Ti-0.4Mn ($\sim 100\%$ α) alloy. The alloy was heat treated 200 h at 963 K and water quenched. Grain size is $\sim 45 \mu\text{m}$.

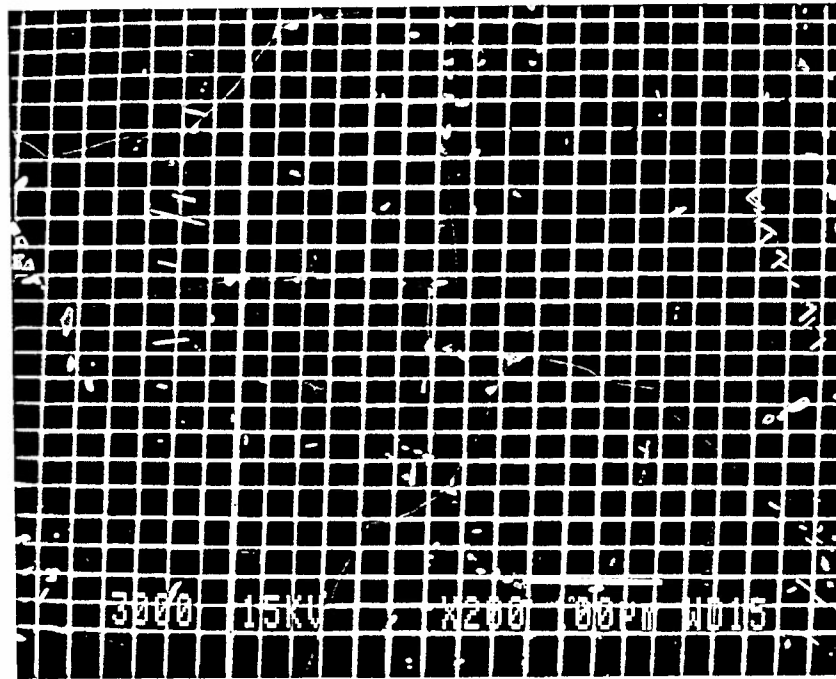


Fig. 5 Typical microstructure of Ti-13.0Mn (~100% β) alloy. The alloy was heat treated 200 h at 963 K and water quenched. Grain size is ~ 200 μm .

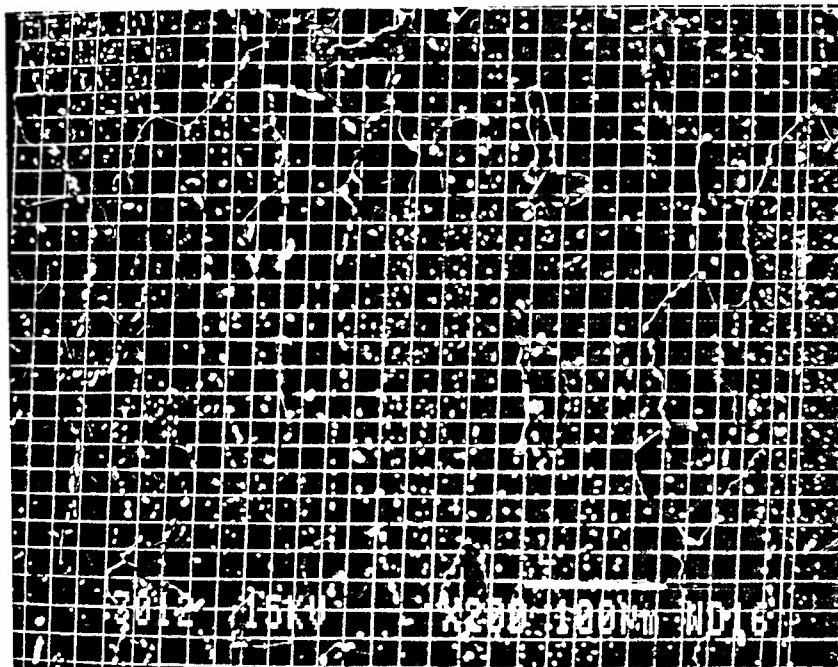


Fig. 6 Typical microstructure of Ti-14.8V (~100% β) alloy. The alloy was heat treated 200 h at 963 K and water quenched. Grain size is ~ 30 μm .

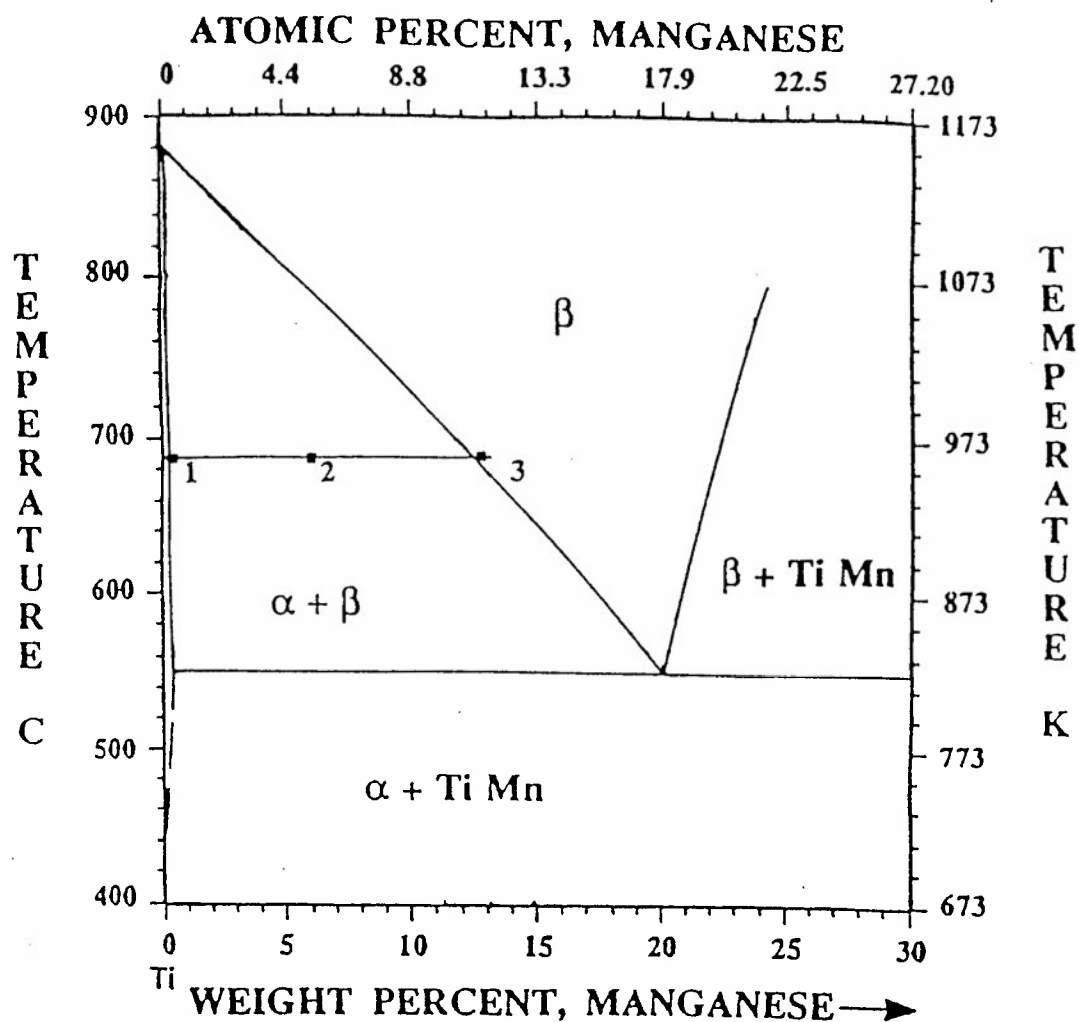


Fig. 7 Partial Ti end of the Ti-Mn phase diagram [45]. The compositions of Alloys 1-3 are indicated with solid squares. The annealing temperature, 690° C (963 K), is also indicated.

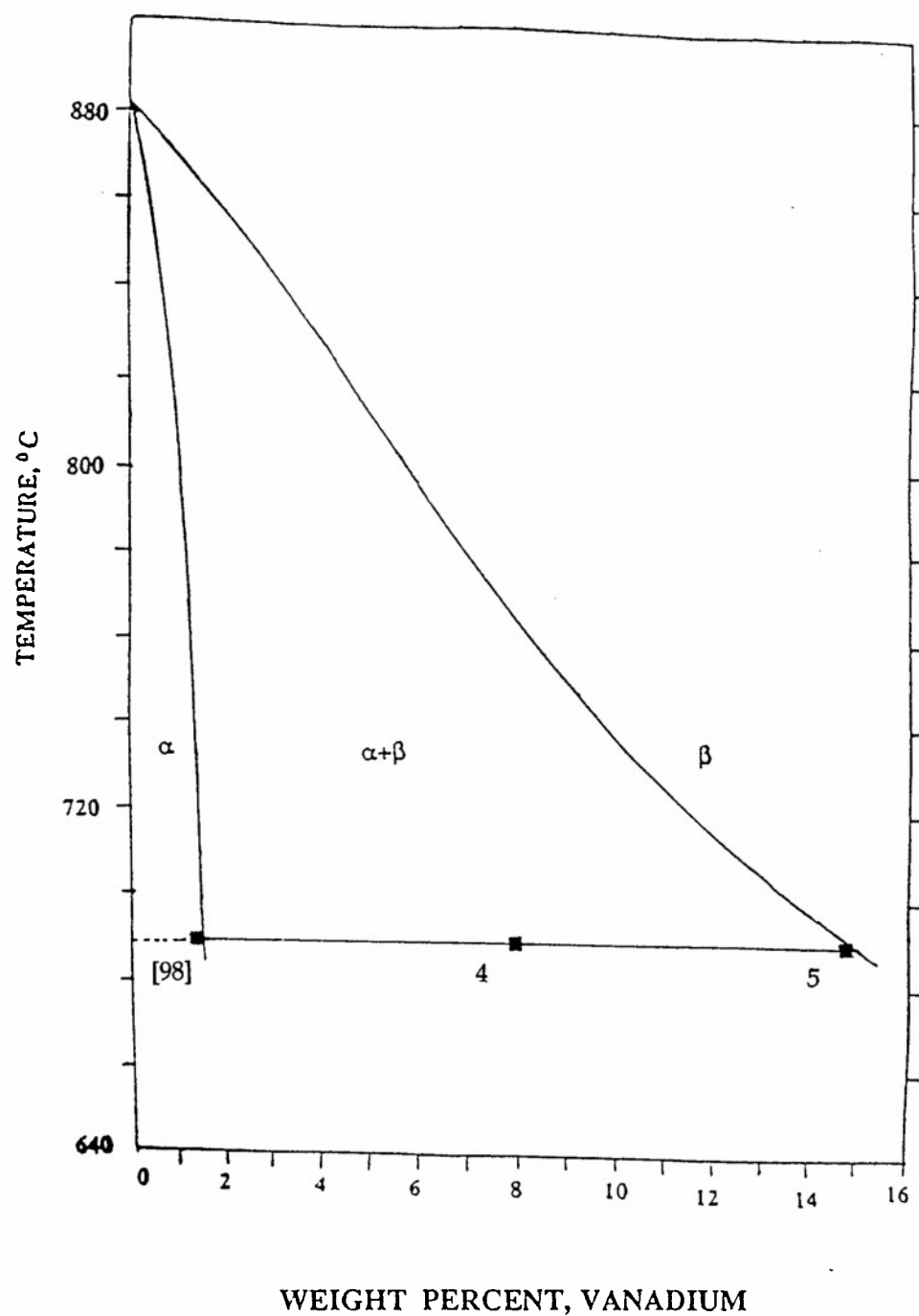
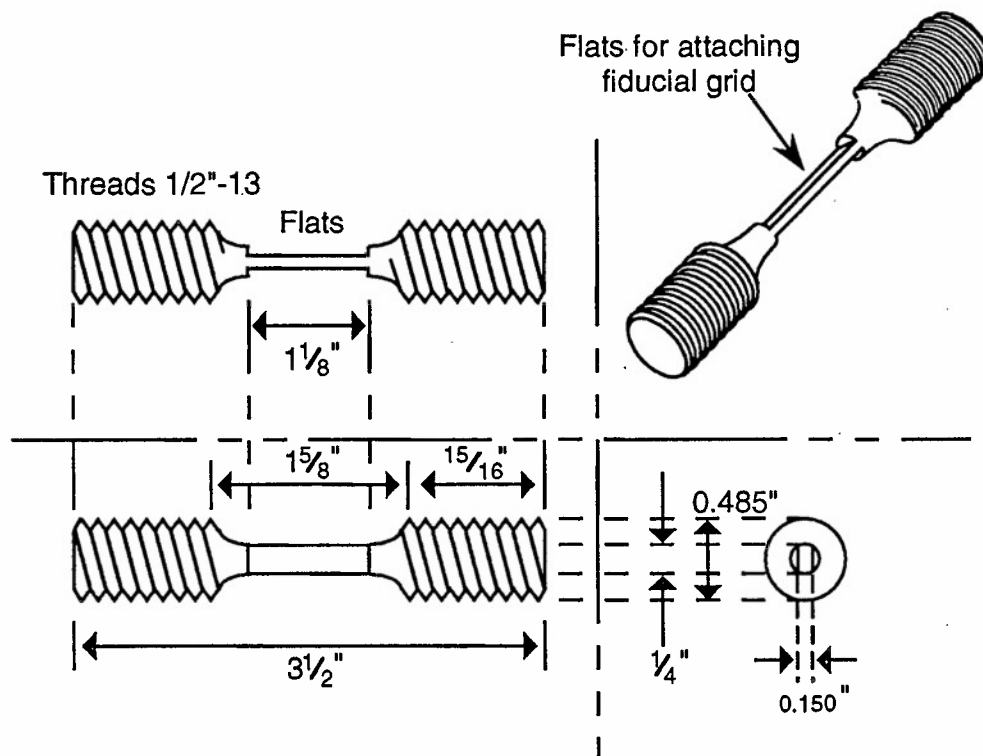
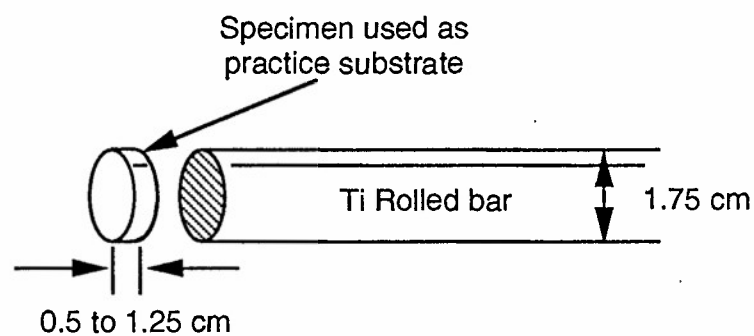


Fig. 8 Partial Ti end of the Ti-V phase diagram [46]. The compositions of alloys 4 and 5 are indicated with solid squares. The annealing temperature of interest, 690° C (963 K), is also indicated.



(a)



(b)

Fig. 9 Diagram of (a) room temperature creep and tensile specimens and (b) specimens used to develop the electron lithography technique of making fiducial grids.

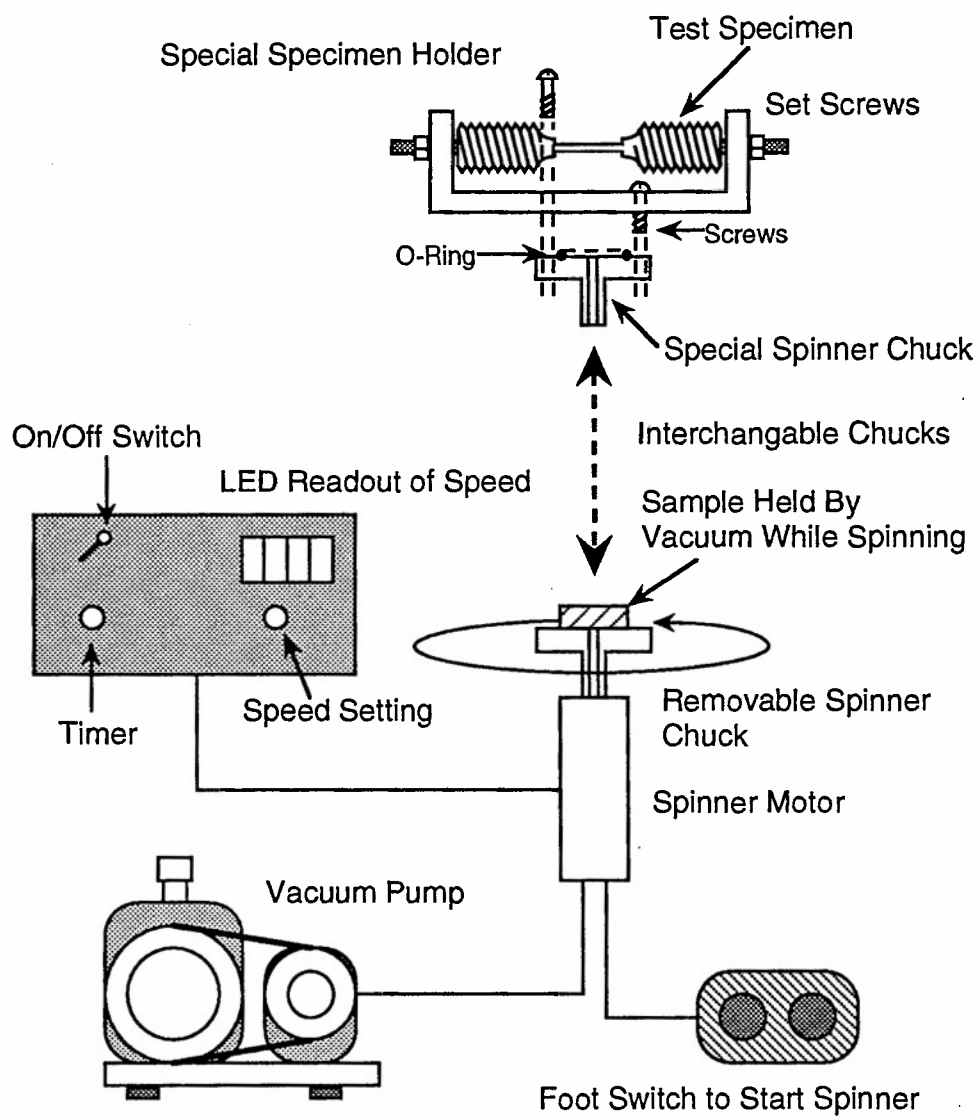


Fig. 10 Vacuum Spinner and Specimen Holder used to spin-coat machined and polished creep and tensile test specimens with photo resist.

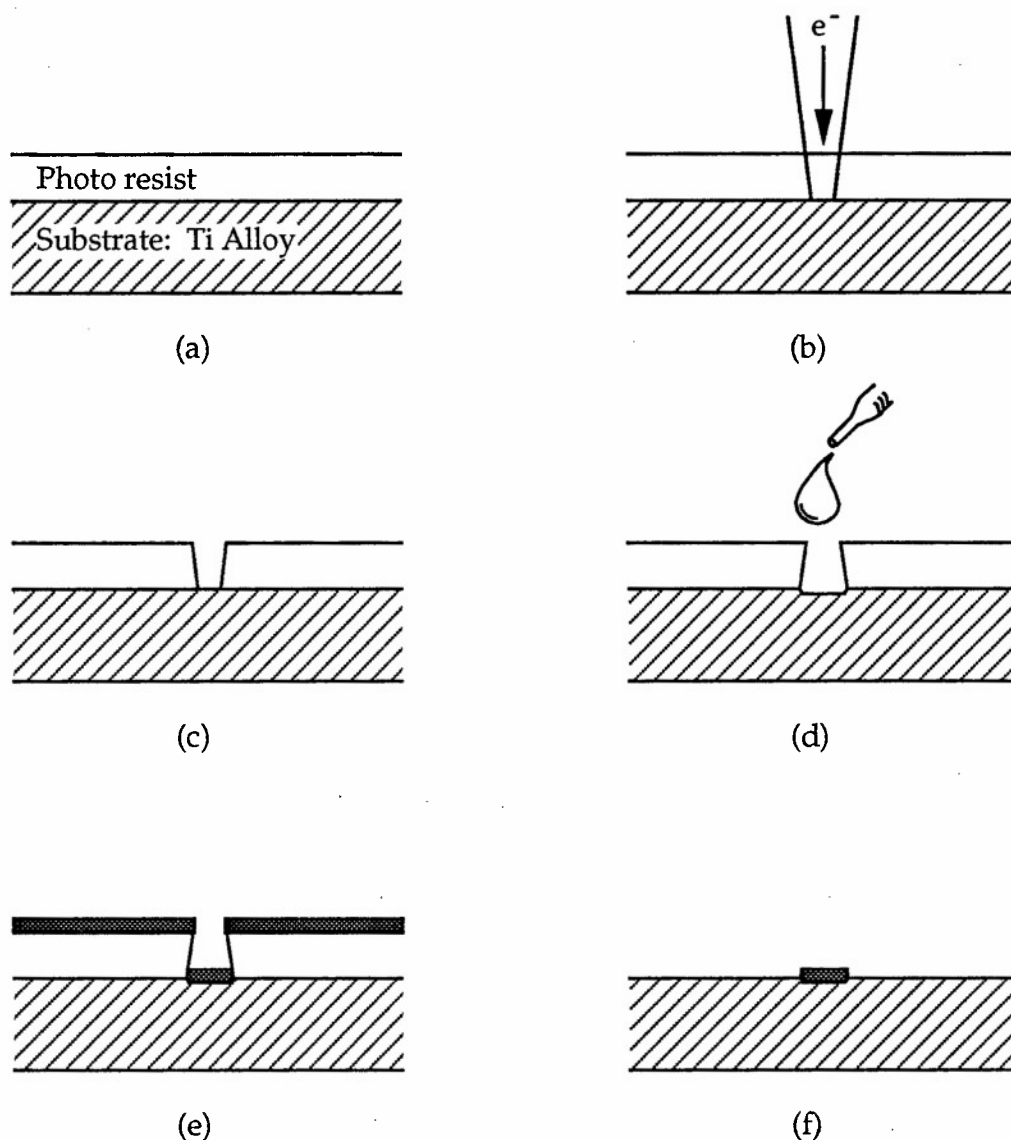


Fig. 11 A schematic of the entire process for producing fiducial grids. a) The substrate is spin coated with a thin layer of photo resist, then b) exposed to the electron beam in line mode perpendicular to the plane of the figure, the exposed photo resist is developed away c), then the specimen is etched with a dilute substrate etchant d), coated with $\sim 250 \text{ \AA}$ of Cu or Au by vacuum evaporation e), and in f) the unexposed photo resist is removed.

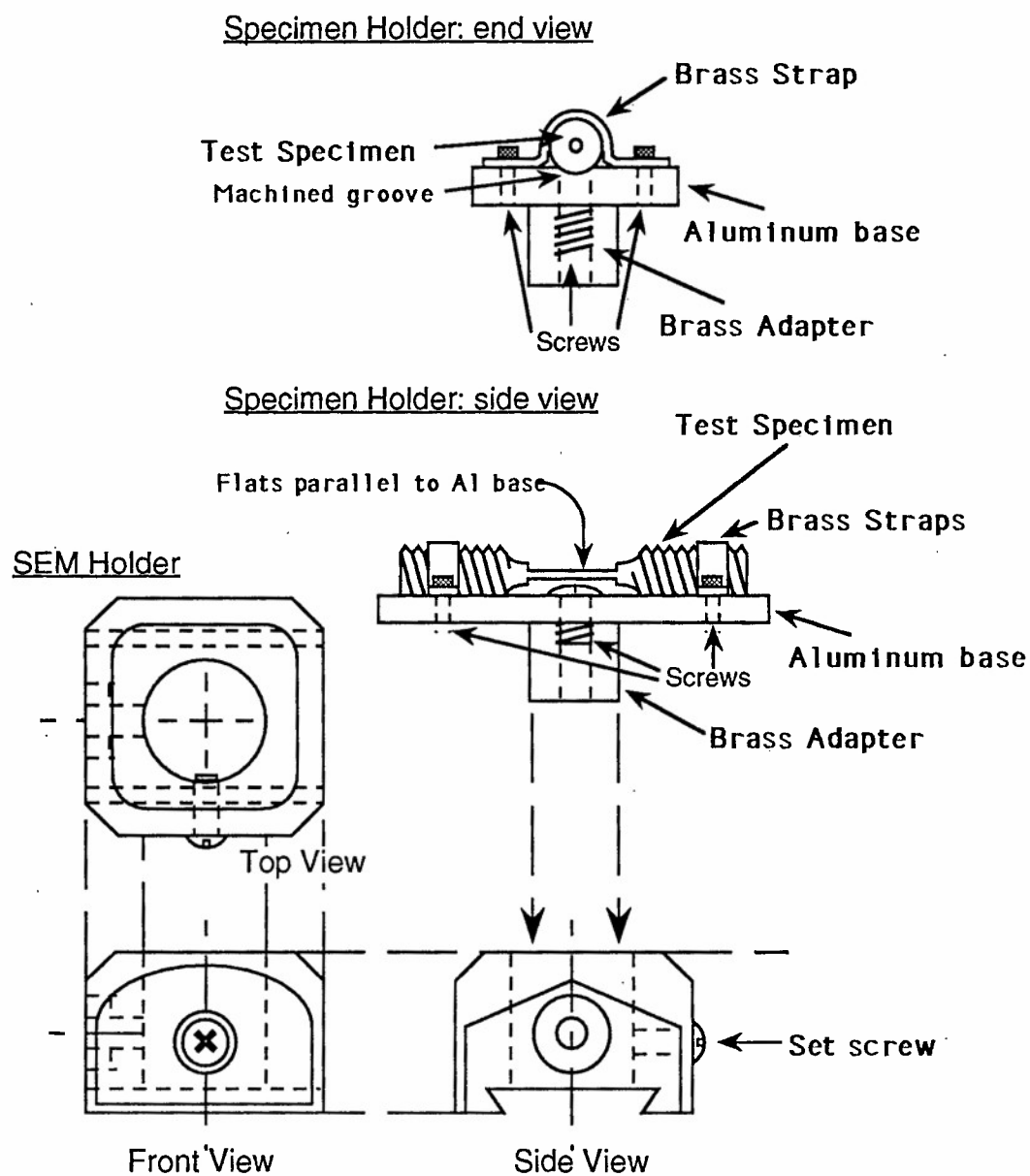
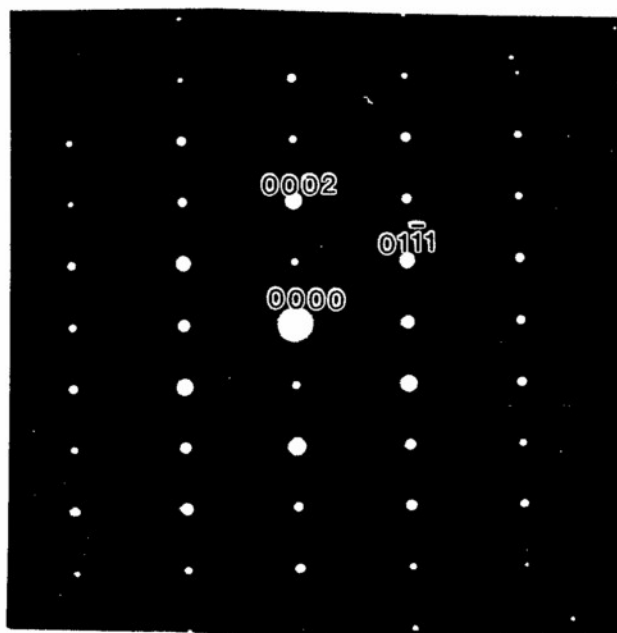


Fig. 12 Schematic of Specimen Holder for electron beam writing.

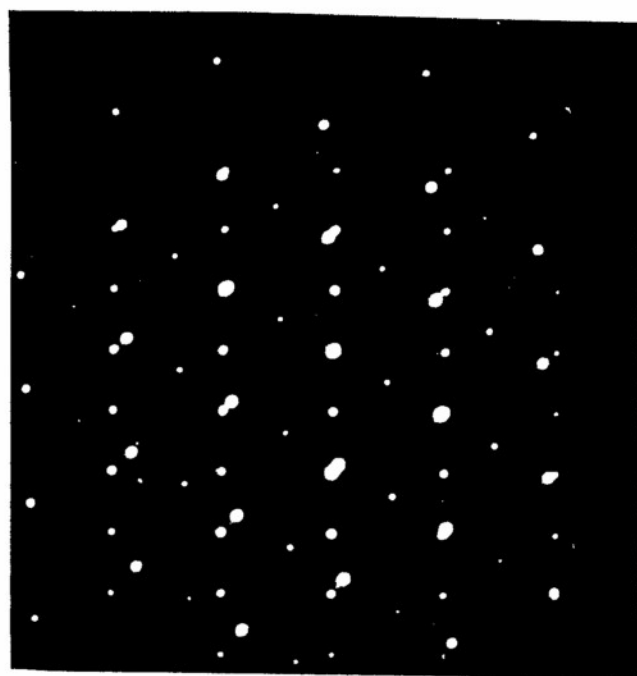
Fig. 13 Deformation twinning in a coarse grained α Ti-0.4Mn alloy crept to 2.7% at 298 K: (a) Bright field TEM micrograph showing twins, (b) Selected Area Diffraction Pattern (SADP) of matrix, (c) SADP of matrix/twin interface at location "A". Note extra spots corresponding to $\{10\bar{1}2\}$ twin.



(a)



(b)

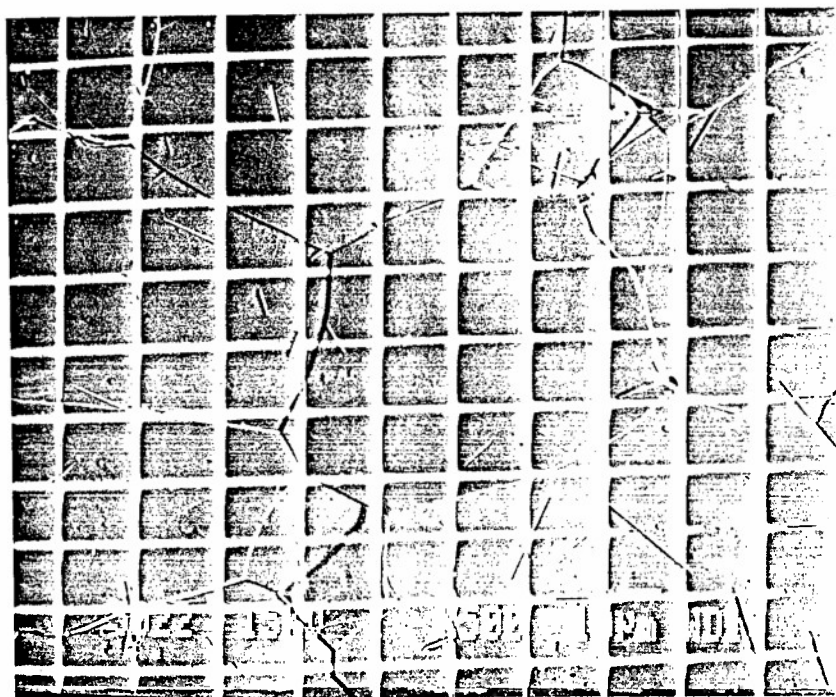


(c)

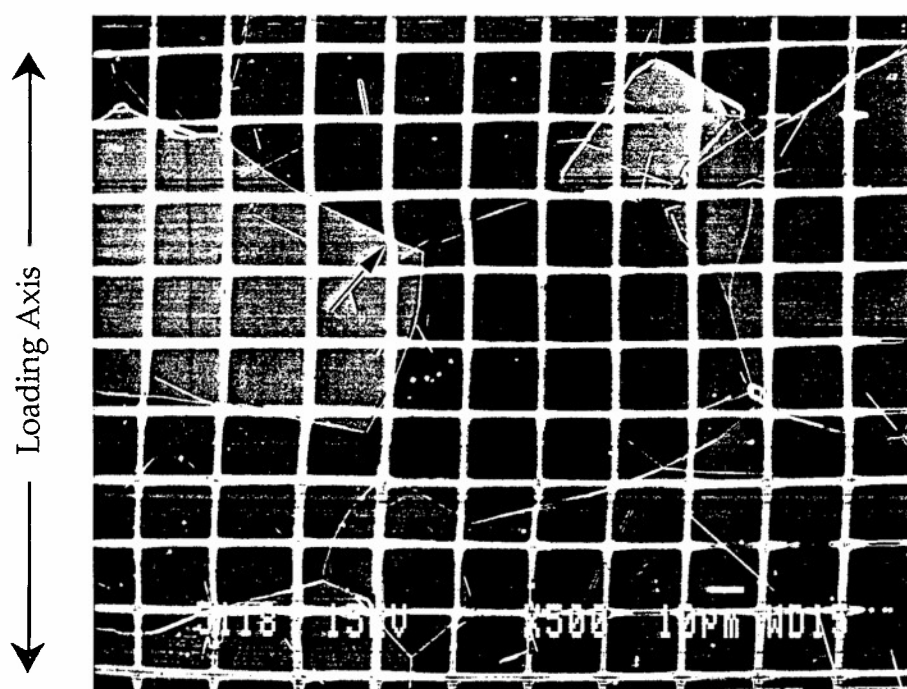
Fig. 14 Transmission electron micrograph of 500 μm grain size α Ti-0.4 wt% Mn alloy after room temperature creep deformation to 2.8% creep strain. Note large twins at bottom and small lenticular twins at center and upper left.



Fig. 15 Typical microstructure of Ti-0.4Mn (~100% α) alloy: (a) before tensile deformation and, (b) after tensile deformation. Note grid distortion at arrow. Total plastic strain is 2.68% at a strain rate of 3.28×10^{-5} per second. The grain size is $\sim 45 \mu\text{m}$.



(a)



(b)

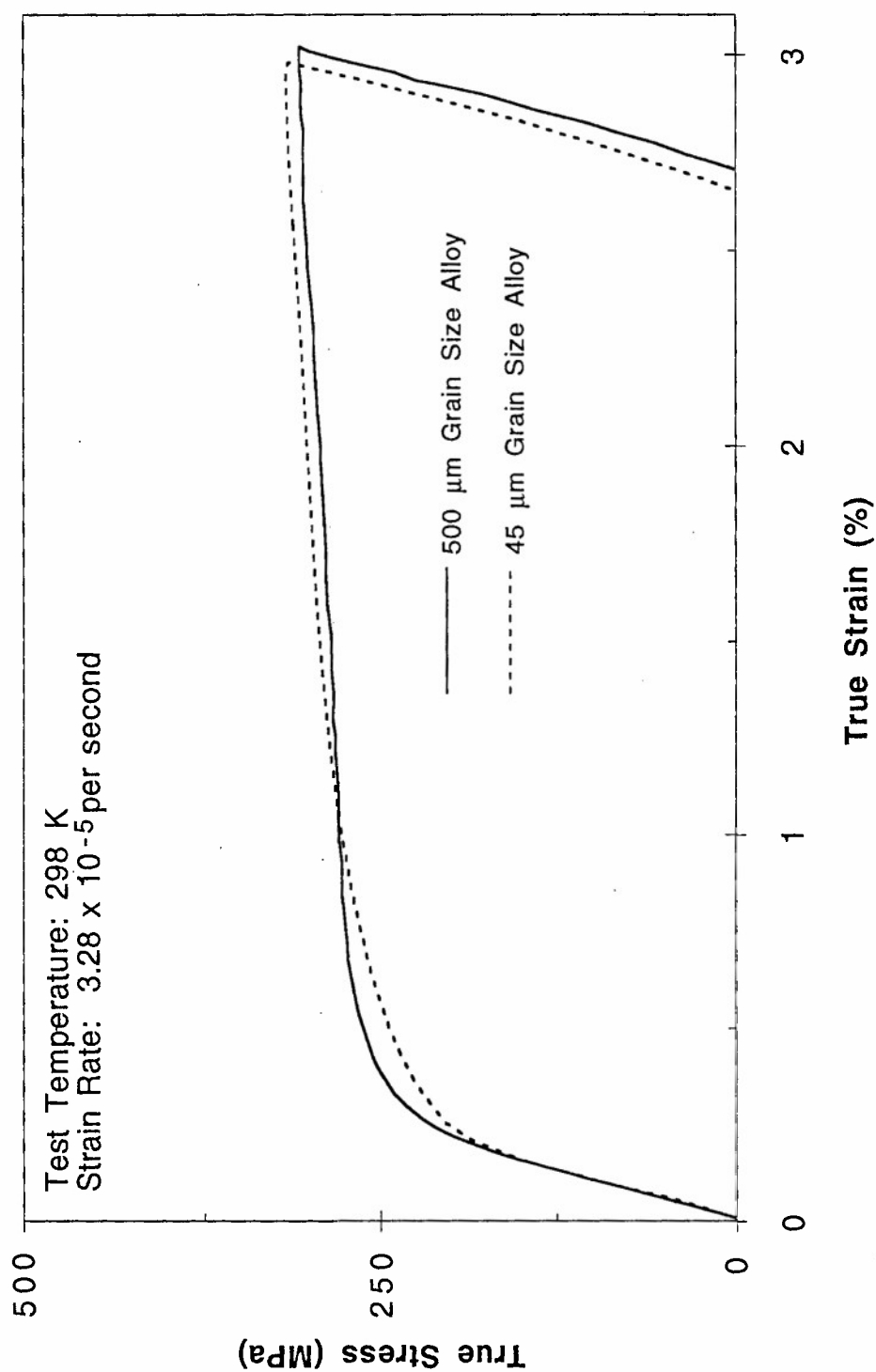
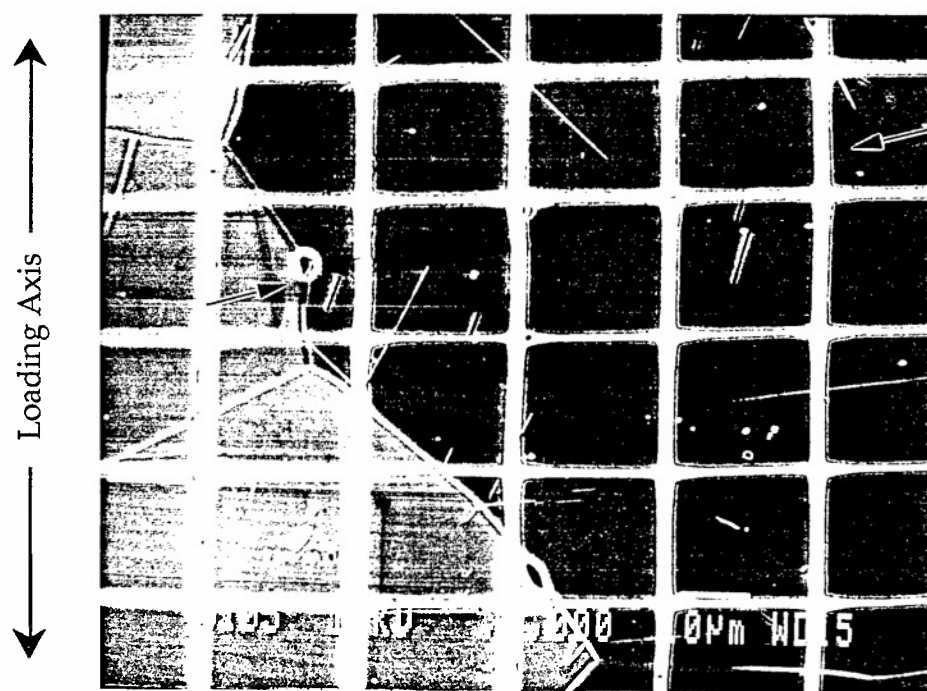


Fig. 16 Ambient temperature true stress-true strain curves of Ti-0.4Mn ($\sim 100\%$ α) alloy. The 45 μm grained alloy was heat treated for 200 h at 963 K followed by water quench. The 500 μm grained alloy was heat treated for 2 h at 1173 K, FC to 963 K, annealed for 200 h followed by water quench.

Fig. 17 Microstructure of $\sim 45\ \mu\text{m}$ grained Ti-0.4Mn ($\sim 100\% \alpha$) alloy: (a) before tensile deformation and, (b) after tensile deformation. Note twinning between arrows. Total plastic strain is 2.68% at a strain rate of 3.28×10^{-5} per second.



(a)



(b)



← Loading Axis →

Fig. 18 Optical micrograph of α Ti-0.4Mn alloy after tensile deformation to 2.68% plastic strain, note twinning.

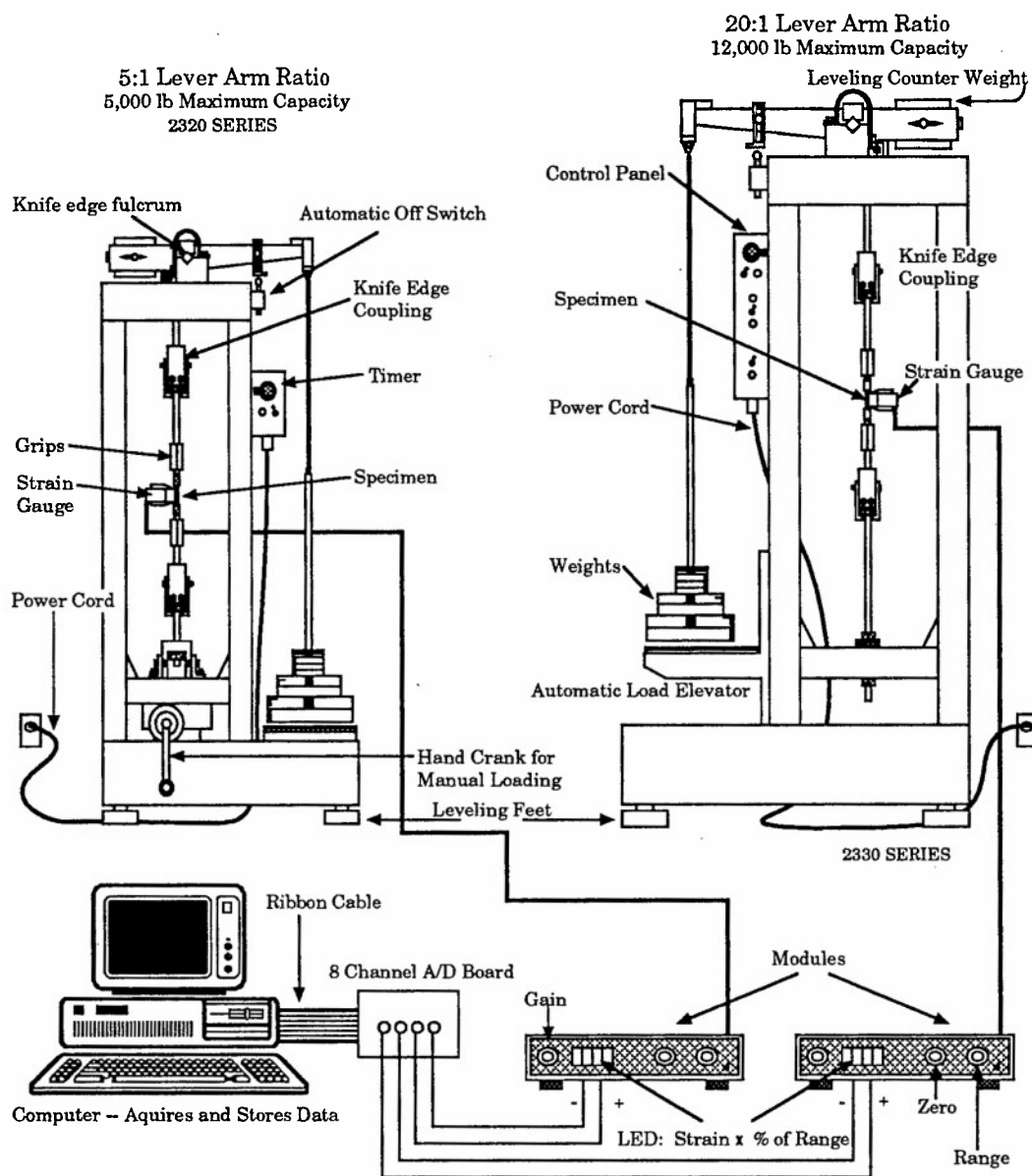


Fig. 19 Creep Test and Data Acquisition Setup.

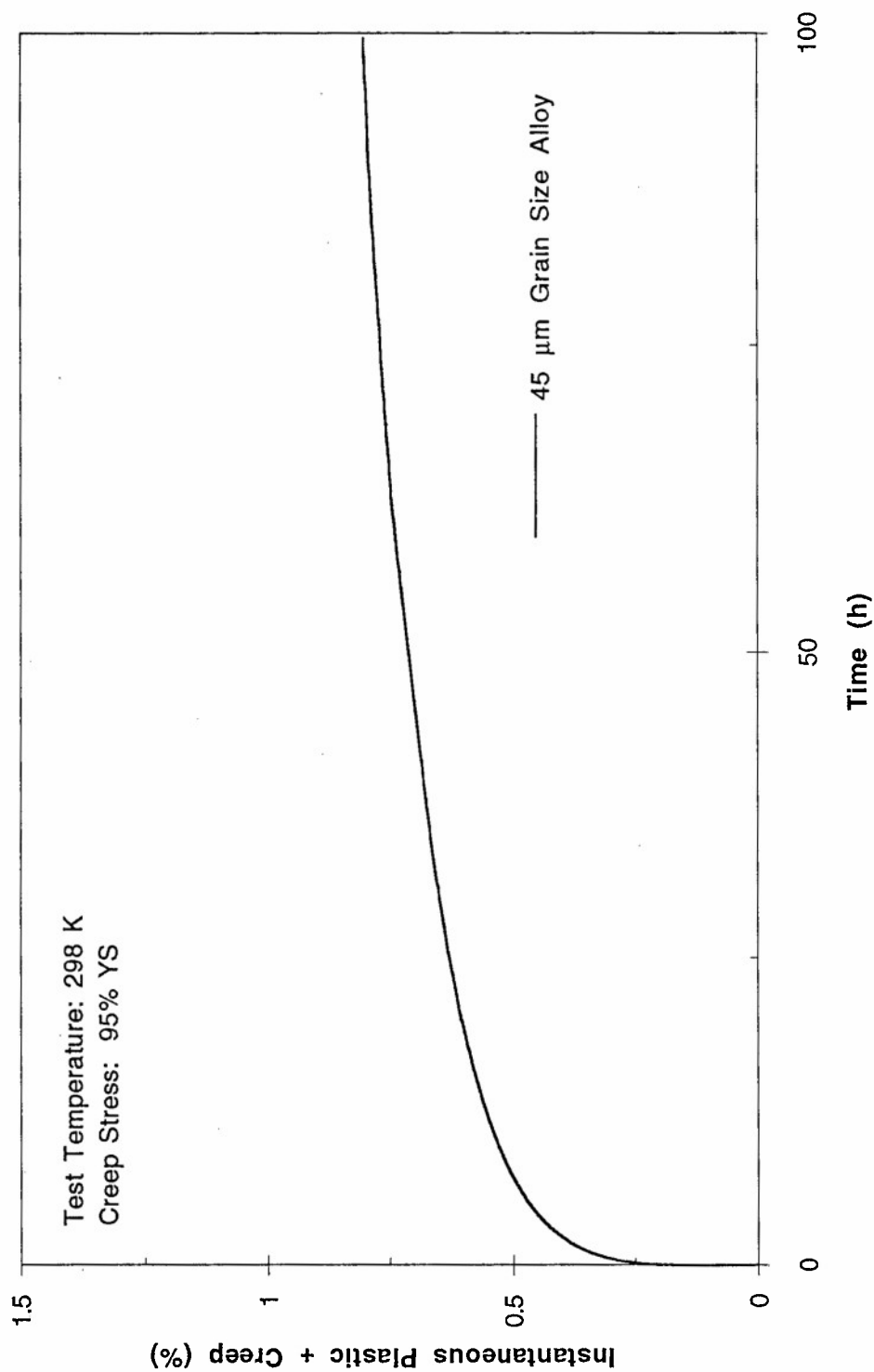
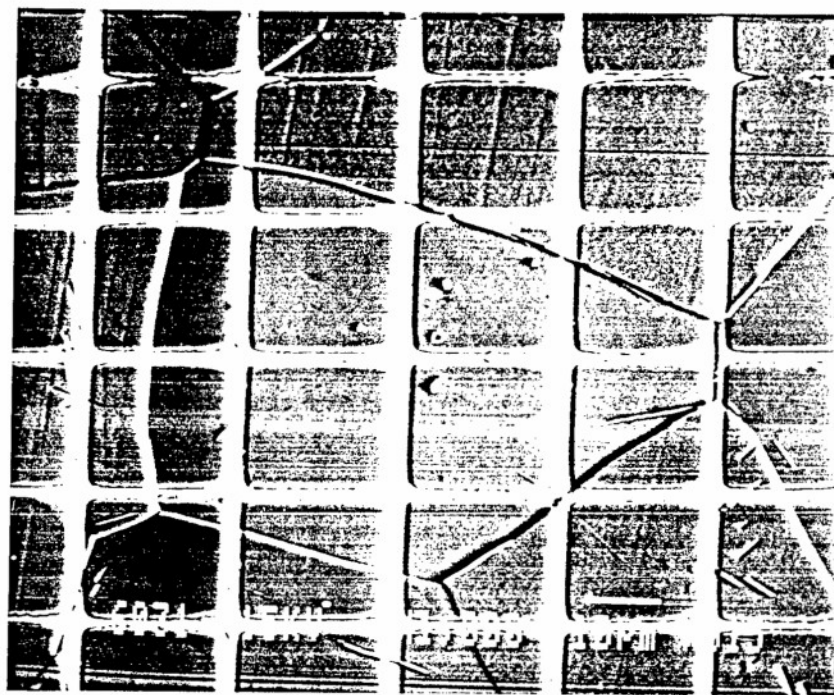
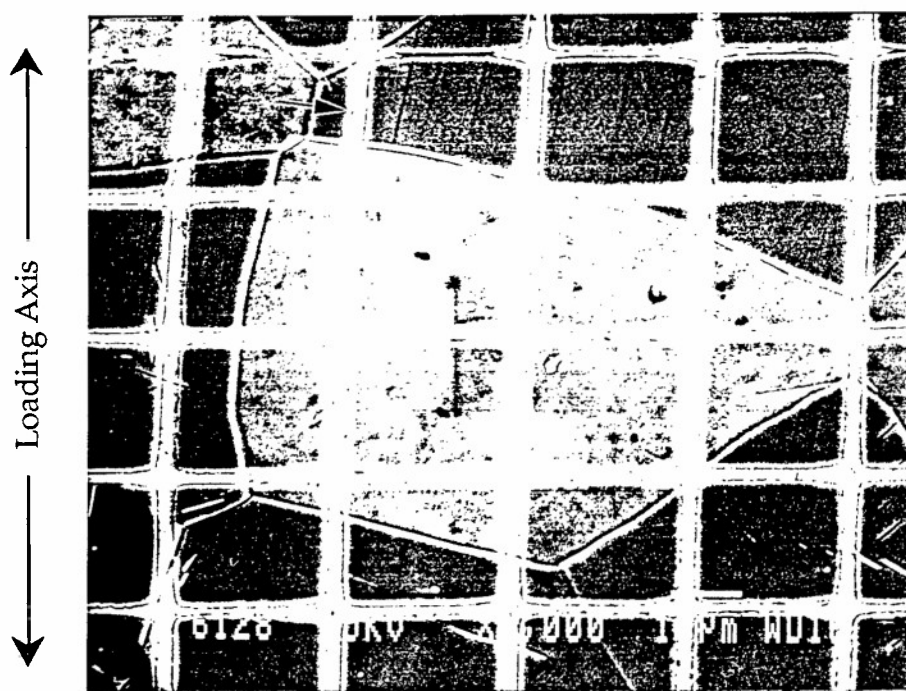


Fig. 20 Ambient temperature creep curve for Ti-0.4Mn ($\sim 100\%$ α) alloy, crept at 95% YS. Alloys were heat treated for 200 h at 963 K followed by water quench.

Fig. 21 SEM micrographs of Ti-0.4Mn (~100% α) alloy (a) before creep deformation and, (b) the same area after creep deformation, note grid distortion at arrow; (c) after deformation, note twinning. Creep strain is 1.30% in 550 h. The grain size is ~45 μm .



(a)

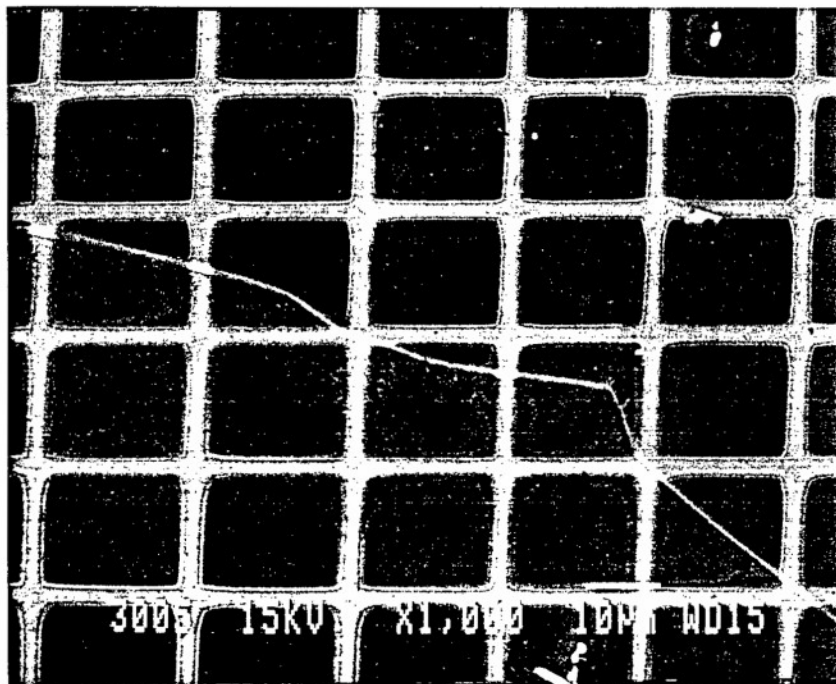


(b)

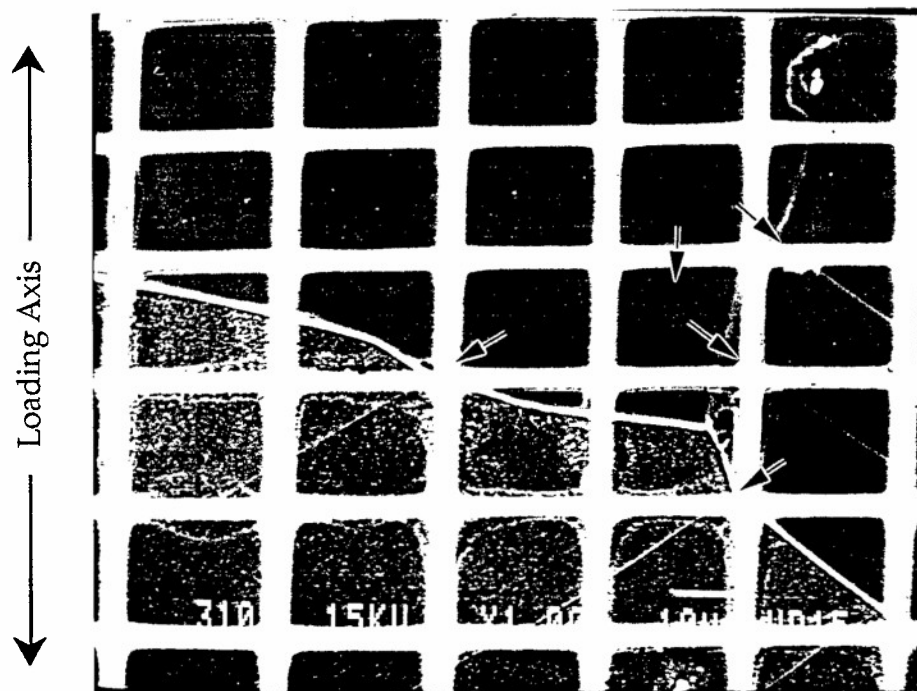


(c)

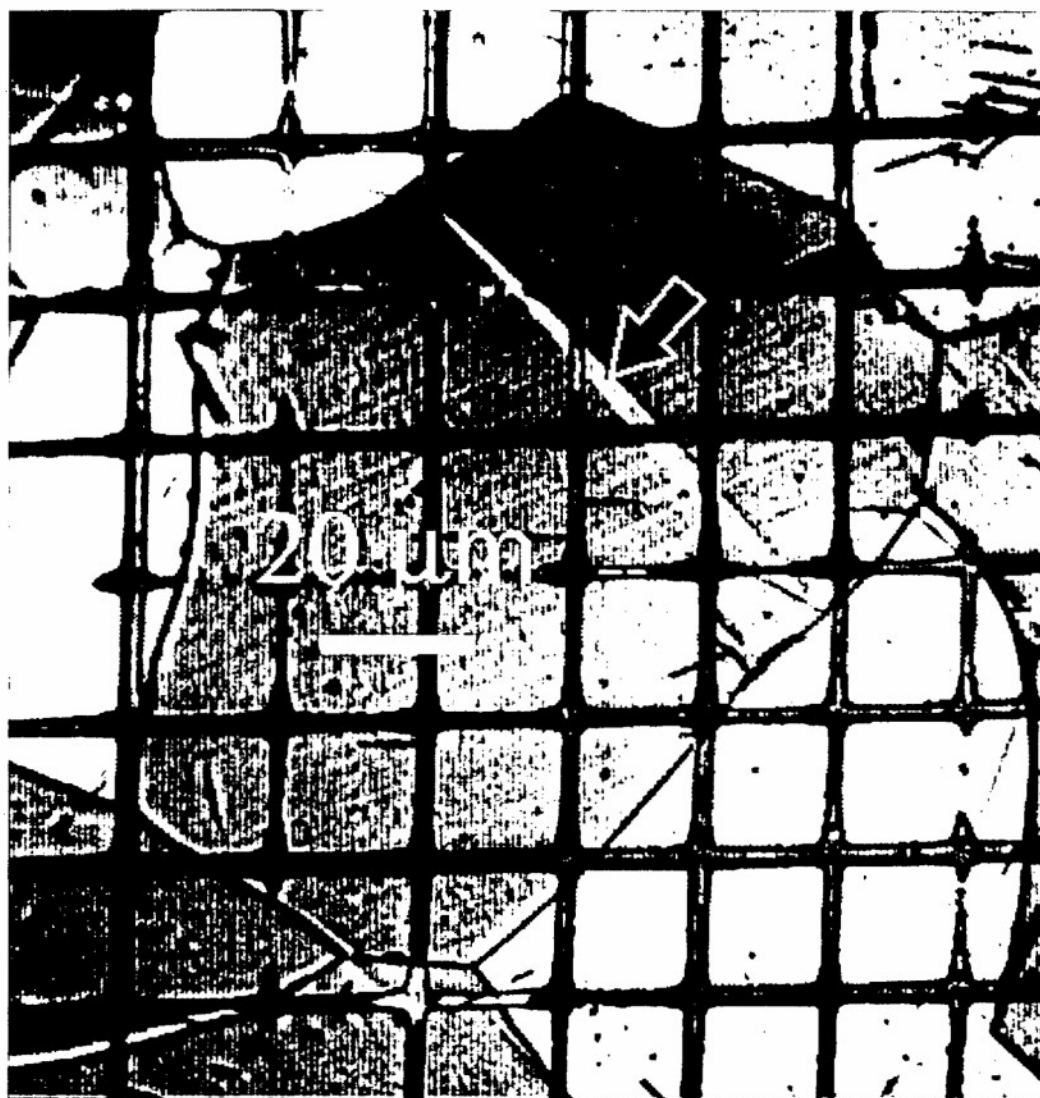
Fig. 22 SEM micrographs of Ti-13.0Mn (~100% β) alloy: (a) before creep deformation and, (b) the same area after creep deformation, note slip bands at the arrows. Total creep strain is 0.03% in 408 h. The grain size is ~ 200 μm .



(a)



(b)



← Loading Axis →

Fig. 23 Optical micrograph of α Ti-0.4Mn alloy after creep deformation to 1.30% creep strain. Note twinning at the arrows.

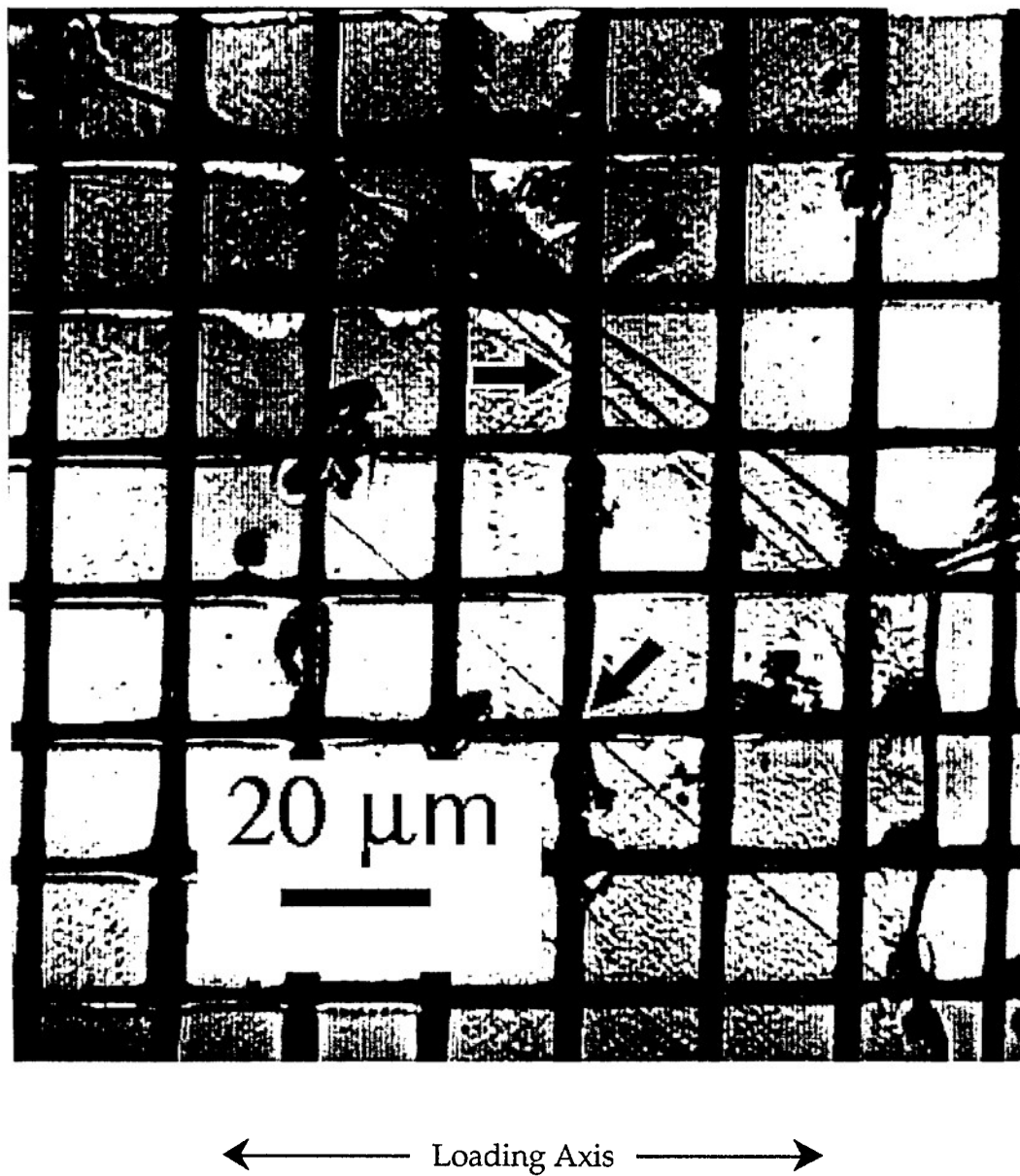
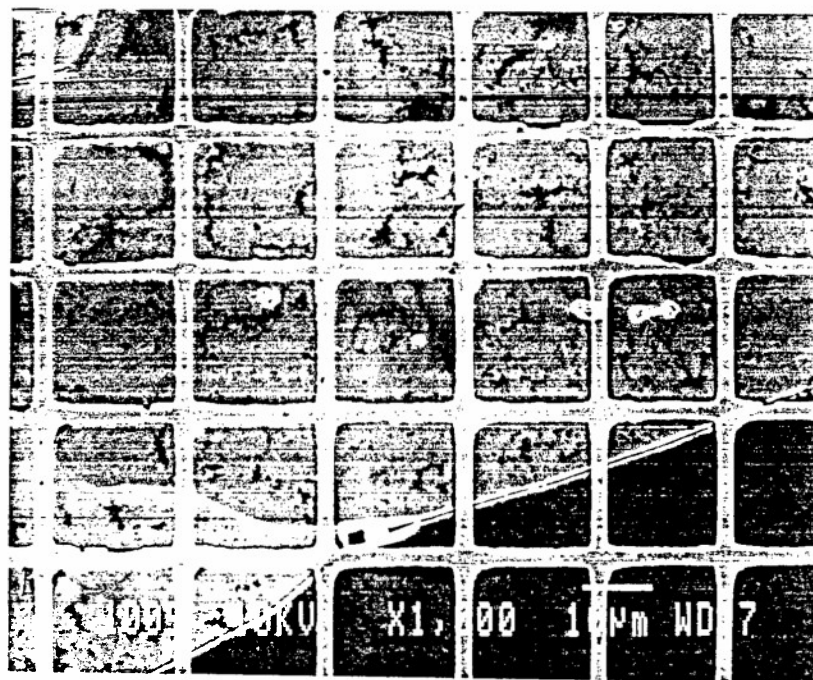
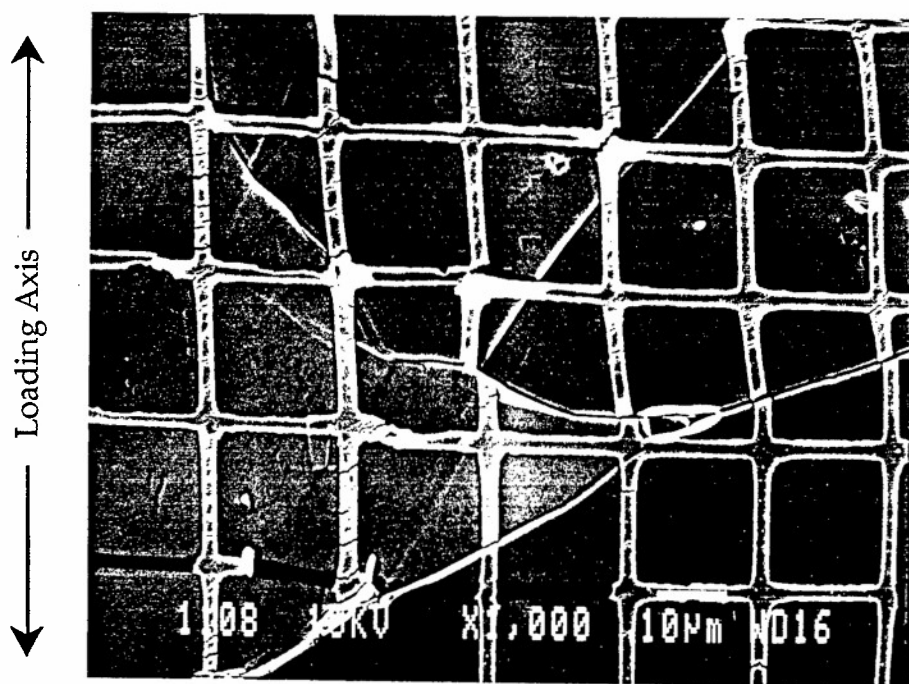


Fig. 24 Optical micrograph of β Ti-13.0Mn alloy after creep deformation to 0.03% creep strain. Note slip lines.

Fig. 25 Typical microstructure of Ti-0.4Mn ($\sim 100\%$ α) alloy: (a) before creep deformation, (b) after creep deformation. Creep strain is 3.71% in 474.4 h. The alloy was heat treated for 2 h at 1173 K, FC to 963 K, 200 h, water quenched.



(a)

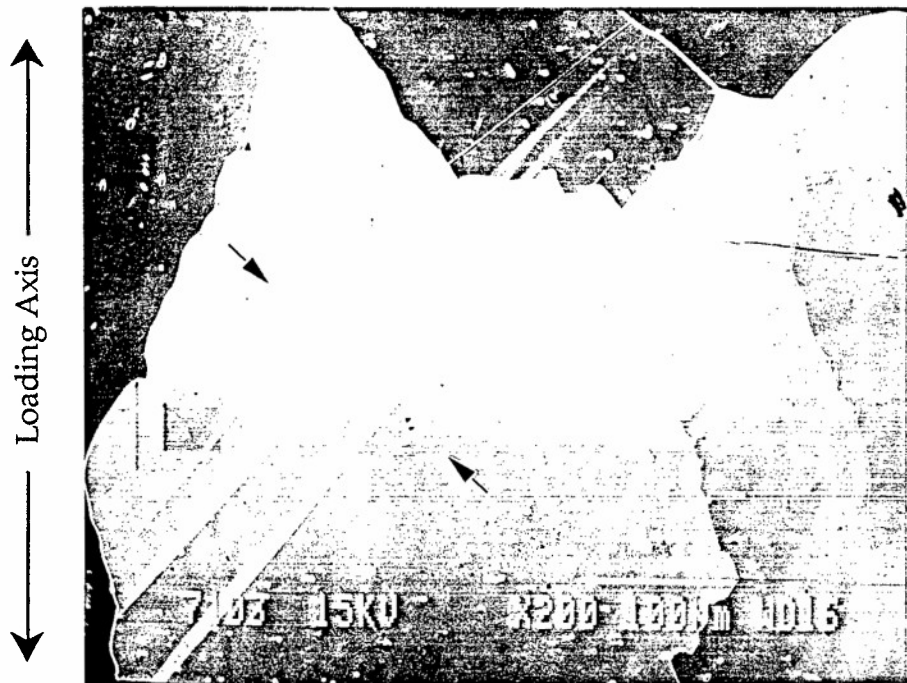


(b)

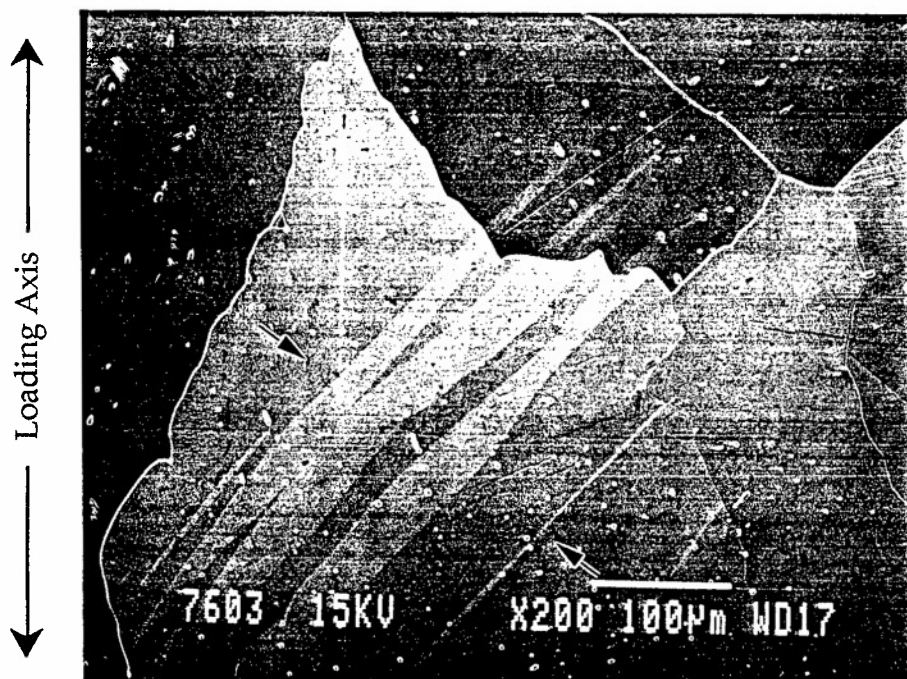


(a)

Fig. 26 Microstructure of α Ti-0.4Mn alloy, grain size ~ 0.5 mm. Note that the twinning length and width increase with creep time: (a) before deformation, (b) after creep strain of 0.92%, (c) after creep strain of 2.75%.

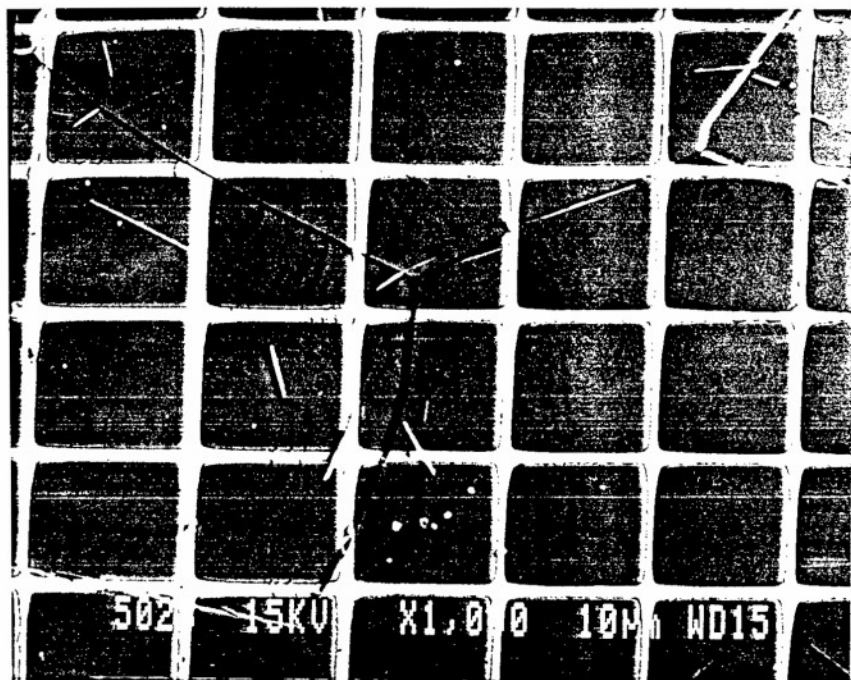


(b)

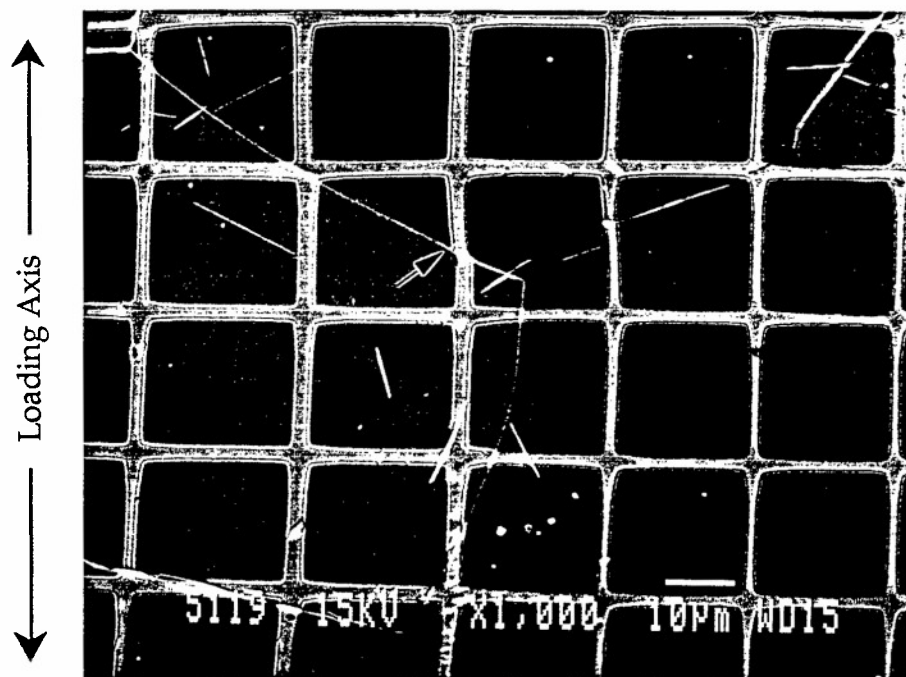


(c)

Fig. 27 Microstructure of small grained Ti-0.4Mn (~100% α) alloy: (a) before tensile deformation and, (b) the same area after tensile deformation, note grid distortion at arrow. Total plastic strain is 2.68% at strain rate 3.28×10^{-5} per second. The alloy was heat treated for 200 h at 963 K, water quenched.

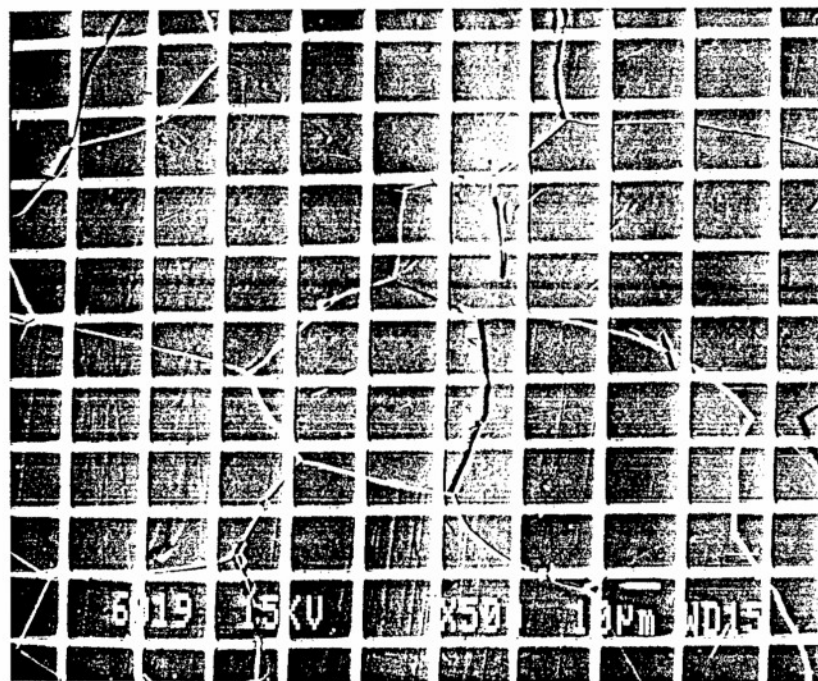


(a)

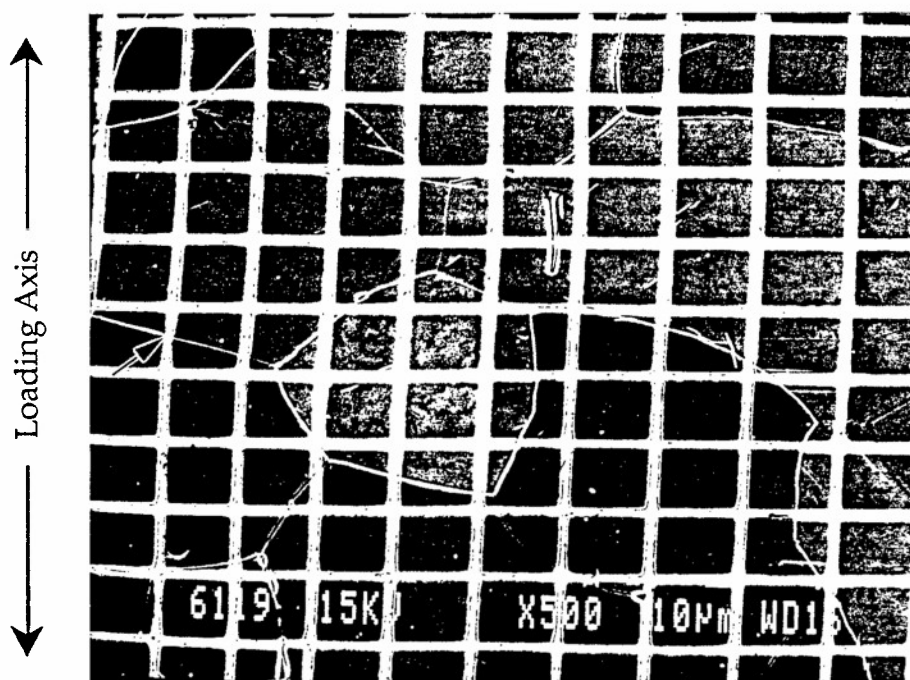


(b)

Fig. 28 Microstructure of small grained Ti-0.4Mn (~100% α) alloy: (a) before creep deformation and, (b) the same area after creep deformation. Note grid distortion at arrow. Creep strain is 1.30% in 500 h. The grain size is ~ 45 μm .

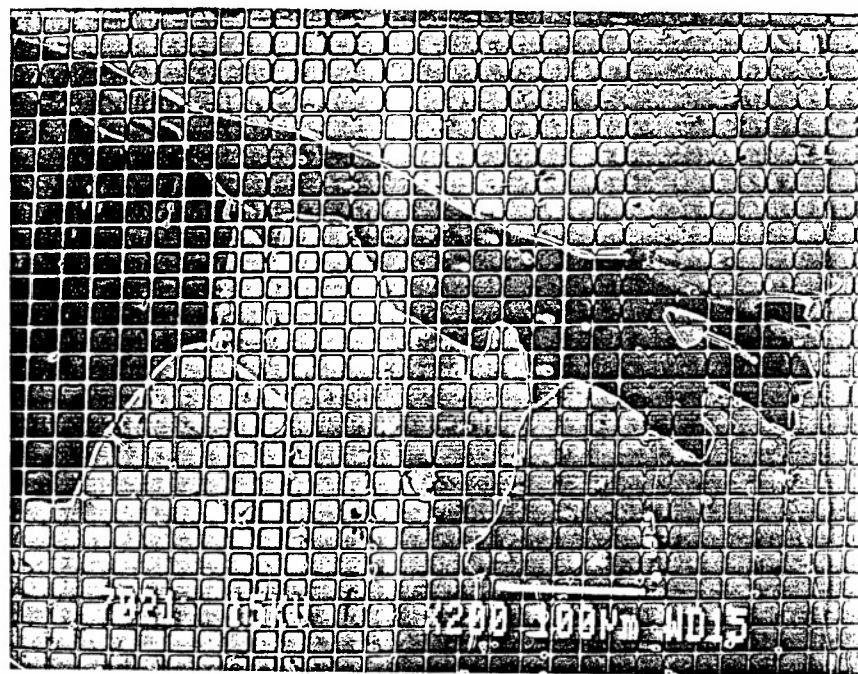


(a)

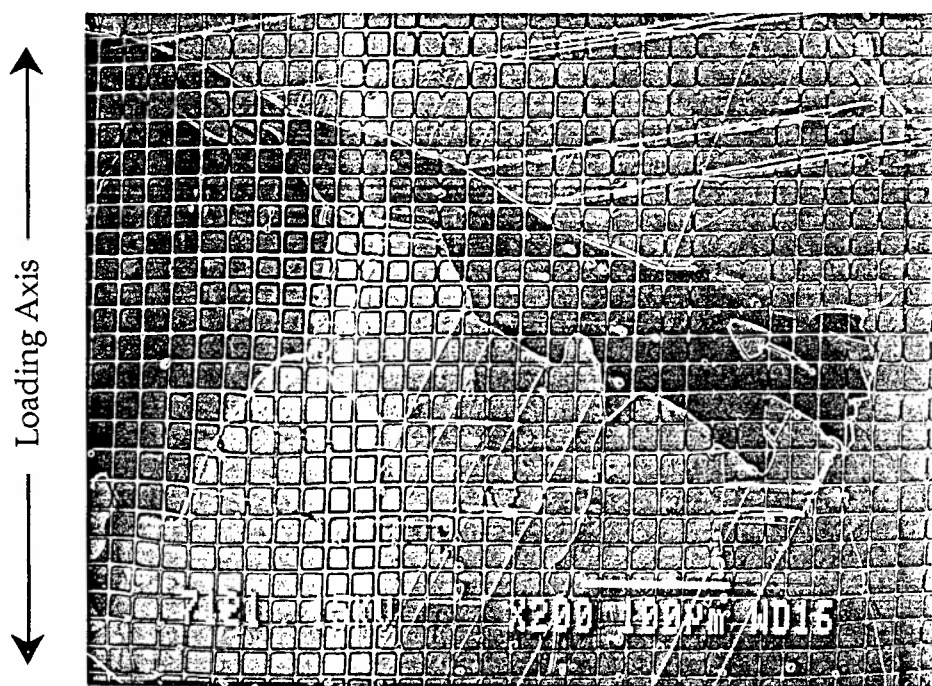


(b)

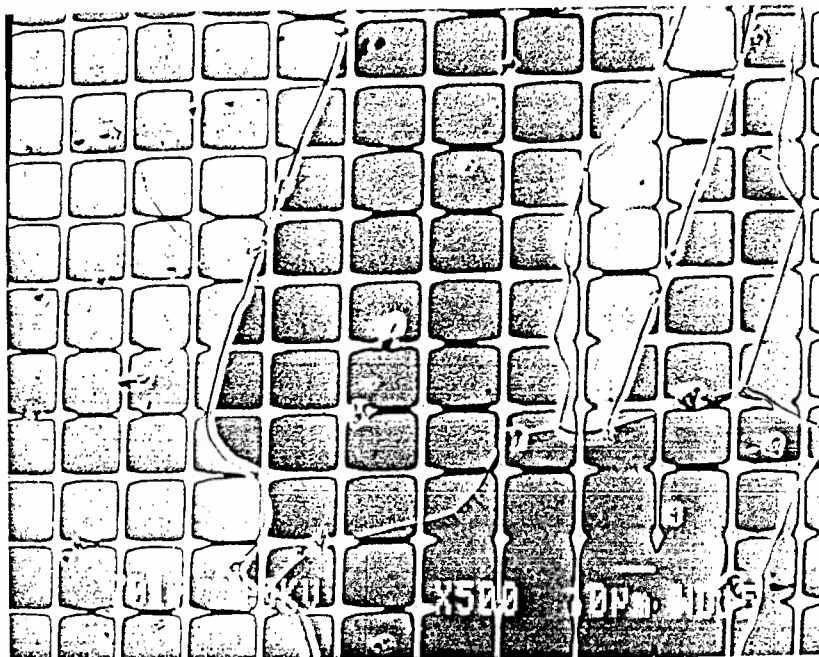
Fig. 29 Microstructure of large grained Ti-0.4Mn (~100% α) alloy: (a) before tensile deformation and, (b) the same area after tensile deformation, note twinning, (c) another area of the same specimen, at higher magnification, before tensile deformation and, (d) the same area after tensile deformation, note twinning. Total plastic strain is 2.26% at strain rate 3.28×10^{-5} per second. The alloy was heat treated for 2 h at 1173 K, FC to 963 K, annealed for 200 h, water quenched. Grain size is ~ 500 μm .



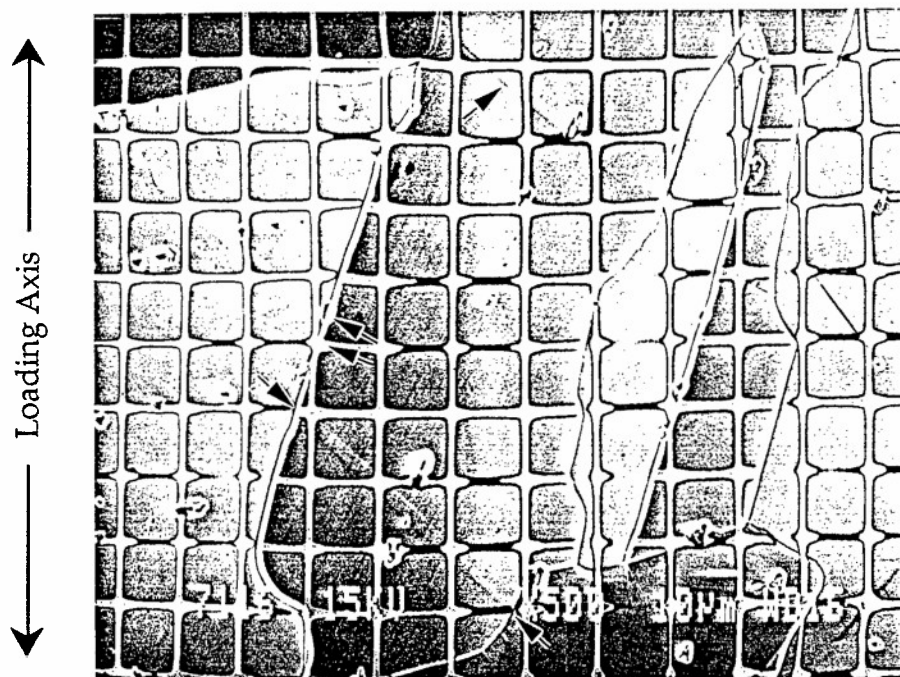
(a)



(b)

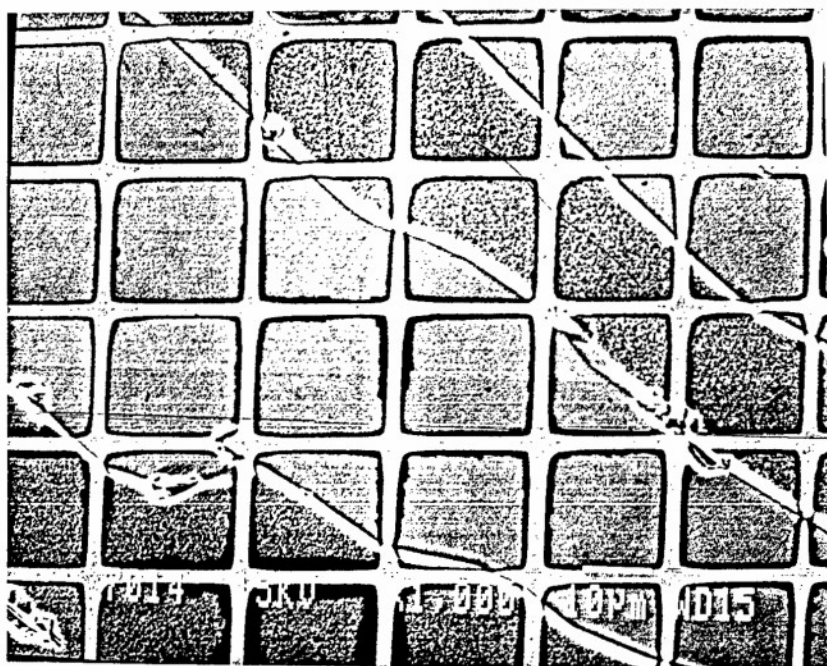


(c)

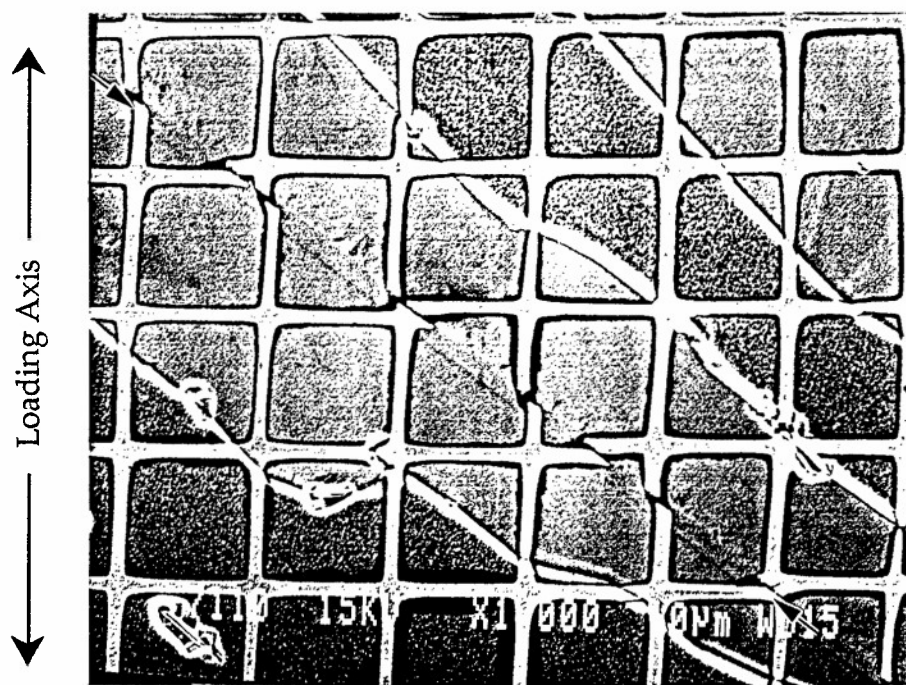


(d)

Fig. 30 Microstructure of Ti-0.4Mn (~100% α) alloy: (a) before tensile deformation and, (b) the same area after tensile deformation. Note twinning. Total plastic strain is 2.26% at strain rate 3.28×10^{-5} per second. The alloy was heat treated for 2 h at 1173 K, FC to 963 K, annealed for 200 h, water quenched.



(a)



(b)

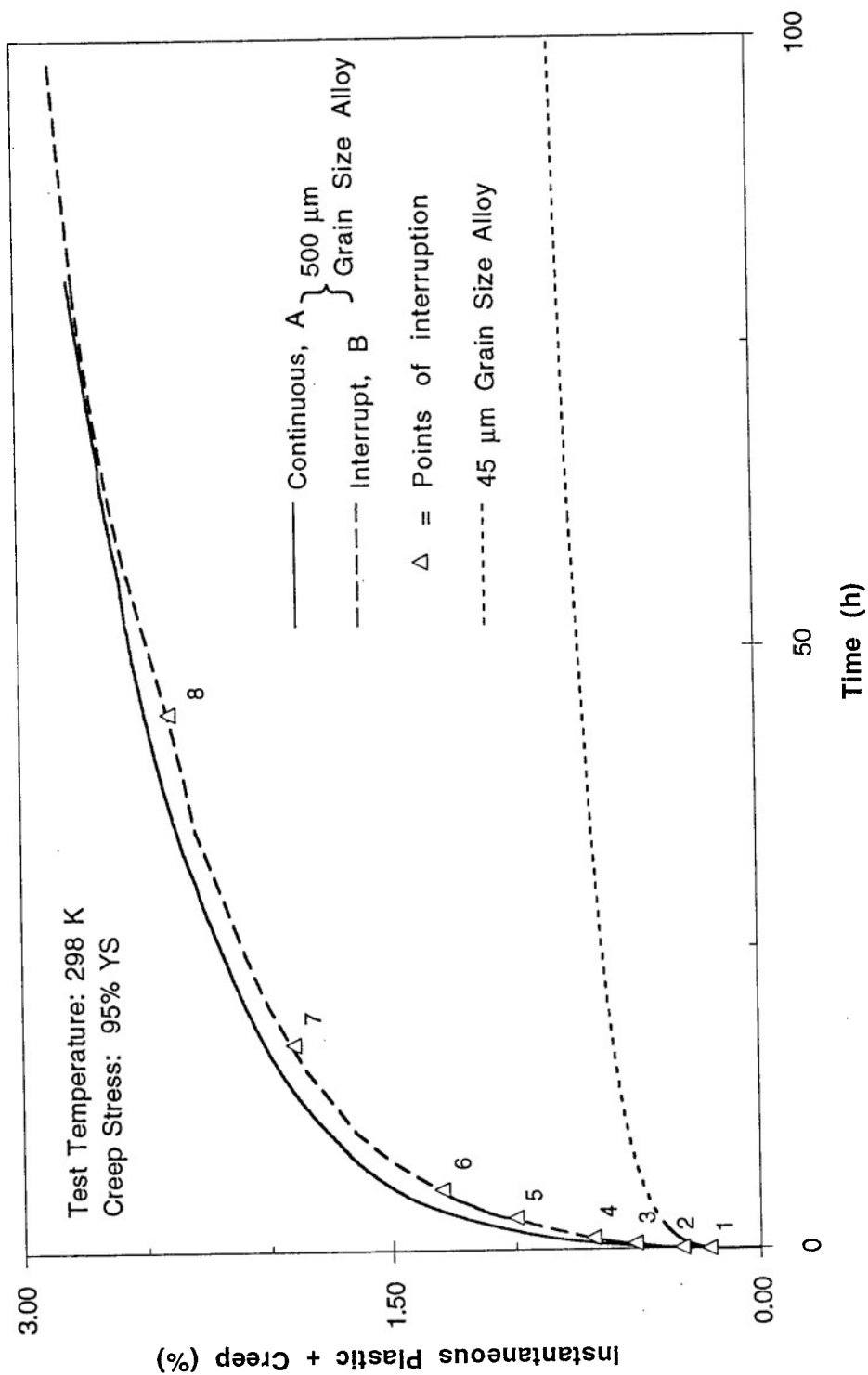
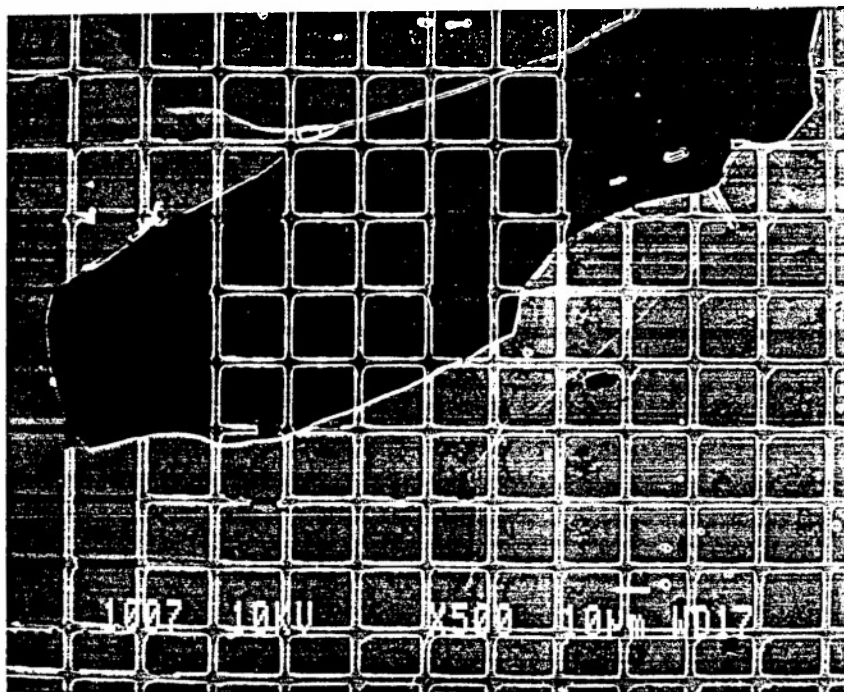
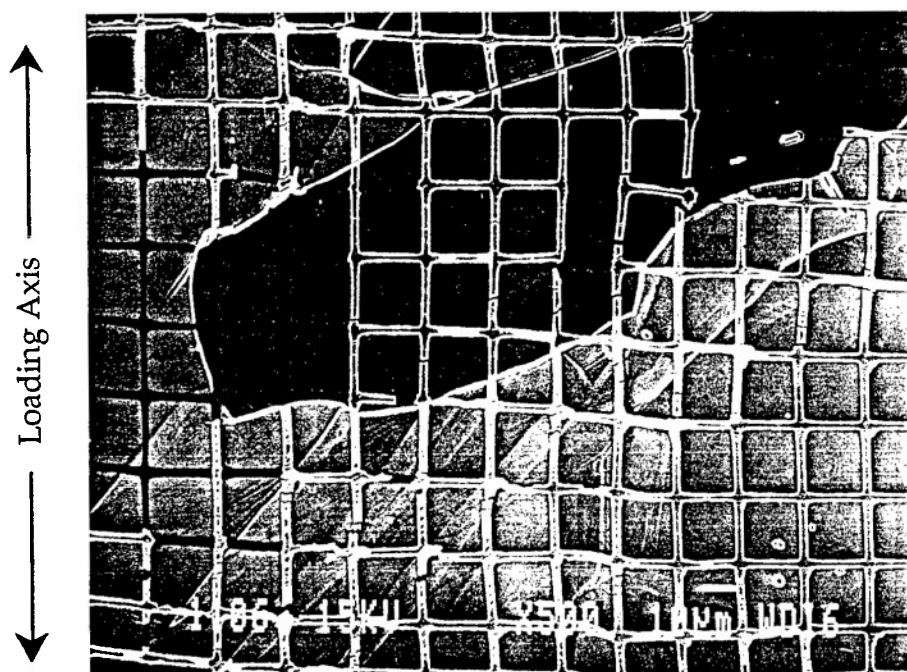


Fig. 31 Instantaneous plastic + creep strain vs. time for α Ti-0.4Mn alloy. Creep stress: 95% YS. The triangles and the associated numbers correspond to test interruptions.

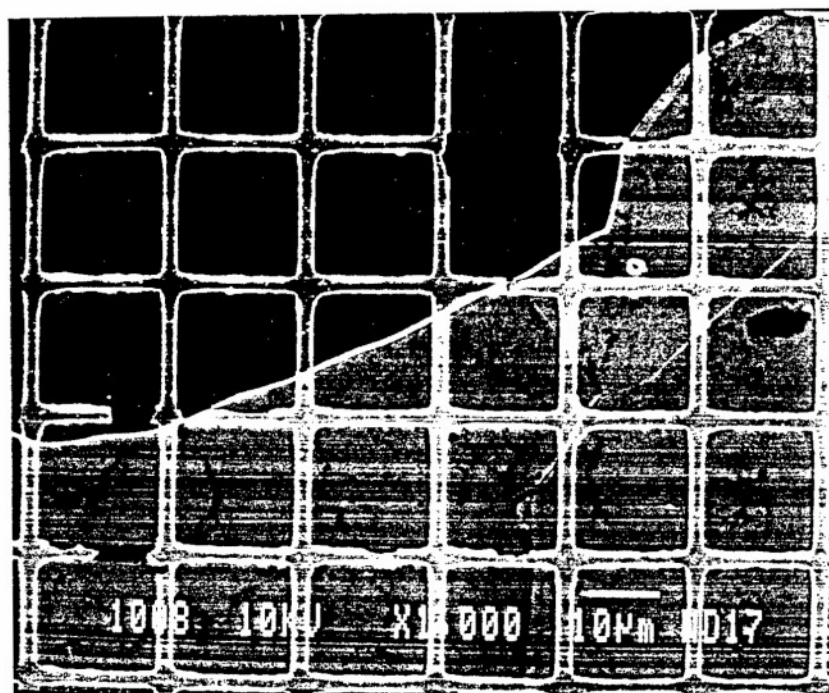
Fig. 32 Microstructure of large grained Ti-0.4Mn ($\sim 100\%$ α) alloy: (a) before creep deformation, (b) the same area after creep deformation, (c) the same area at higher magnification before creep deformation and, (d) after creep deformation. Total creep strain was 3.71% in 474.4 h. The alloy was heat treated for 2 h at 1173 K, FC to 963 K, 200 h, water quenched. The grain size is $\sim 500\ \mu\text{m}$.



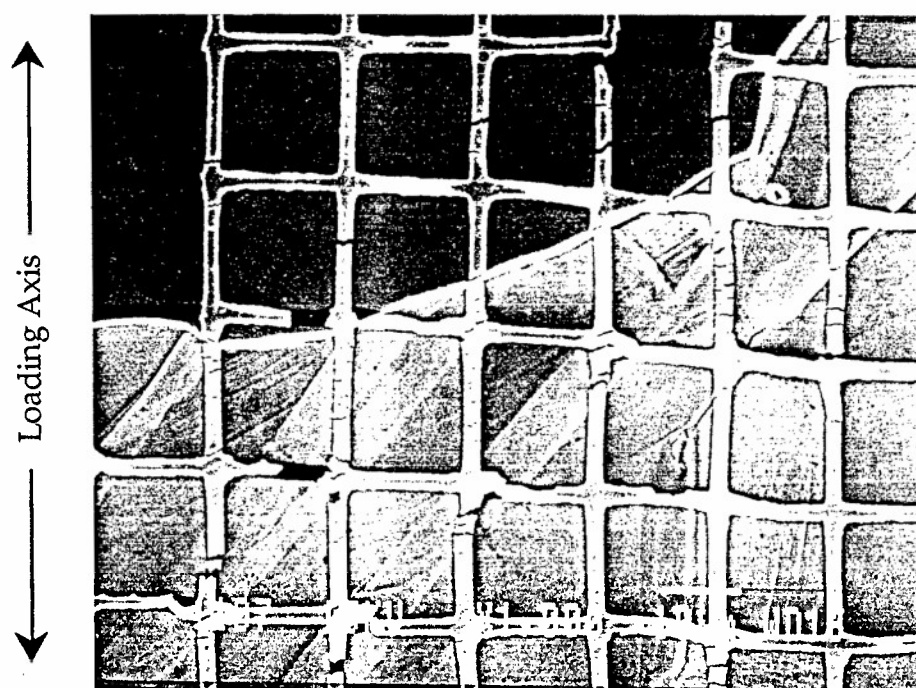
(a)



(b)

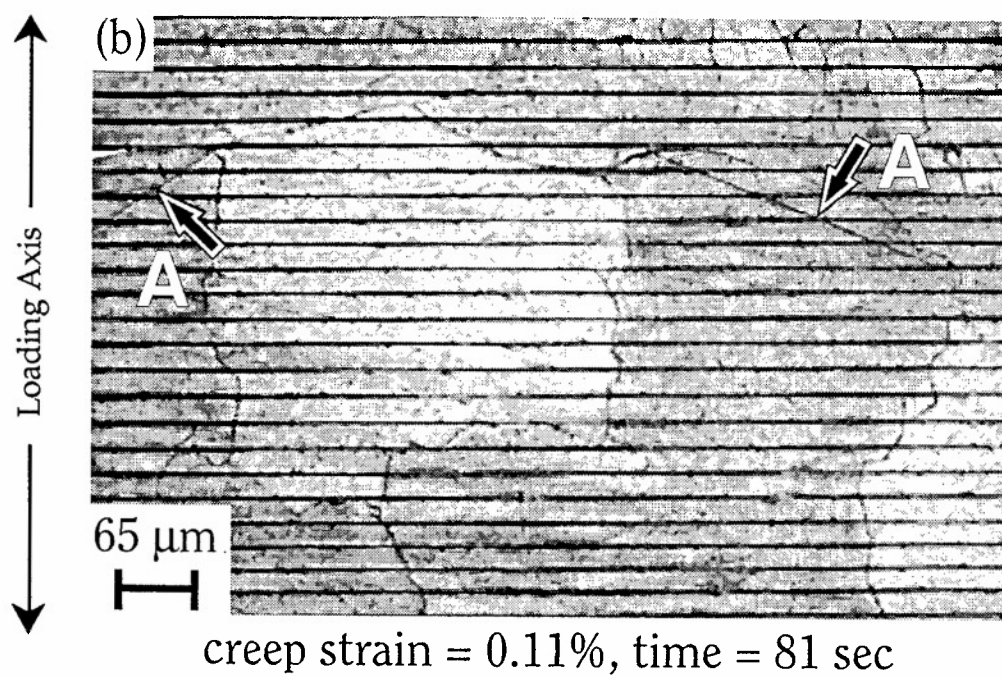
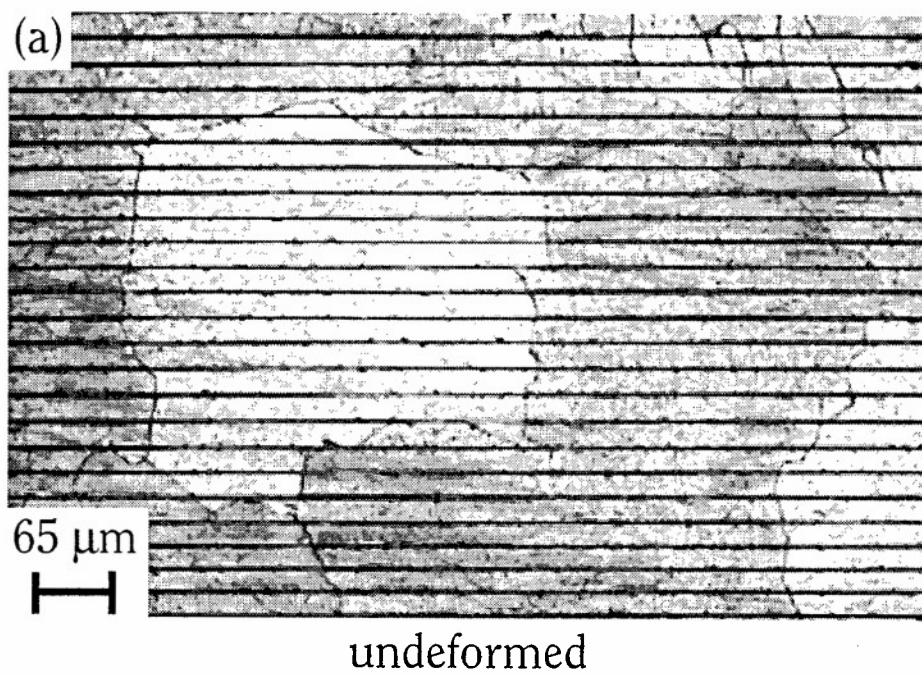


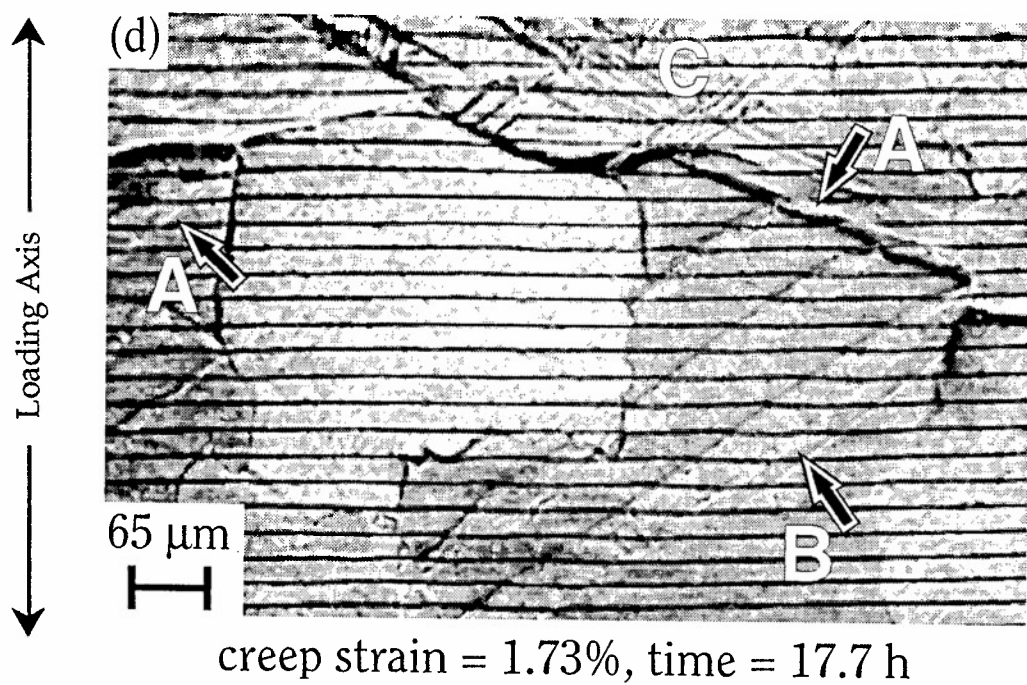
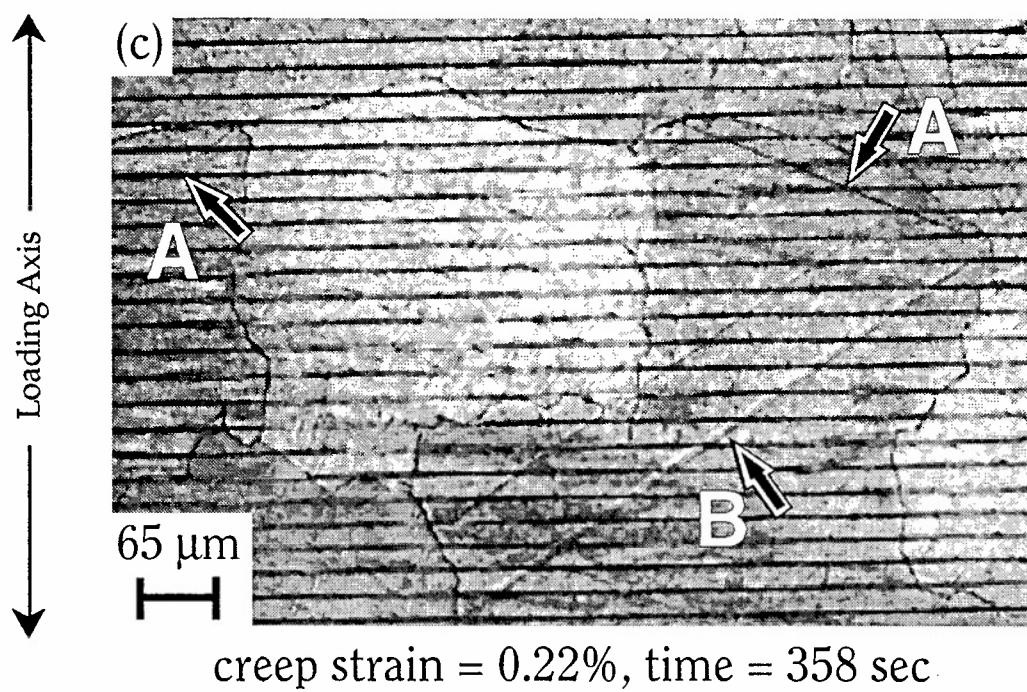
(c)



(d)

Fig. 33 Optical micrographs of (a) undeformed, (b), (c), and (d) deformed α Ti-0.4Mn alloy, Specimen B. Horizontal lines are gold fiducial lines. (b) shows instantaneous twins at "A", (c) shows nucleation of new twins at "B", and (d) shows growth of twins at "A" and "B" and formation of new twins at "C".





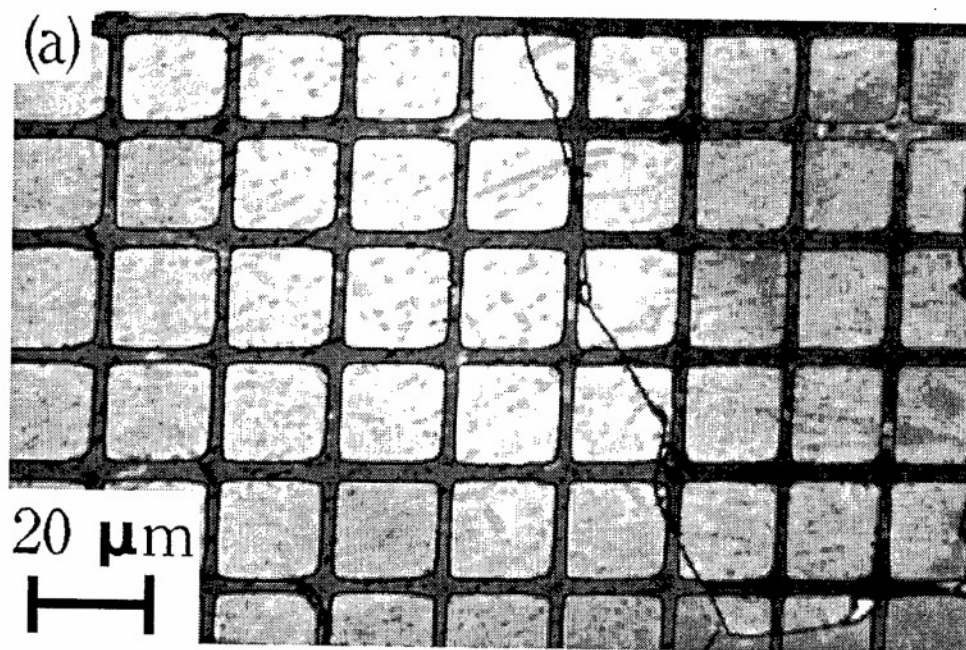
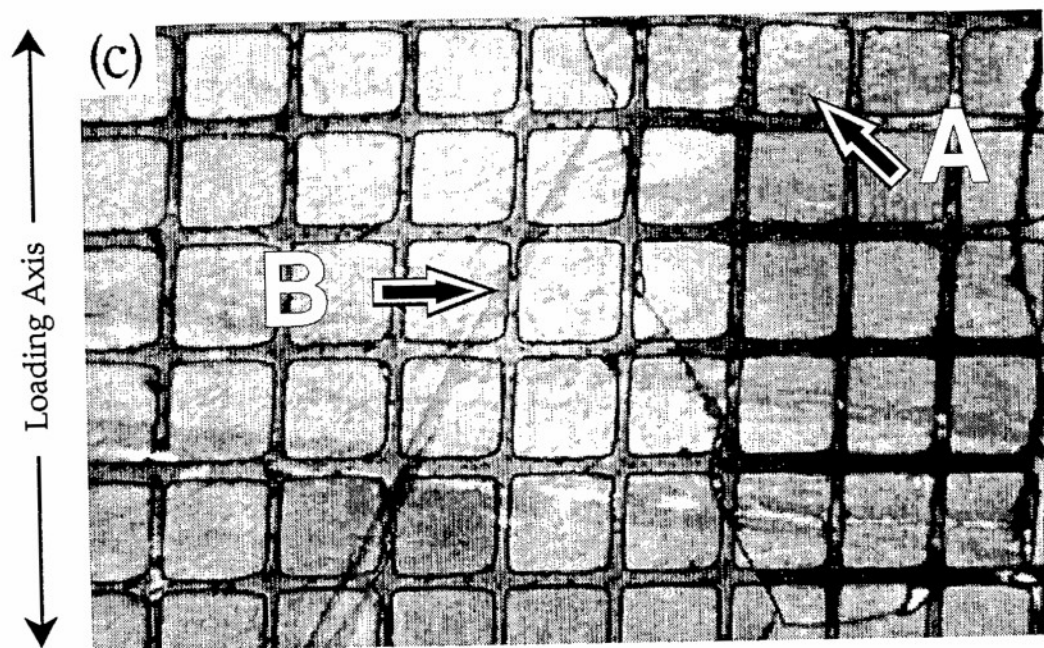
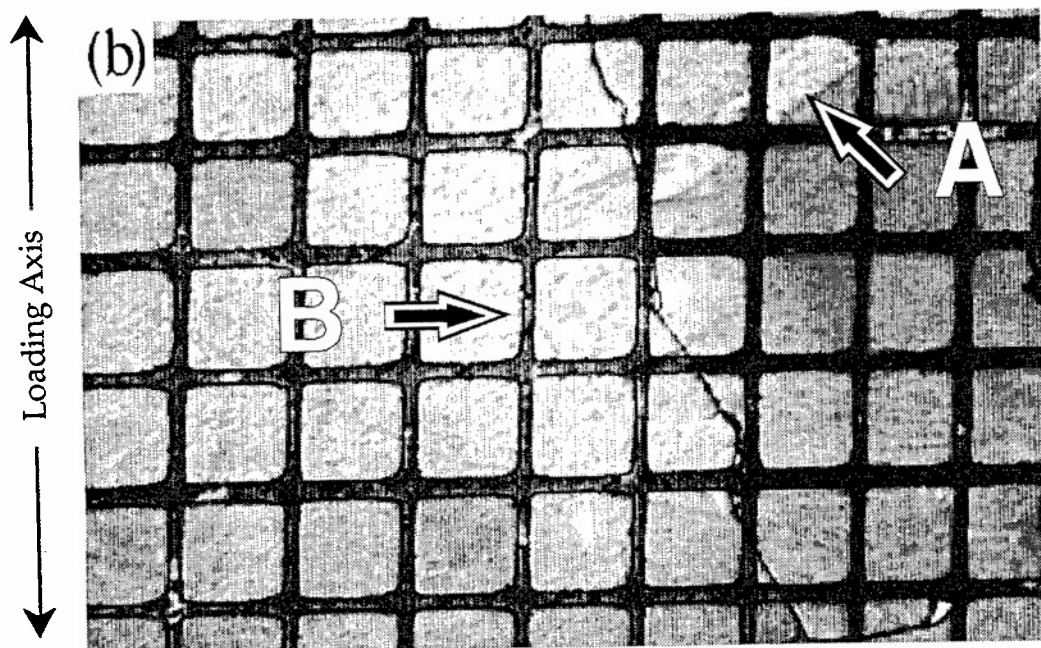


Fig. 34 Optical micrographs of a different area of specimen B. (a) Undeformed, (b) creep strain = 0.61%, time = 0.96 h and (c) creep strain = 1.22%, time = 5.18 h. Note elongation of grid lines in loading direction at "B" in (b), (c) shows formation of twin at "B".



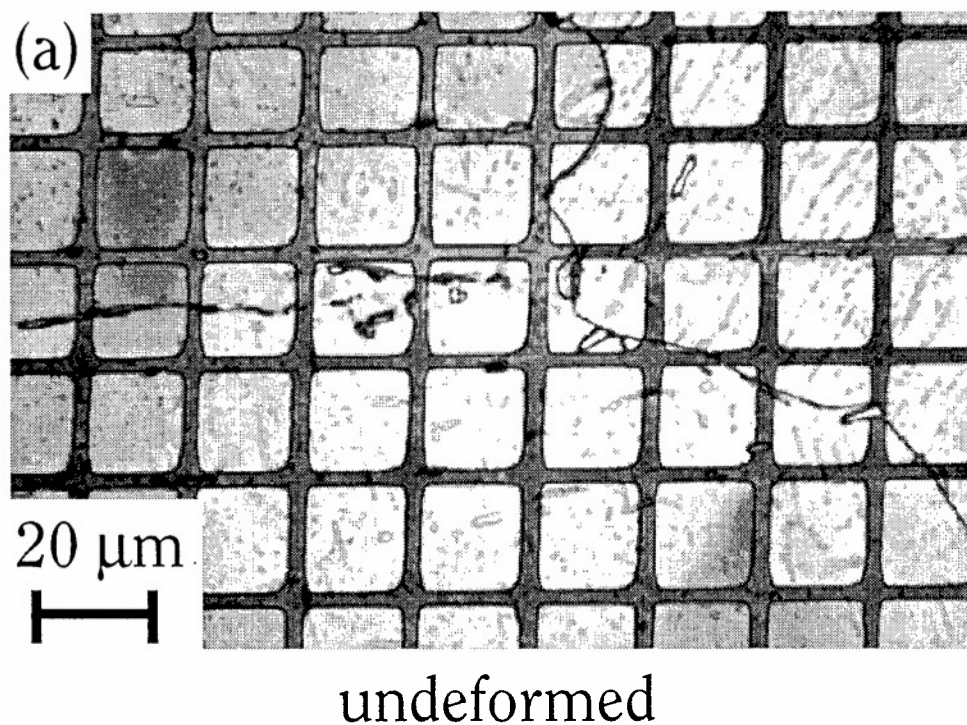
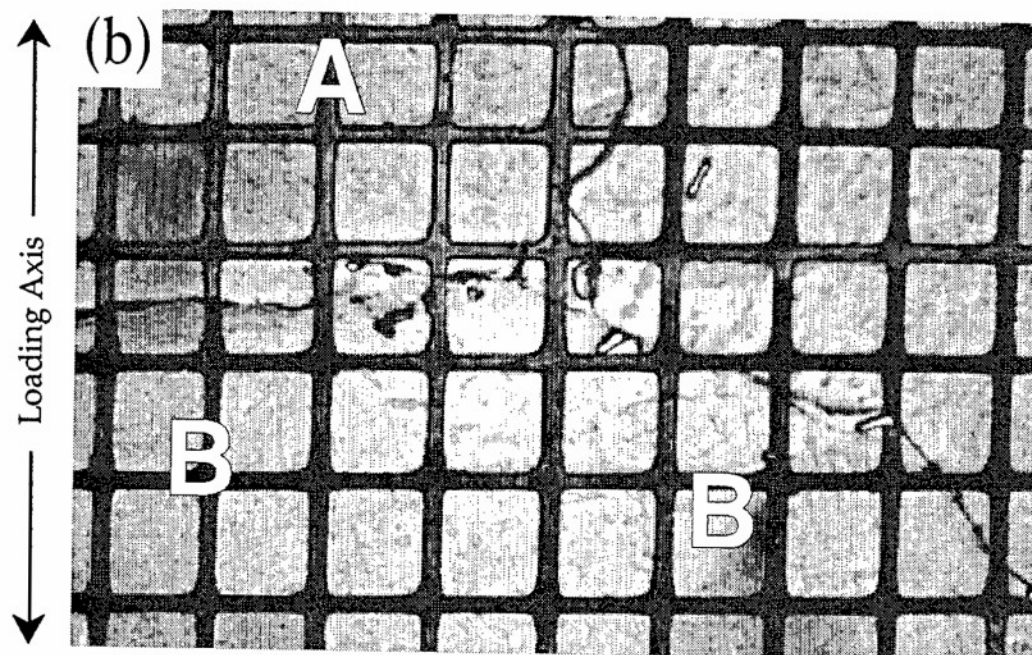
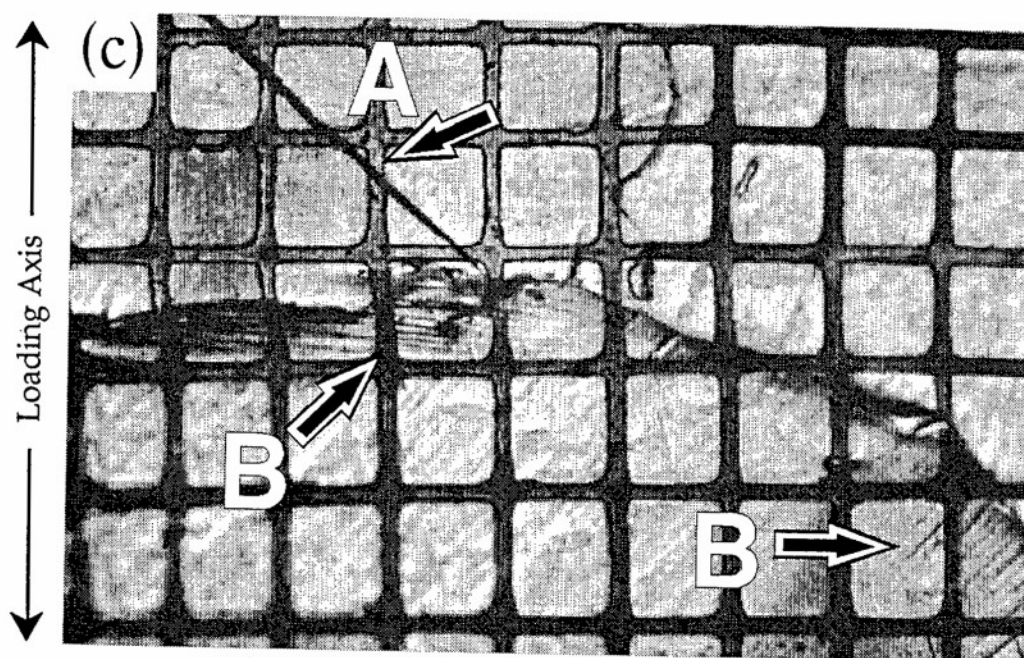


Fig. 35 Optical micrograph of another area of Specimen B. Note grid distortion at "A" and "B" in (b), (c) indicates twinning at "A" and visible coarse slip lines at "B" after large strain.



creep strain = 0.61%, time = 0.96 h



creep strain = 2.82%, time = 115 h

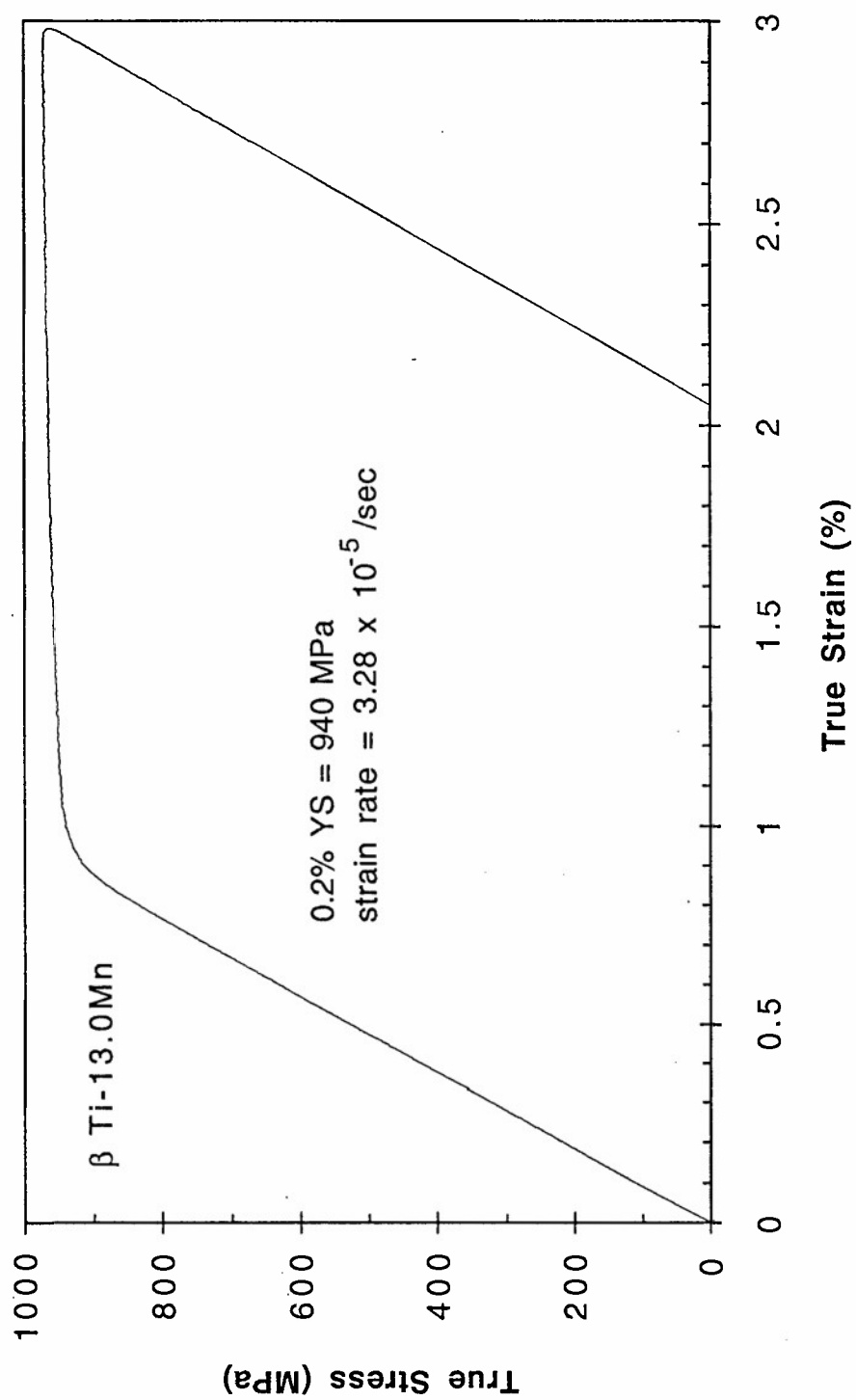
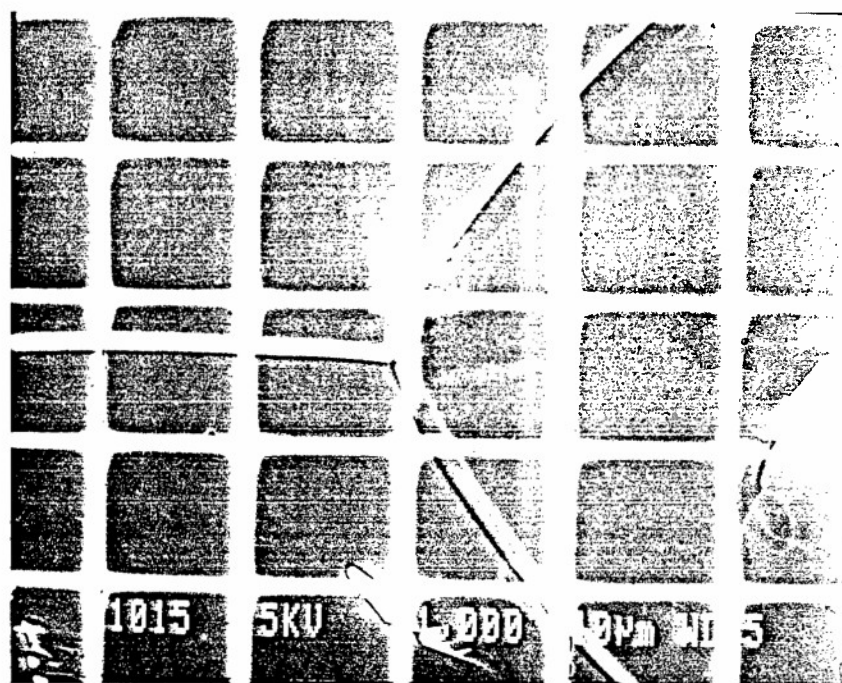
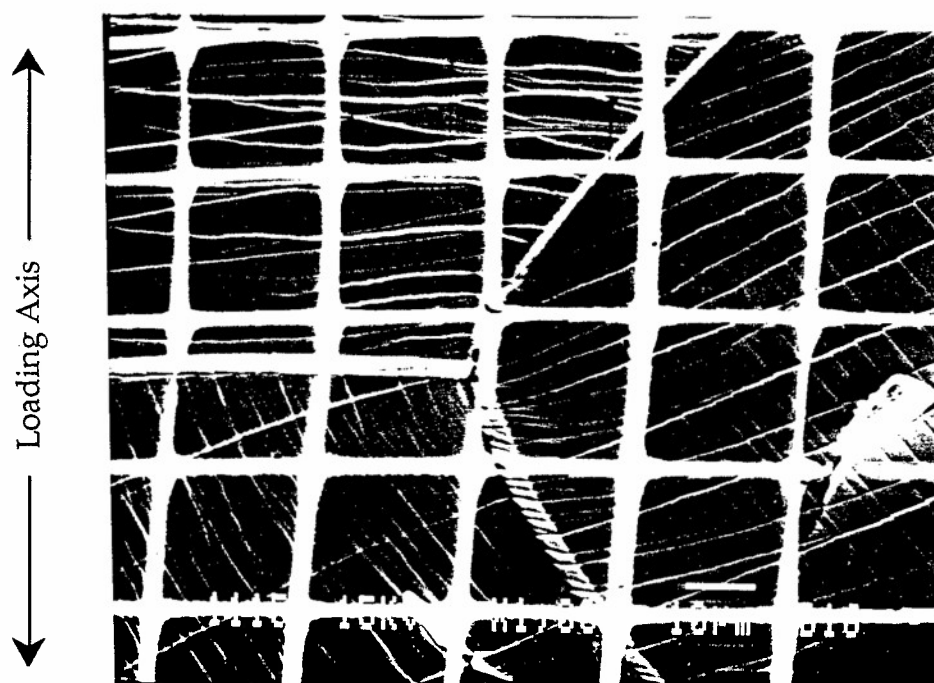


Fig. 36 Ambient temperature true stress - true strain curve of β Ti-13.0Mn alloy.

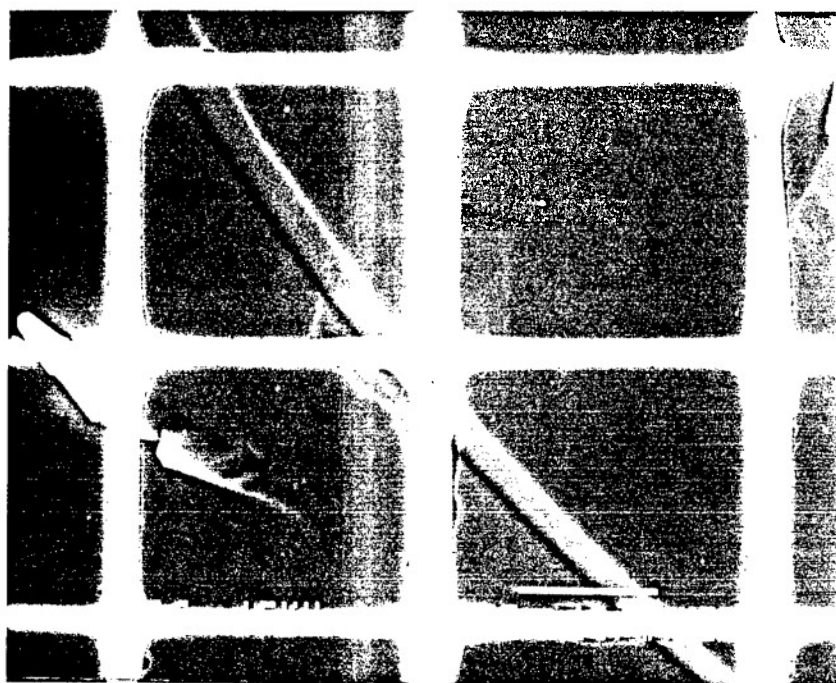
Fig. 37 SEM micrographs of Ti-13.0Mn (~100% β) alloy: (a) before tensile deformation, (b) the same area after tensile deformation, note slip bands, (c) another area of the same specimen before tensile deformation and, (d) after tensile deformation, note slip bands. Total plastic strain is 2.1% at strain rate 3.28×10^{-5} per second. The alloy was heat treated for 200 h at 963 K and water quenched. The grain size is $\sim 200 \mu\text{m}$.



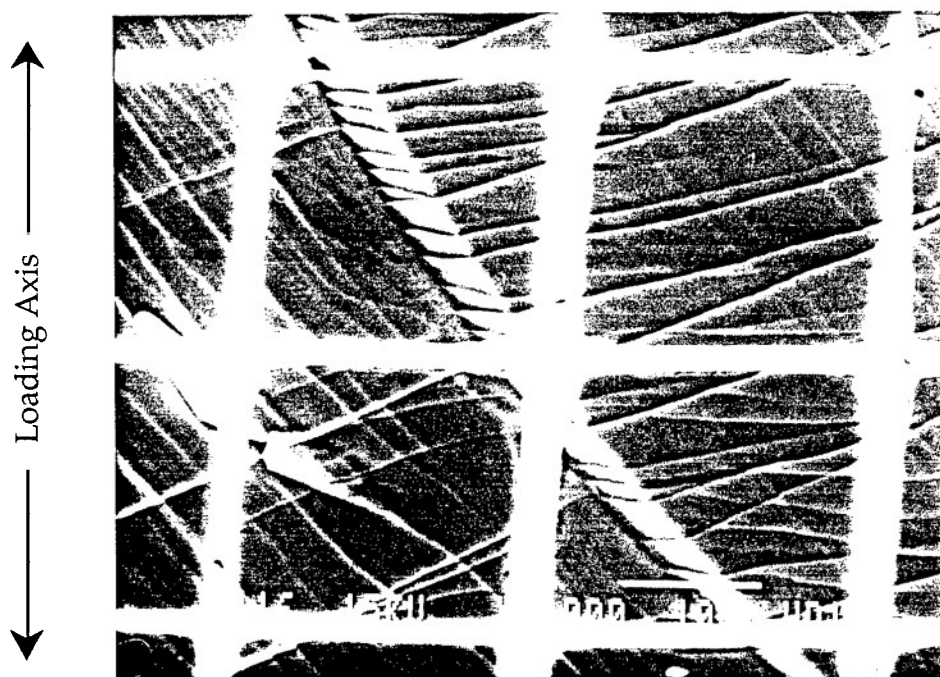
(a)



(b)



(c)



(d)

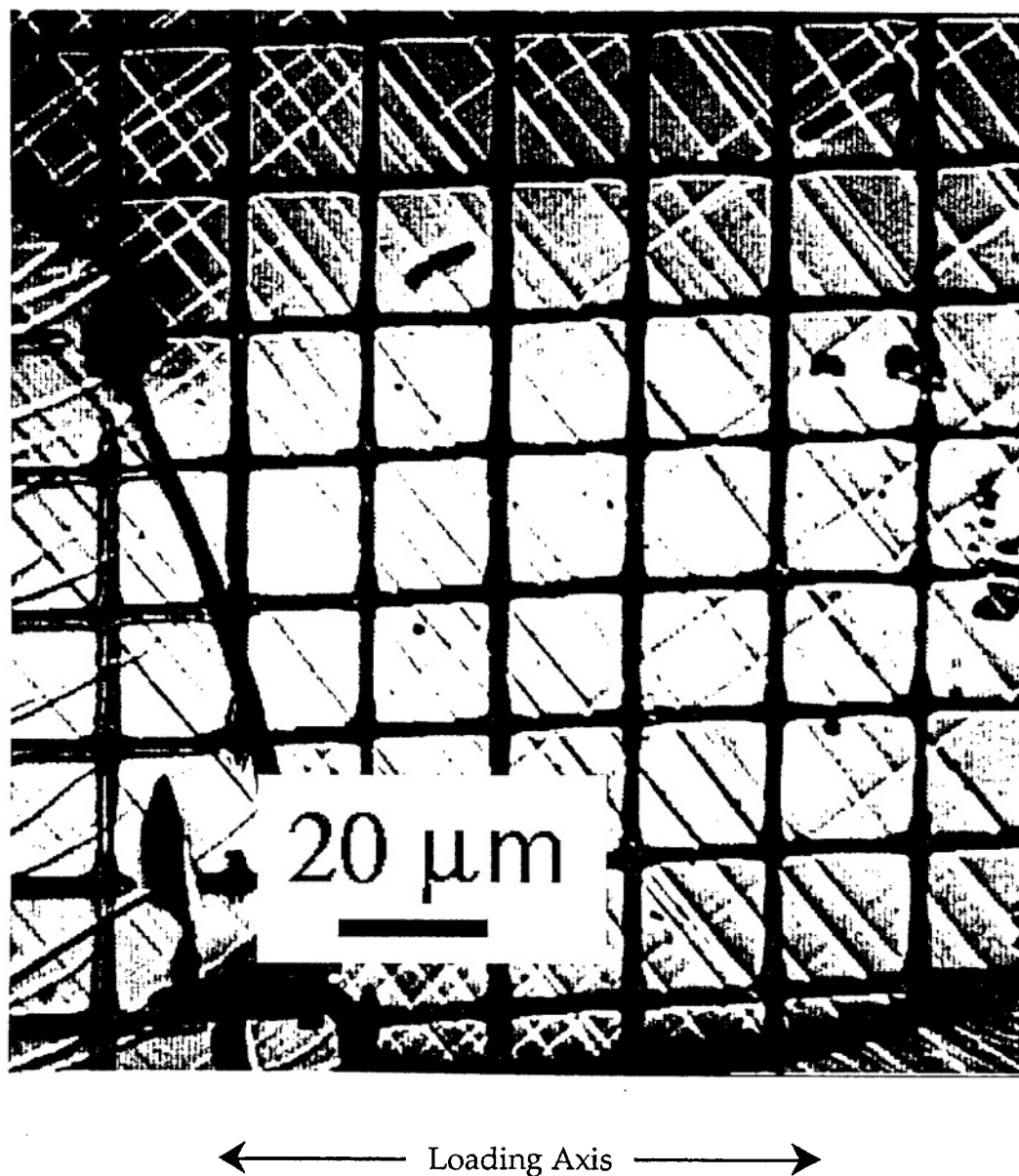


Fig. 38 Optical micrograph of β Ti-13.0Mn alloy after tensile deformation to 2.10% plastic strain, note coarse slip lines.

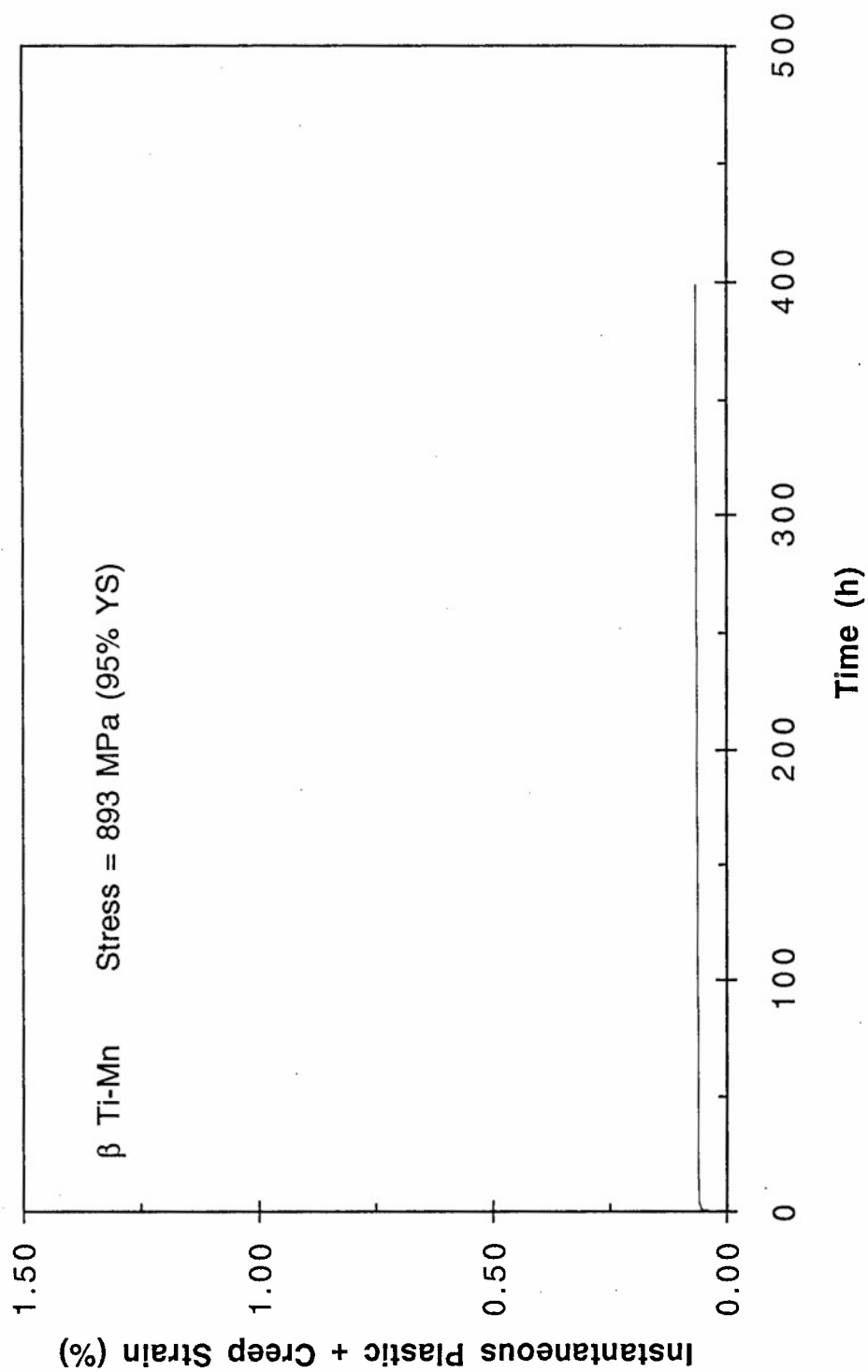
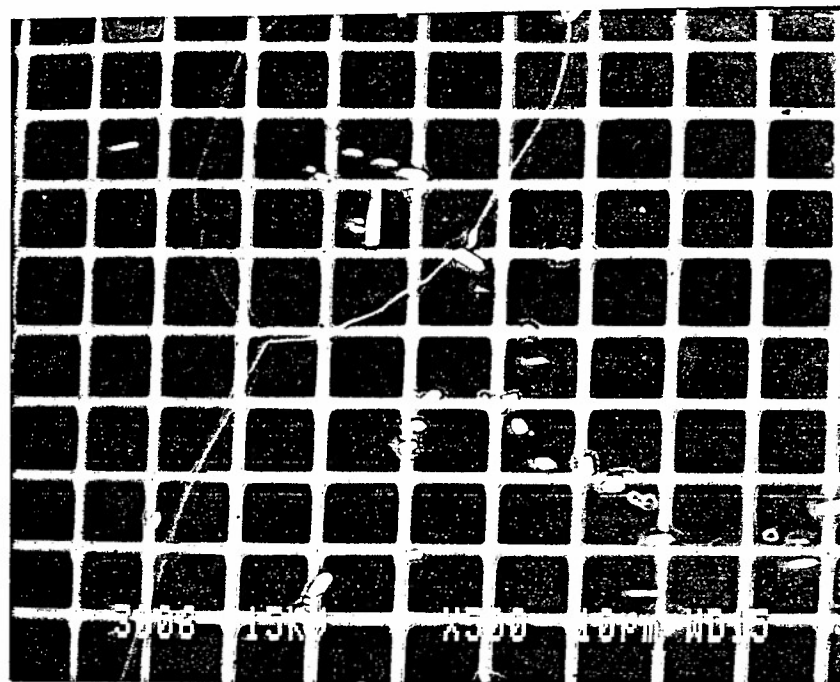
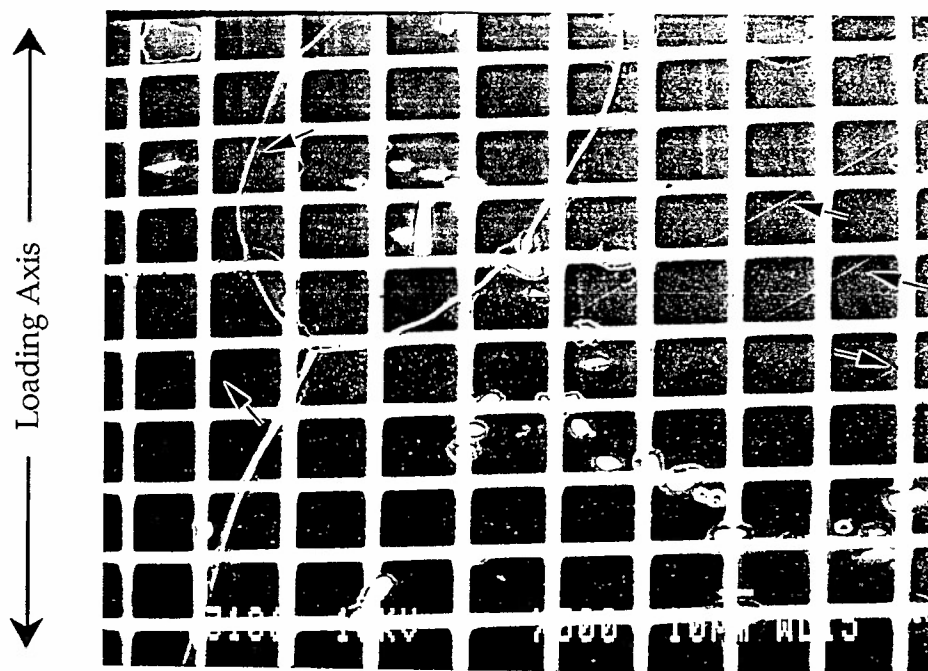


Fig. 39 Ambient temperature creep curve of β Ti-13.0Mn alloy, crept at 95% YS.

Fig. 40 SEM micrographs of Ti-13.0Mn (~100% β) alloy (a) before creep deformation and, (b) the same area after creep deformation, note slip bands at arrows. The total creep is 0.03% in 408 h. The grain size is ~ 200 μm .



(a)



(b)

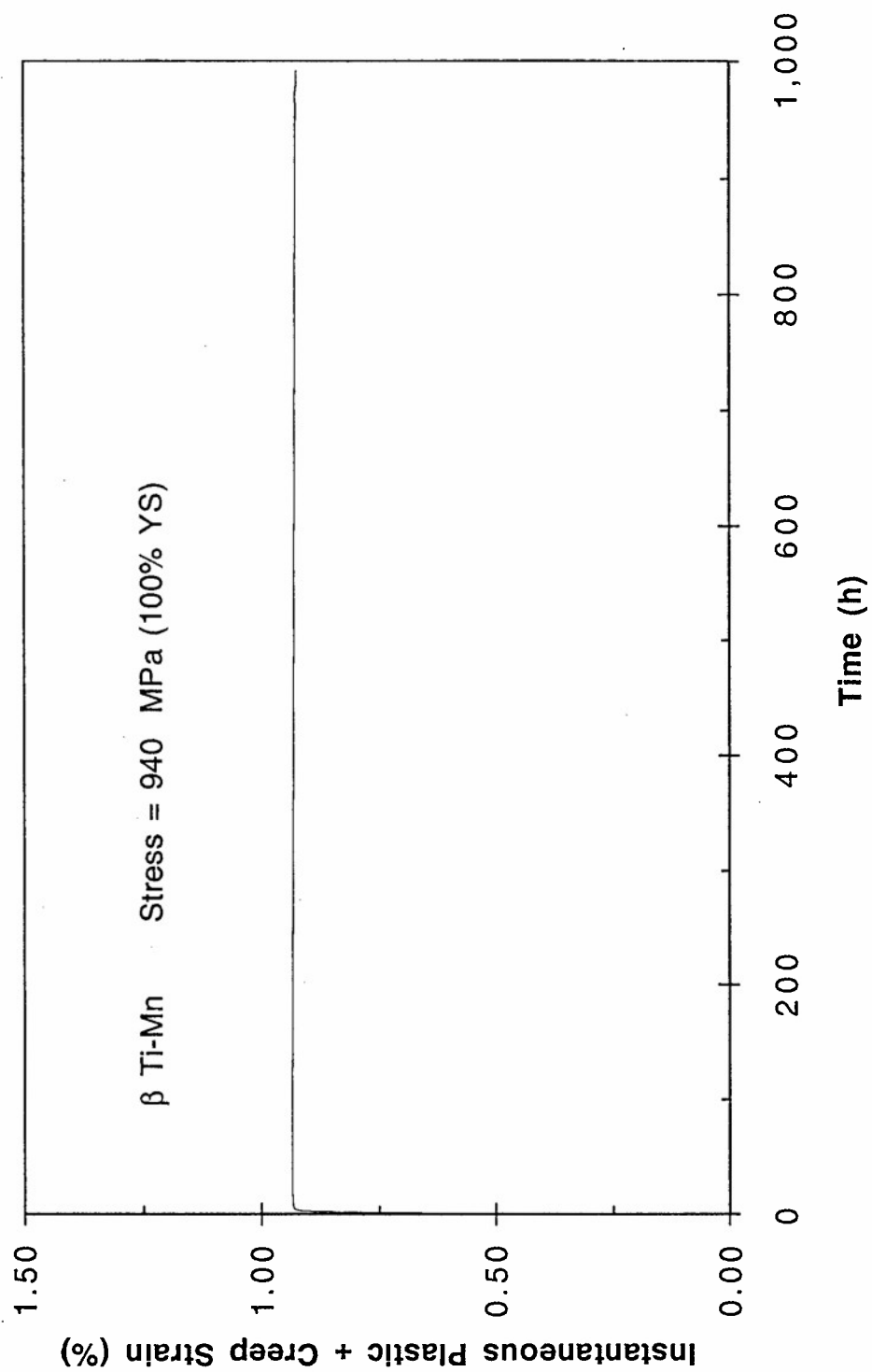


Fig. 41 Ambient temperature creep curve of β Ti-13.0Mn crept at 100% YS.

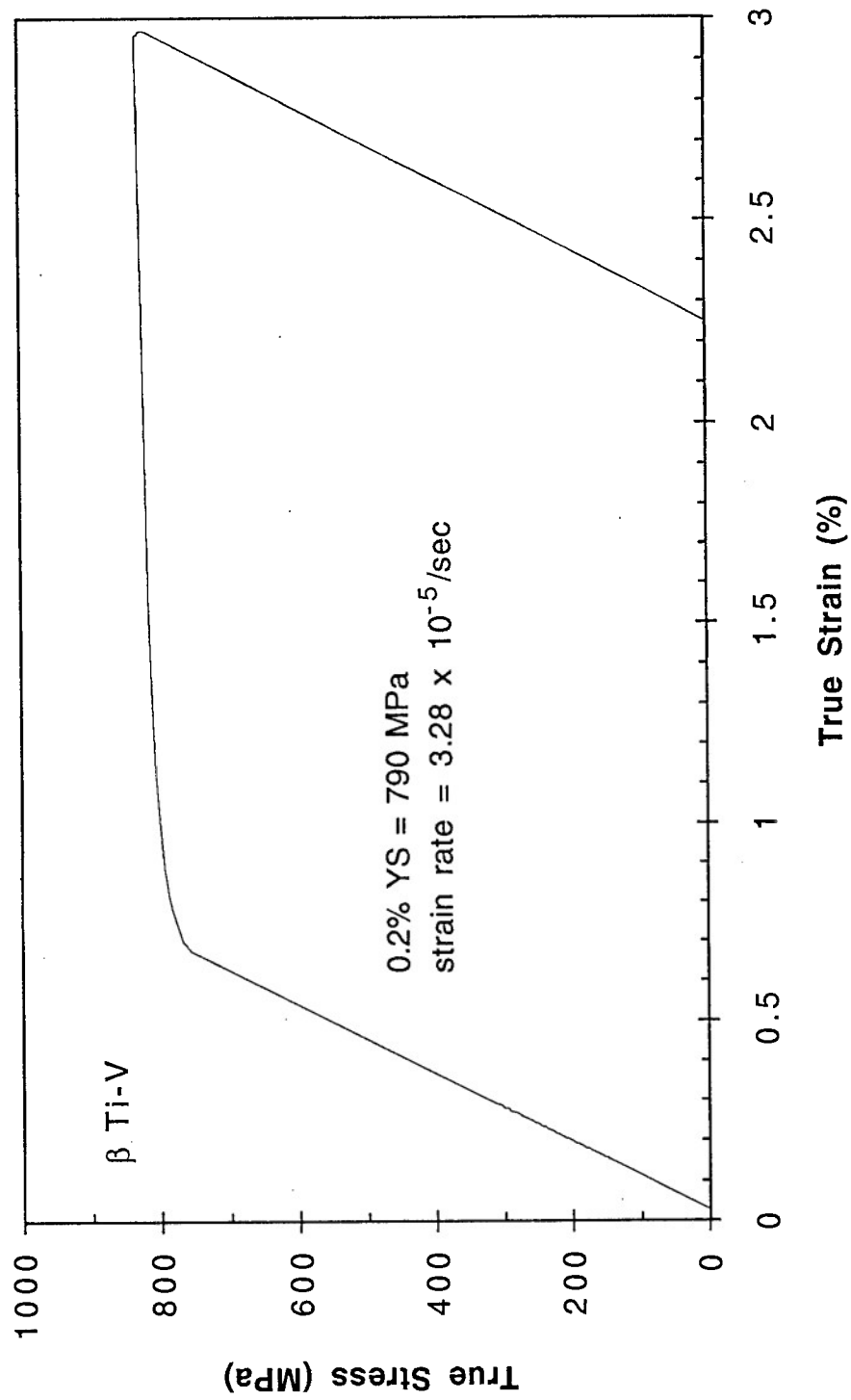
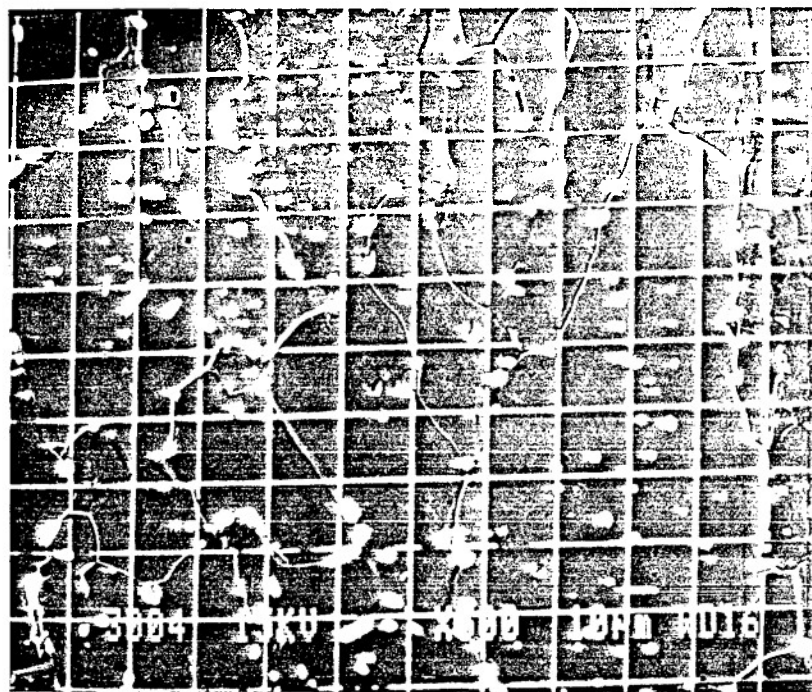


Fig. 42 Ambient temperature true stress - true strain curve of β Ti-14.8V alloy.

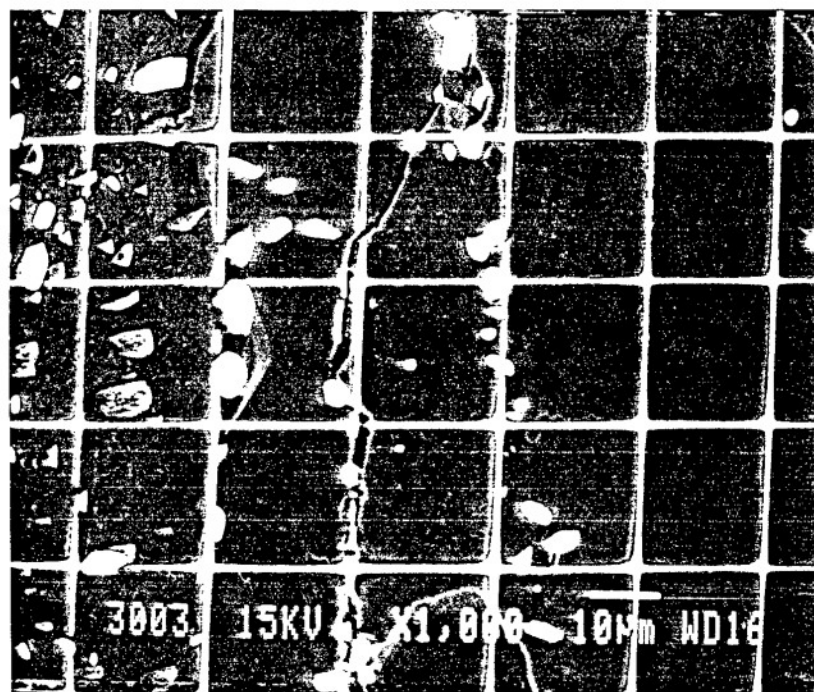
Fig. 43 SEM micrographs of Ti-14.8V (~100% β) alloy: (a) before tensile deformation, (b) the same area after tensile deformation, note twinning at the arrows, (c) another area of the same specimen before tensile deformation and, (d) after tensile deformation, note slip bands and twinning at the arrows. Total plastic strain is 2.25% at a strain rate of 3.28×10^{-5} per second. The grain size is $\sim 30 \mu\text{m}$.



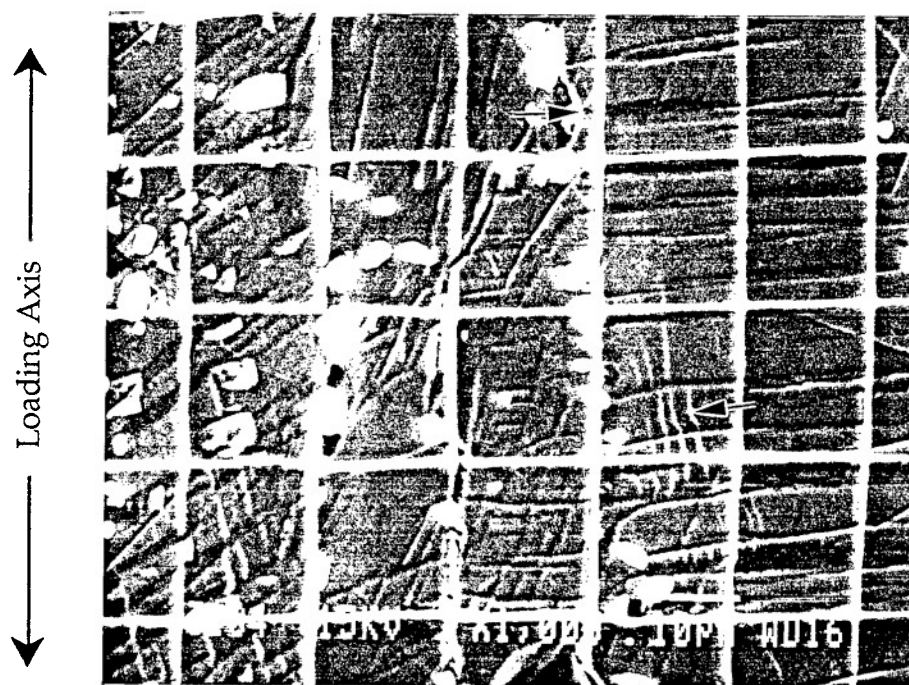
(a)



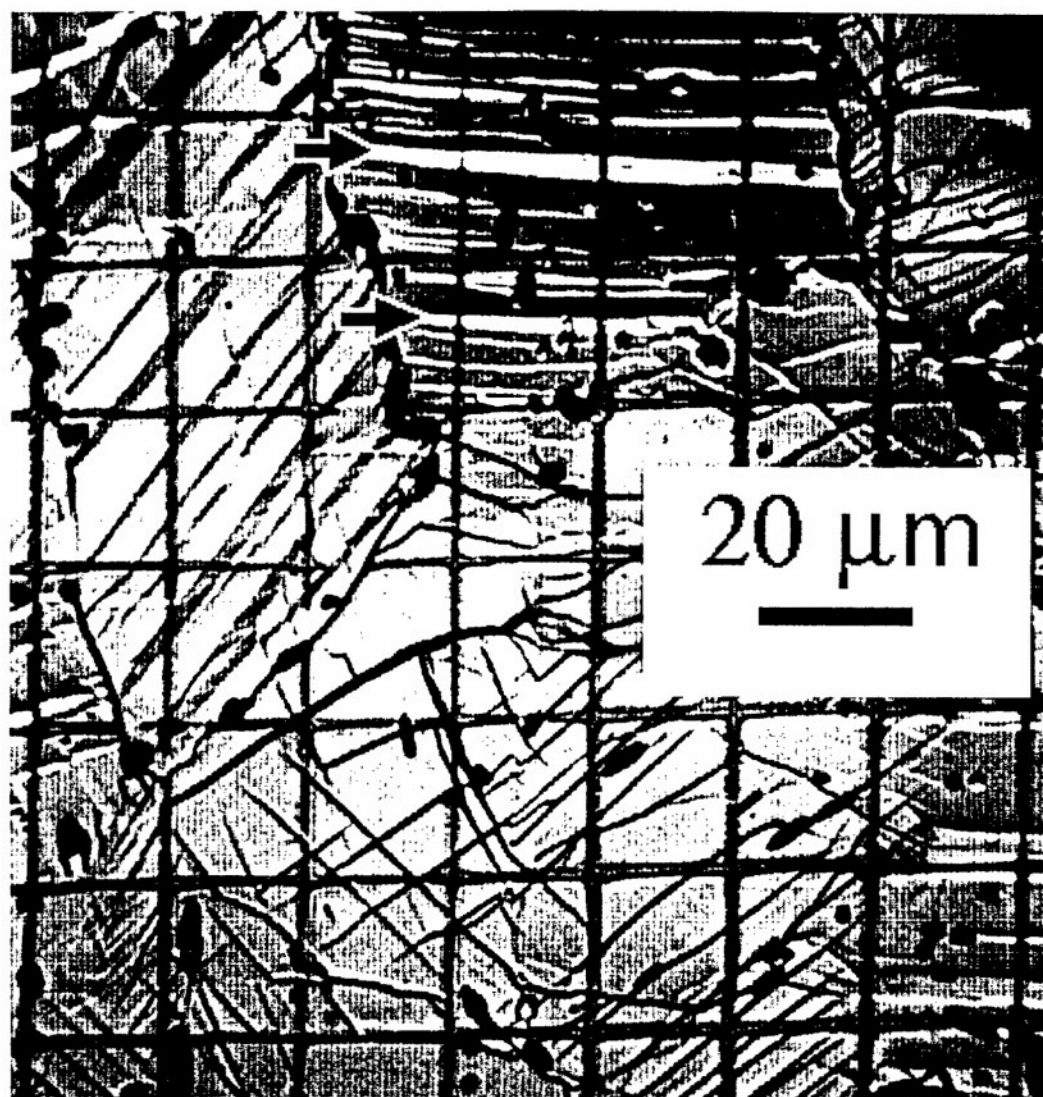
(b)



(c)



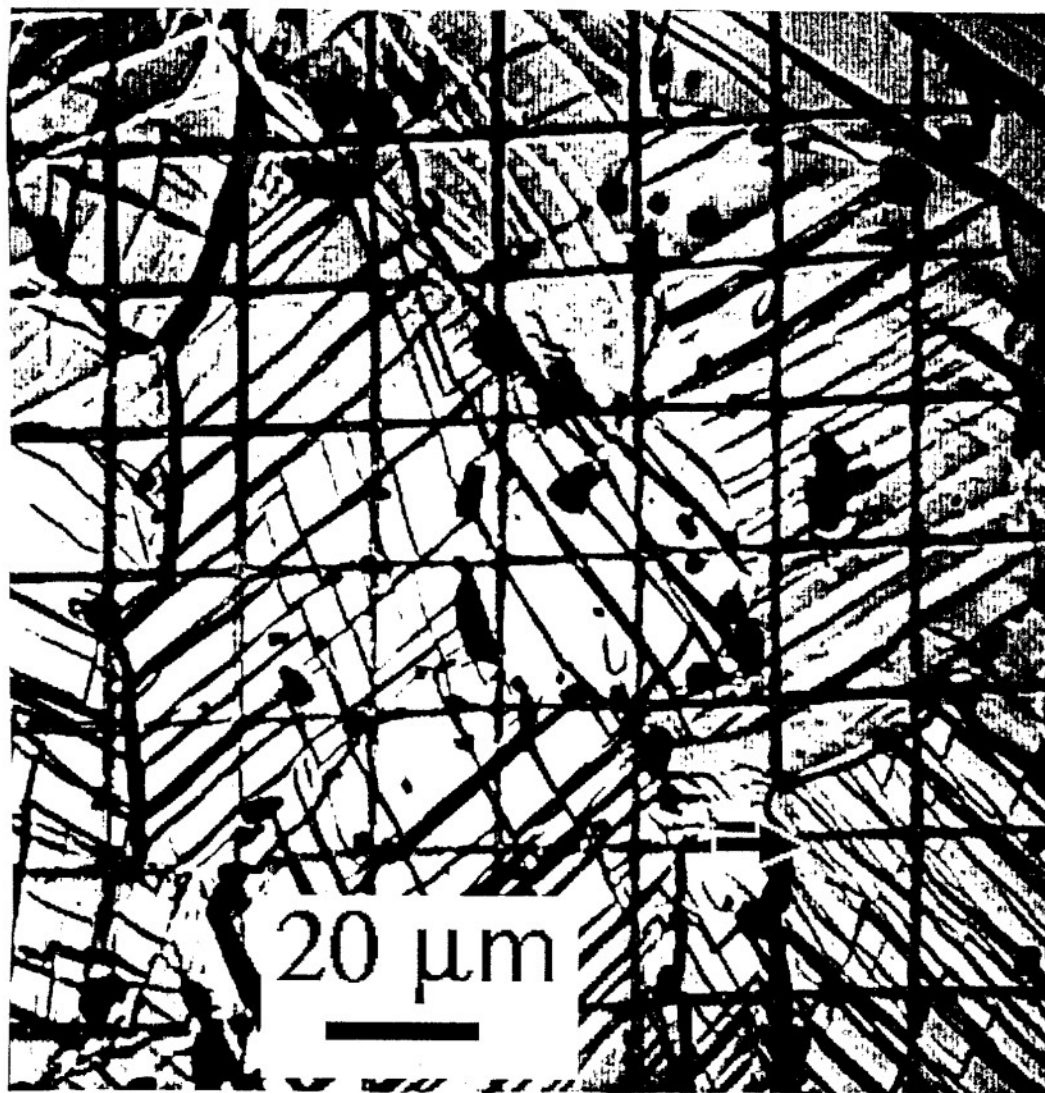
(d)



← Loading Axis →

(a)

Fig. 44 Optical micrograph of β Ti-14.8V alloy after tensile deformation to 2.25% plastic strain. Note twinning in (a) and slip lines in (b).



← Loading Axis →

(b)

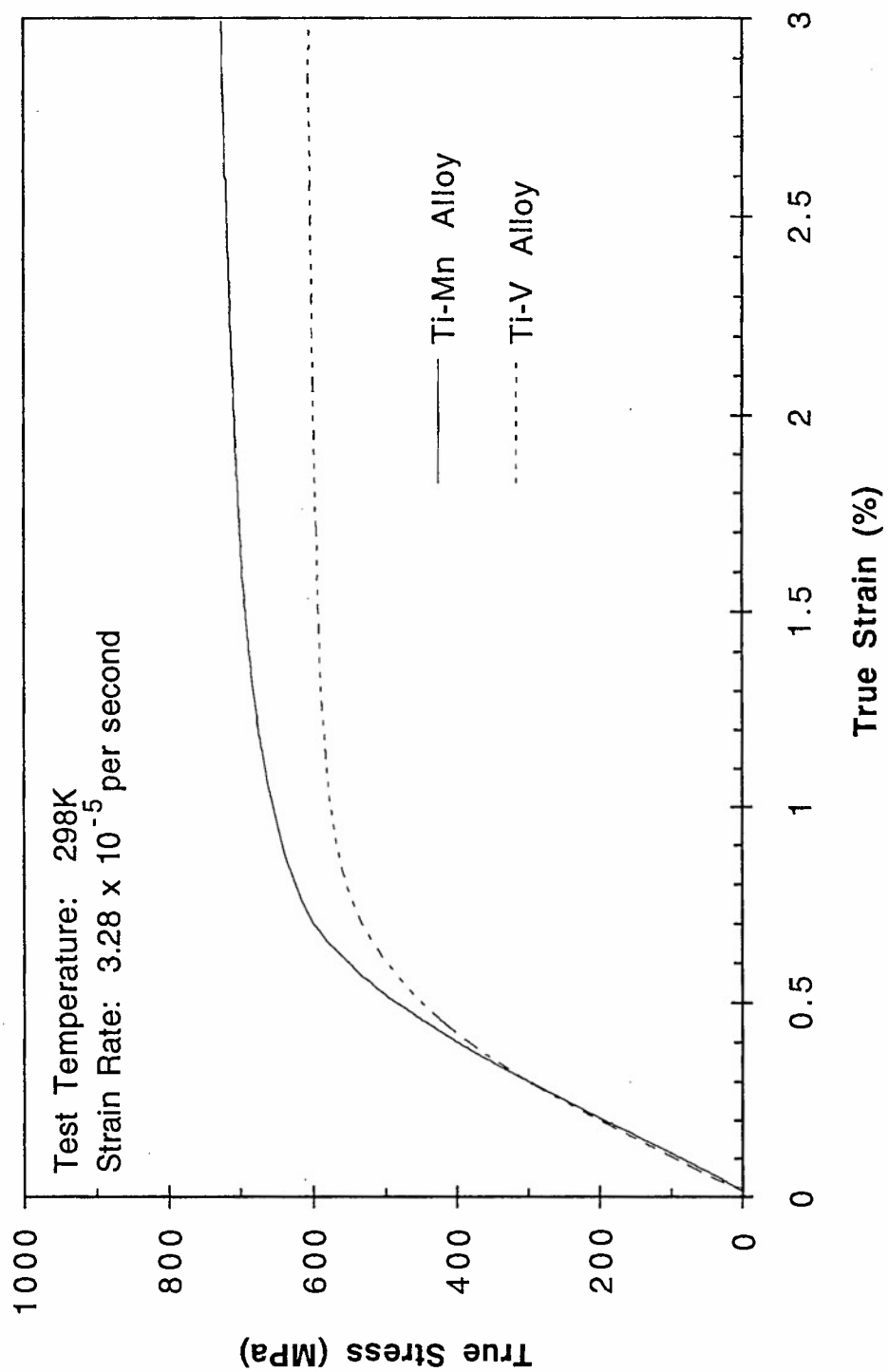
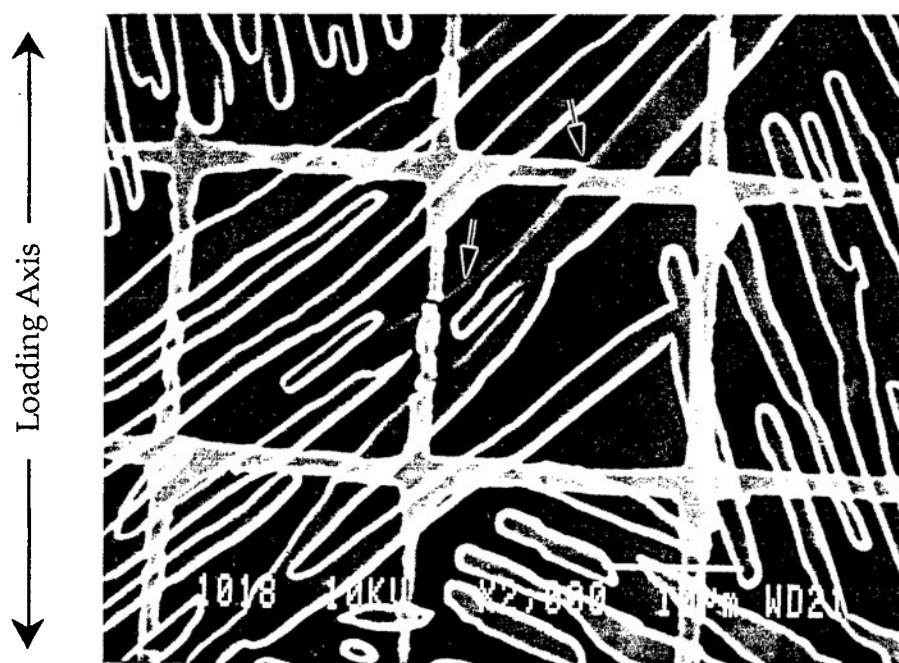


Fig. 45 Ambient temperature true stress - true strain curves of α - β Ti-6.0Mn and Ti-8.1V alloys.

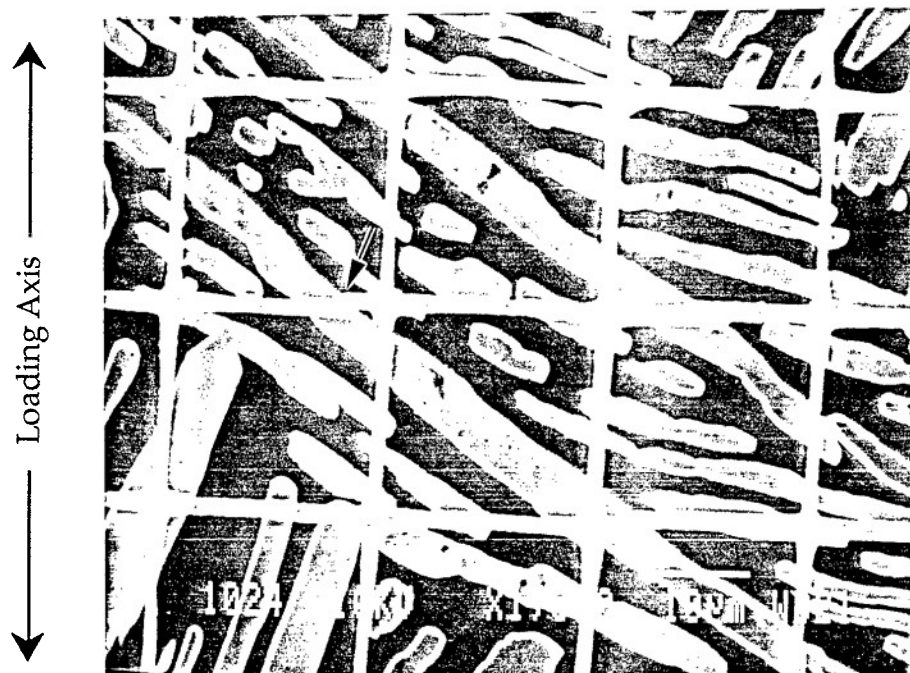
Fig. 46 SEM Micrograph of Ti-6.0Mn (~46% α - 54% β) alloy: (a) before tensile deformation, (b) the same region after tensile deformation, note slip line in the β phase, (c) after deformation, note inter-phase sliding, and (d) after deformation, note twin in α phase. Total plastic strain is 2.25% at strain rate of $3.28 \times 10^{-5} \text{ s}^{-1}$. The alloy was heat treated for 2 h at 1173 K, FC to 963 K, annealed for 200 h at 963 K, and water quenched.



(a)



(b)



(c)



(d)

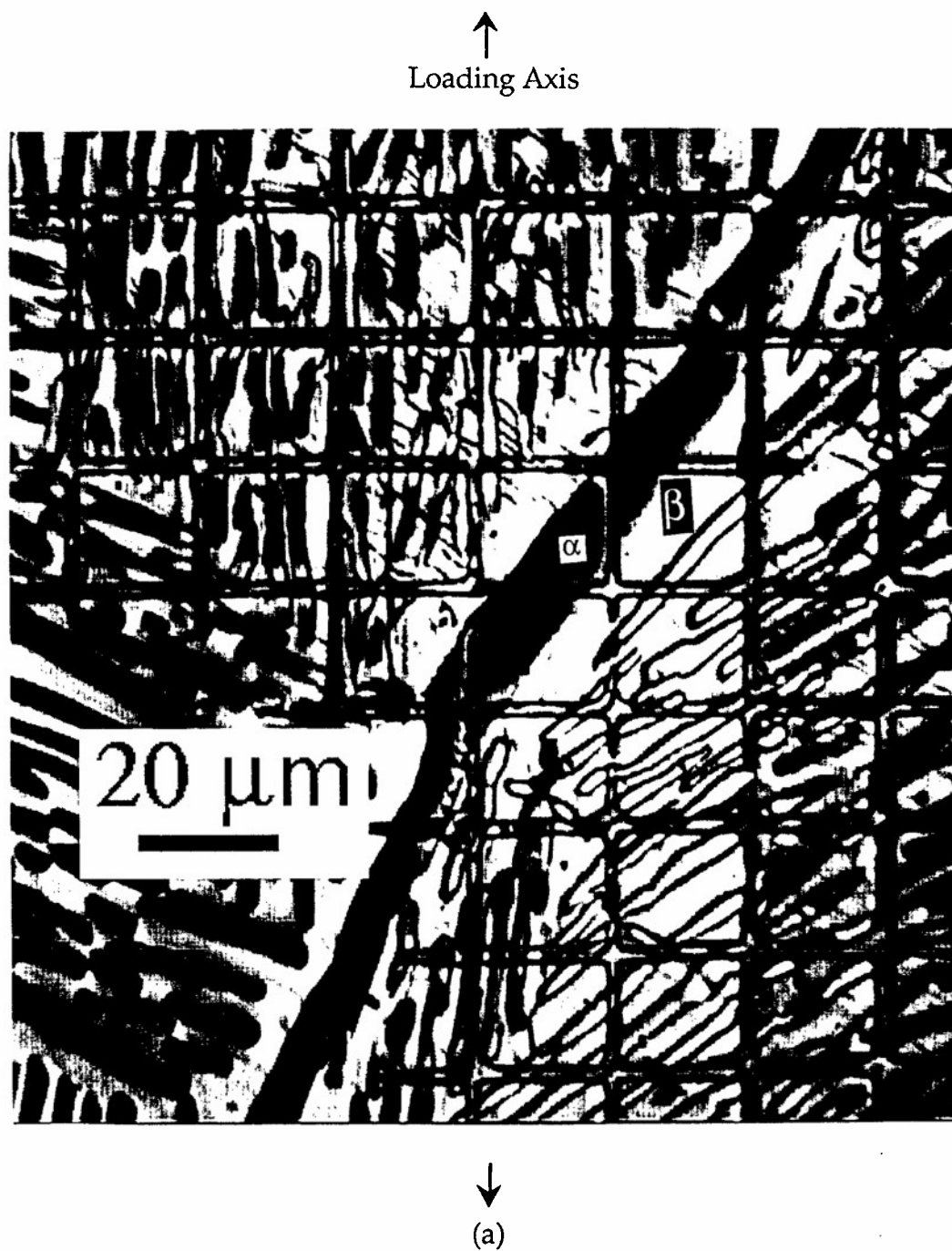
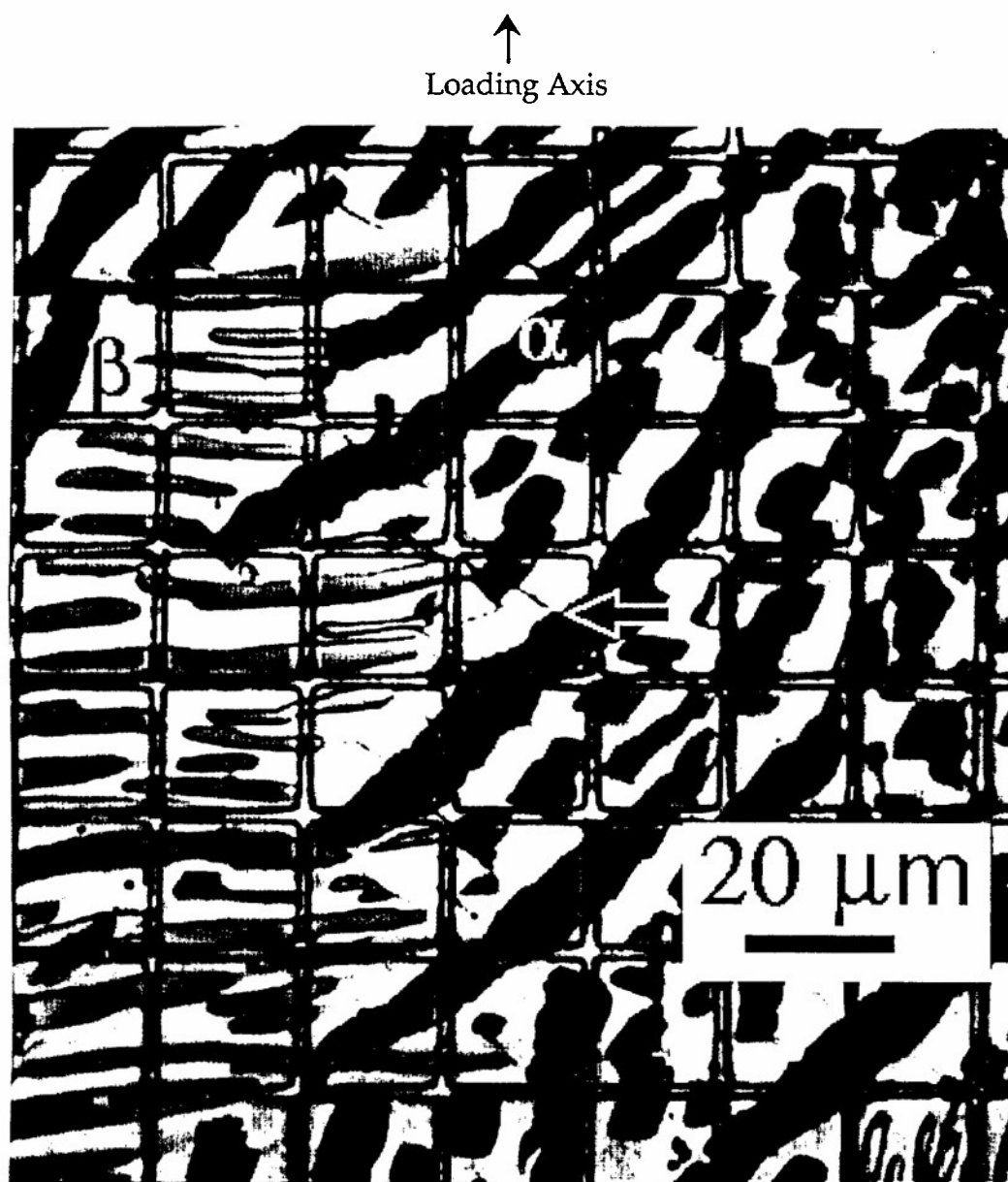


Fig. 47 Optical micrograph of α - β Ti-6.0Mn alloy after tensile deformation to 2.25%, (a) coarse slip in β phase matrix, coarse slip lines do not go through the α phase platelets, (b) another area of the same sample.



(b)

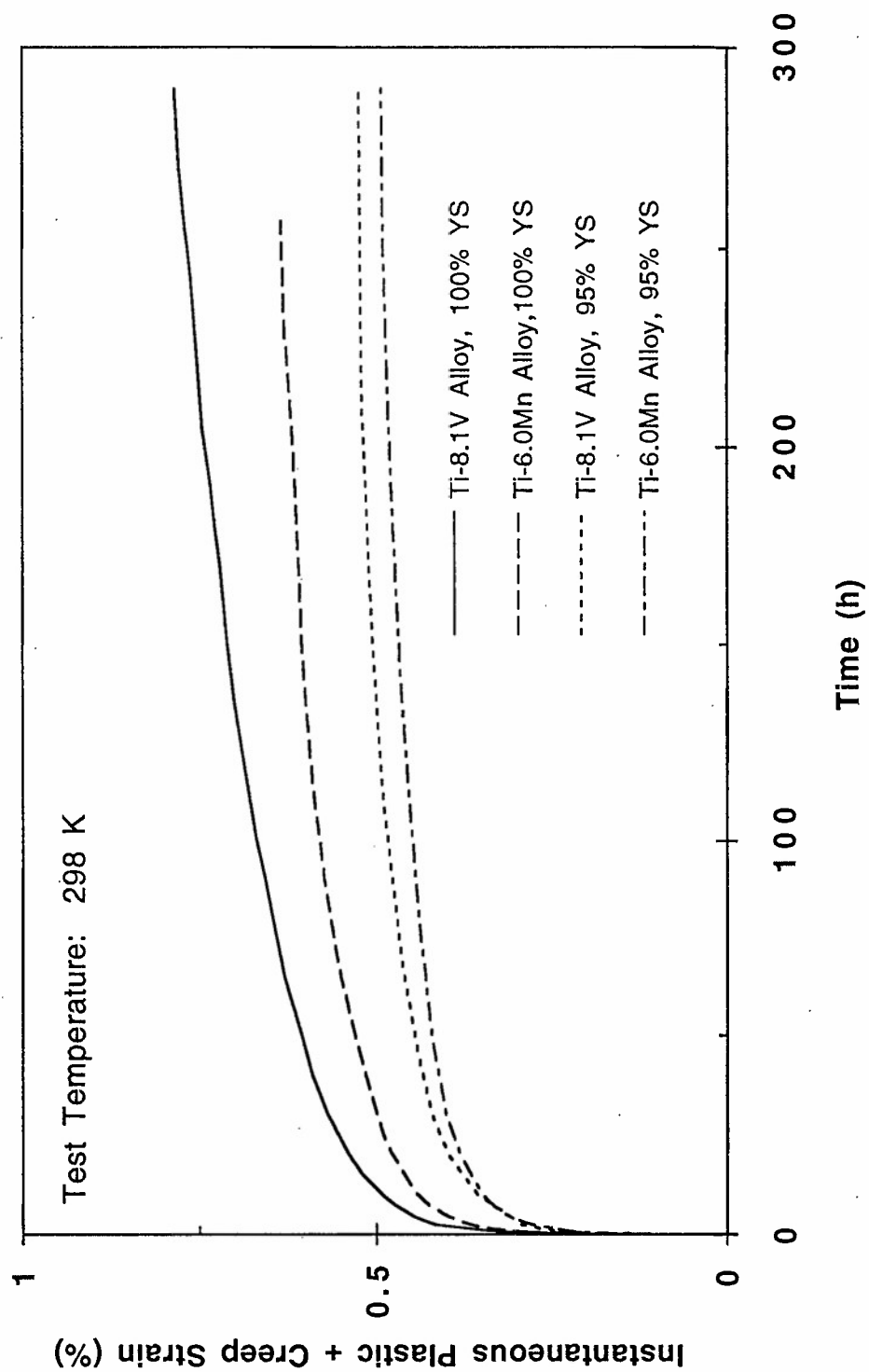
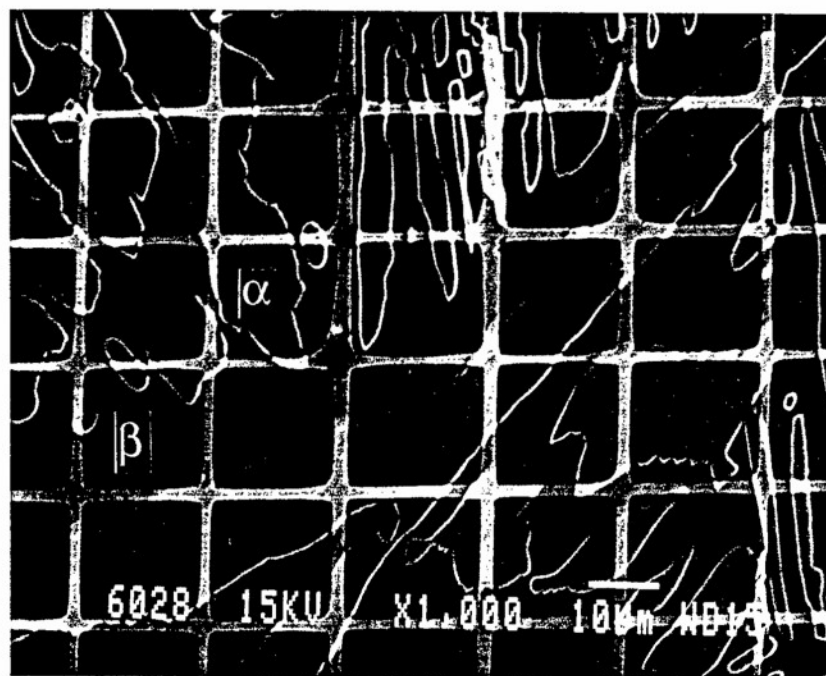


Fig. 48 Ambient temperature creep curves of α - β Ti-6.0Mn and Ti-8.1V alloys at 95% and 100% yield stress.

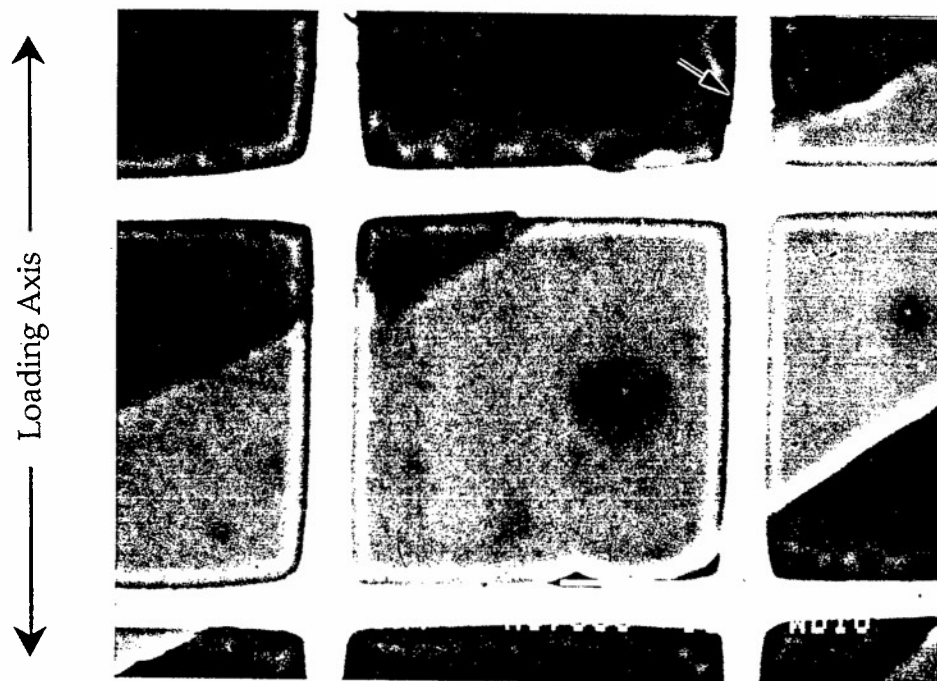
Fig. 49 SEM micrographs of Ti-6.0Mn ($\sim 46\% \alpha - 54\% \beta$) alloy: (a) before creep deformation, (b) the same area after creep deformation and (c) the same area after deformation at a higher magnification. Note interface sliding. Creep strain is 0.62% in 257.8 h at 100% YS. The alloy was heat treated for 2 h at 1173 K, FC to 963 K, annealed for 200 h and water quenched.



(a)

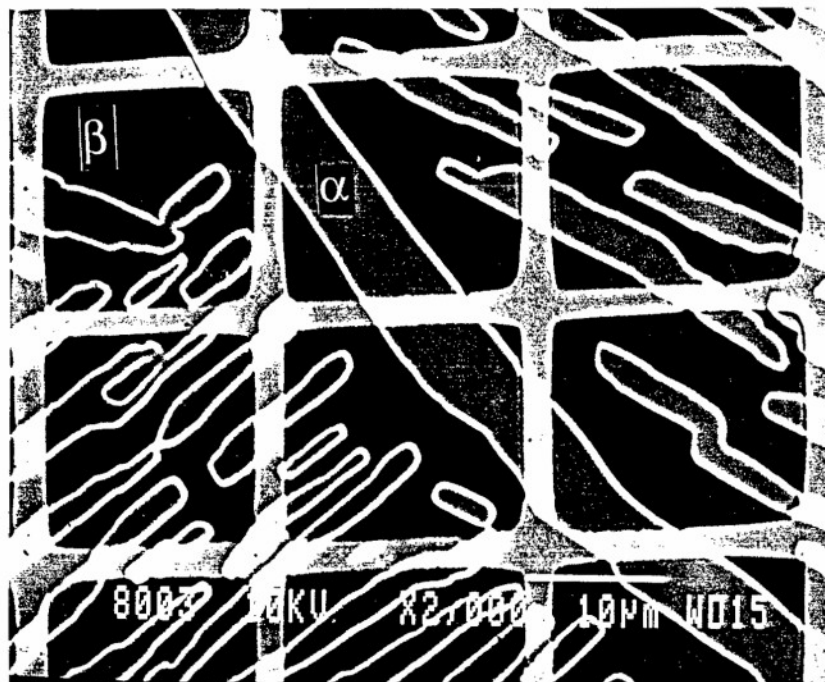


(b)

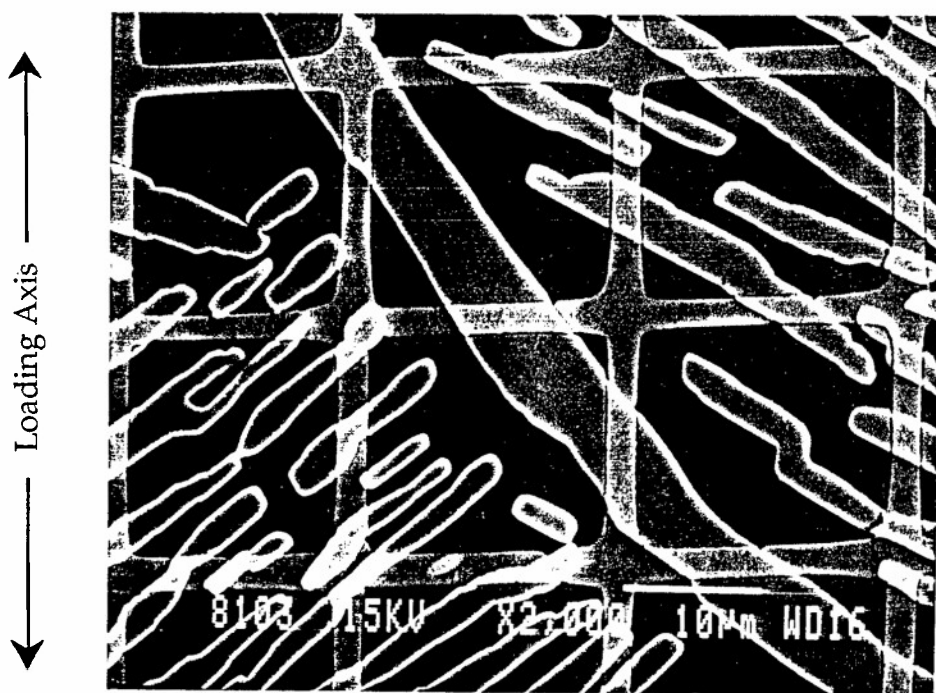


(c)

Fig. 50 SEM micrographs of Ti-6.0Mn ($\sim 46\% \alpha - 54\% \beta$) alloy: (a) before creep deformation and (b) the same area after creep deformation. Creep strain is 0.40% in 405.1 h at 95% YS. The alloy was heat treated for 2 h at 1173 K, FC to 963 K, annealed for 200 h and water quenched.



(a)



(b)

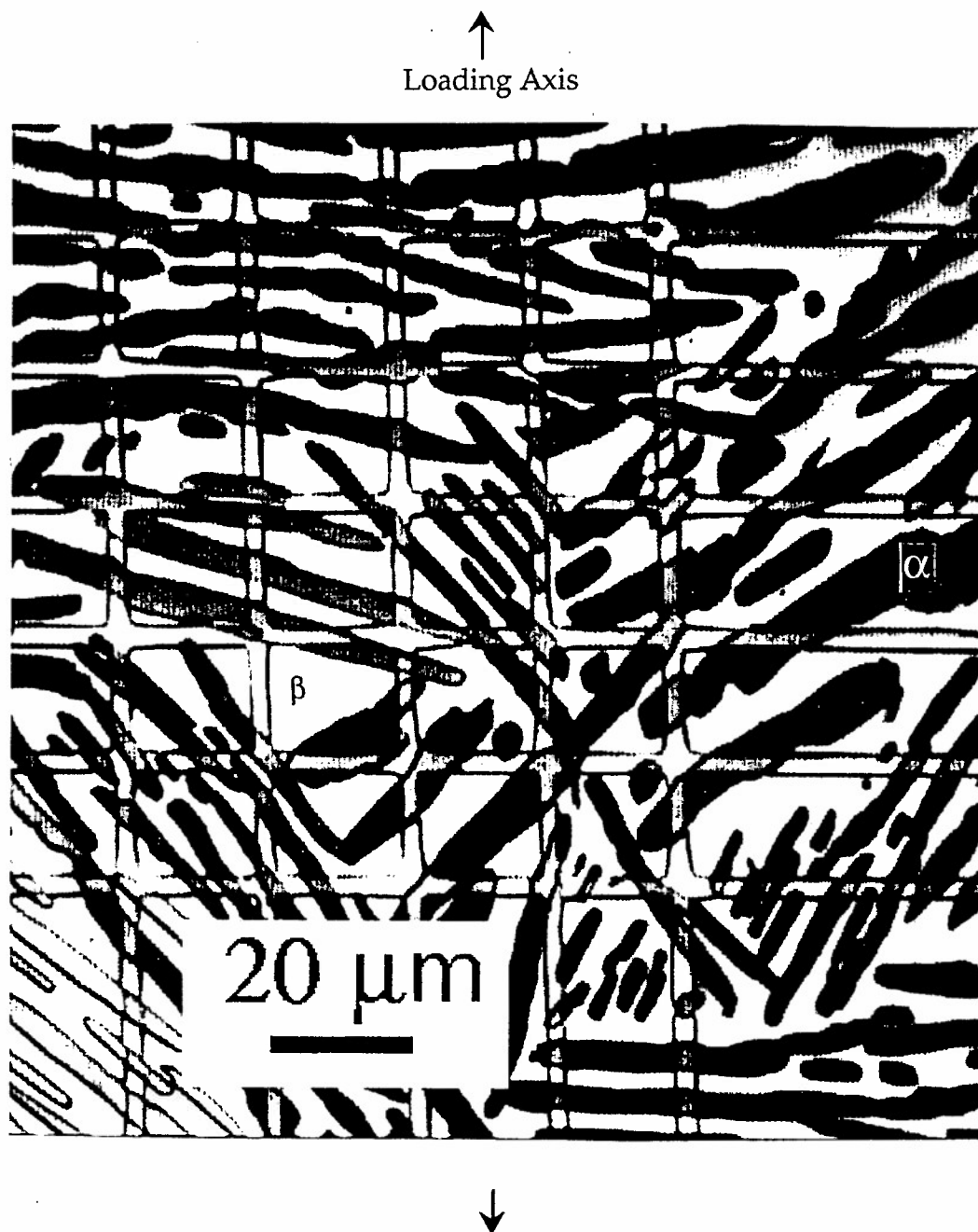
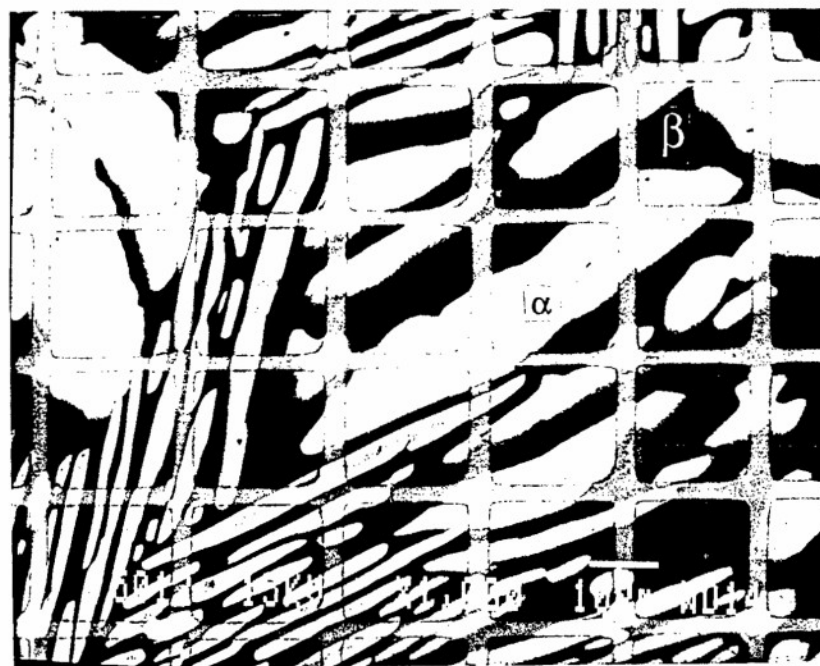


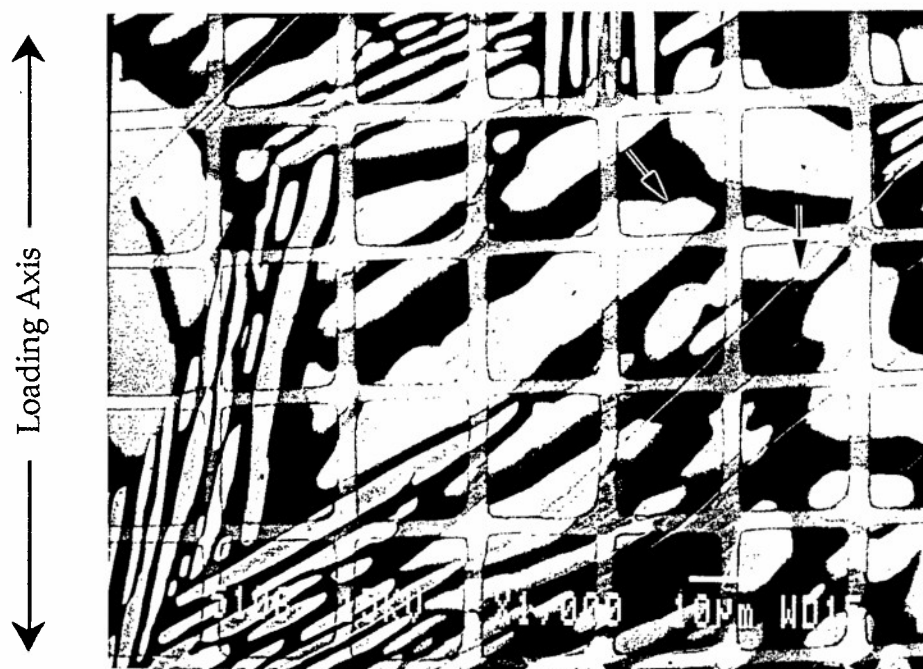
Fig. 51 Optical micrograph of α - β Ti-6.0Mn alloy after creep deformation to 0.62%.

Fig. 52 SEM Micrograph of Ti-8.1V (~ 51% α - 49% β) alloy: (a) before tensile deformation and (b) the same area after deformation, note coarse slip lines. Total plastic strain is 2.33% at a strain rate of $3.28 \times 10^{-5} \text{ s}^{-1}$. The alloy was heat treated for 2 h at 1173 K, FC to 963 K, annealed for 200 h and water quenched.

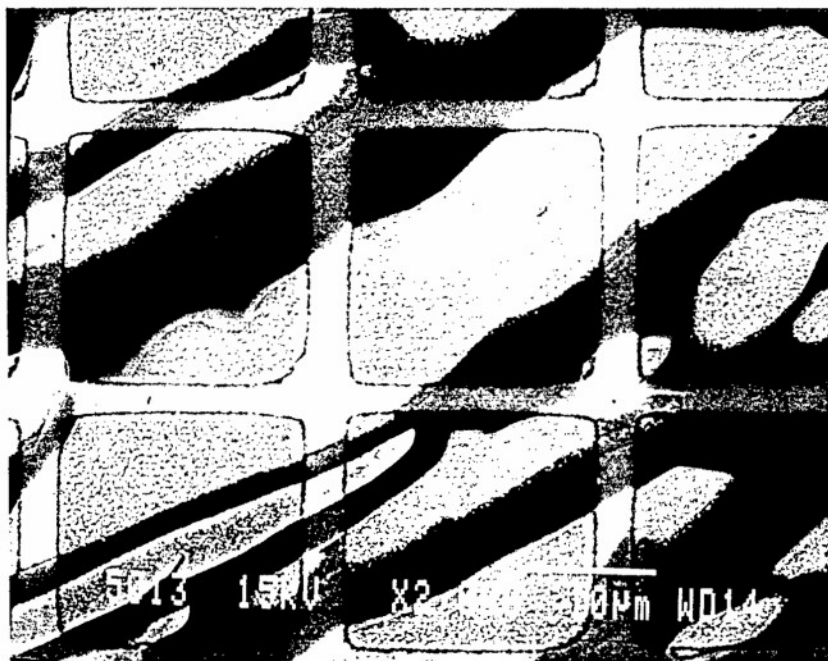
Fig. 53 A different area of the same α - β Ti-8.1V alloy specimen as in Fig. 52, at a higher magnification, (a) before tensile deformation, (b) after deformation, note continuous coarse slip lines penetrating the α and β phases. The same area as shown in (a) and (b), at a higher magnification, (c) before tensile deformation and (d) after deformation, note continuous coarse slip lines penetrating the α and β phases. The alloy was heat treated for 2 h at 1173 K, FC to 963 K, annealed for 200 h and water quenched.



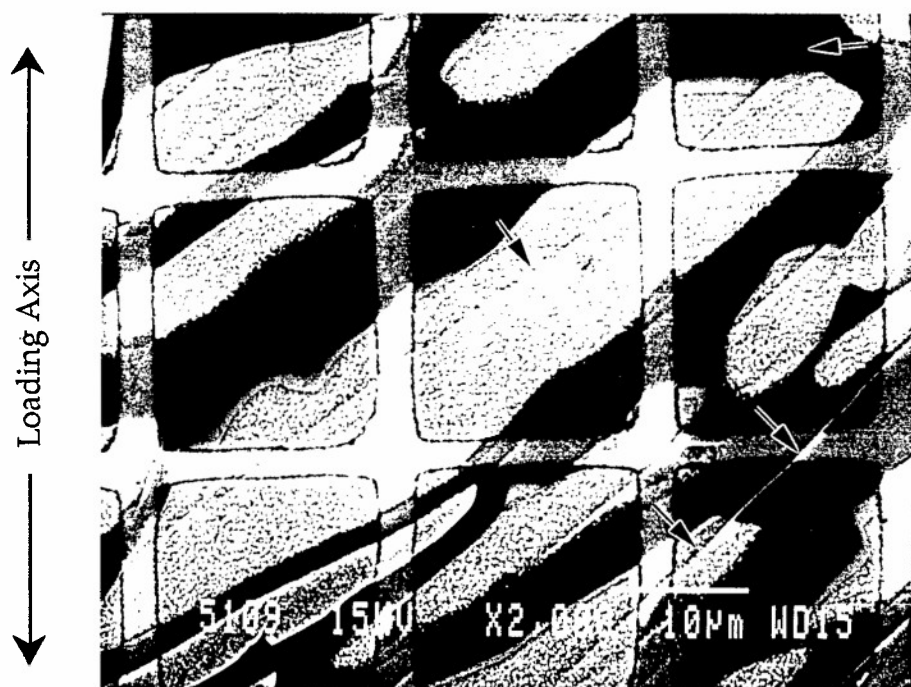
(a)



(b)



(c)



(d)

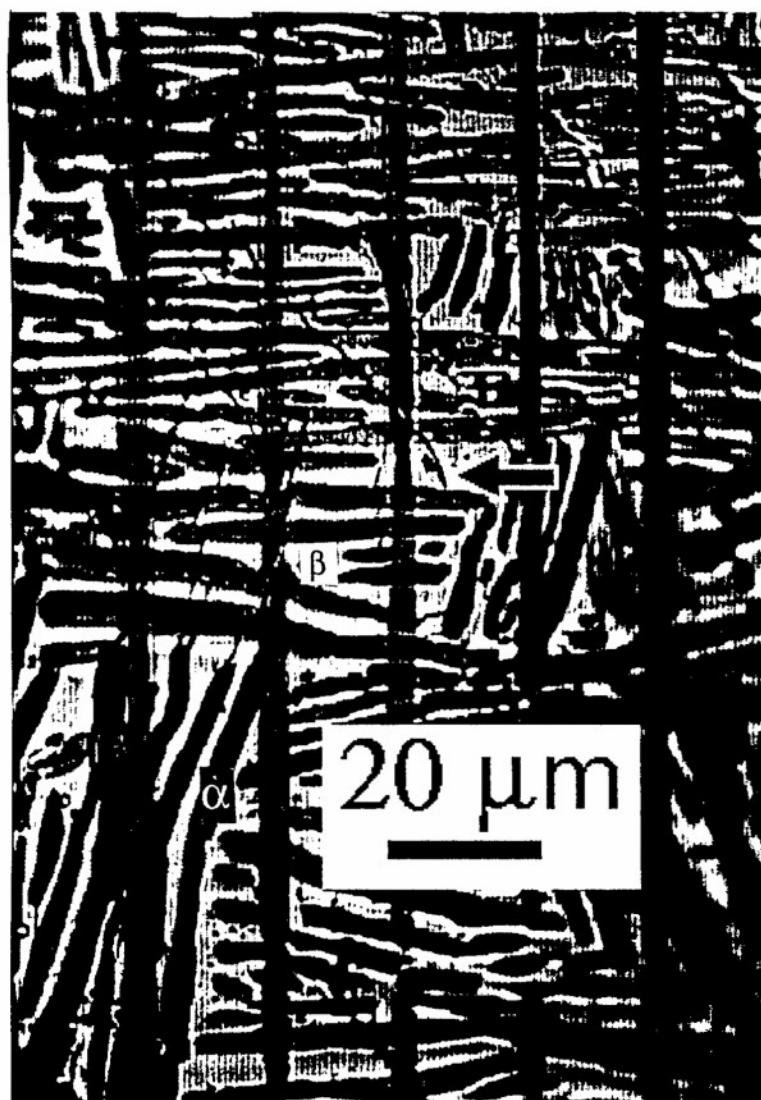
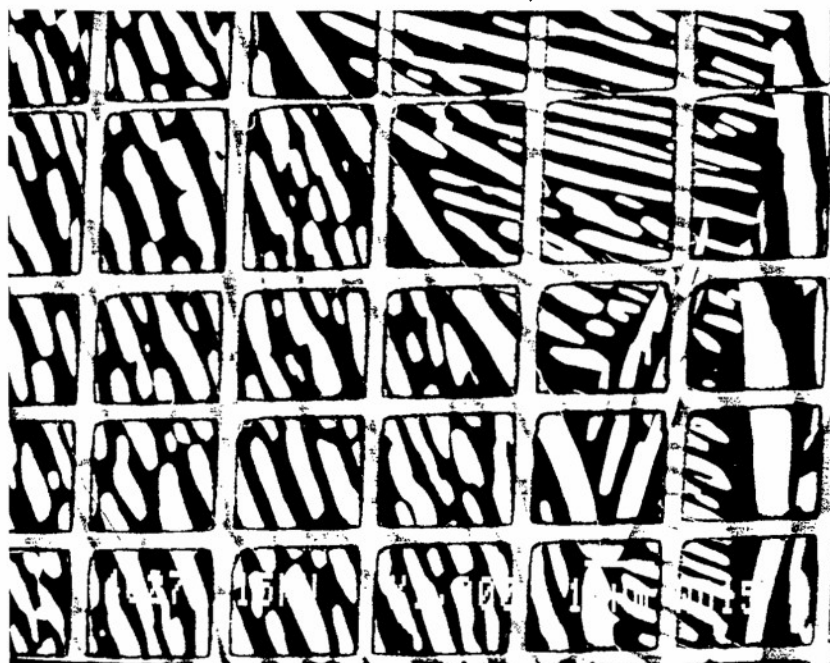
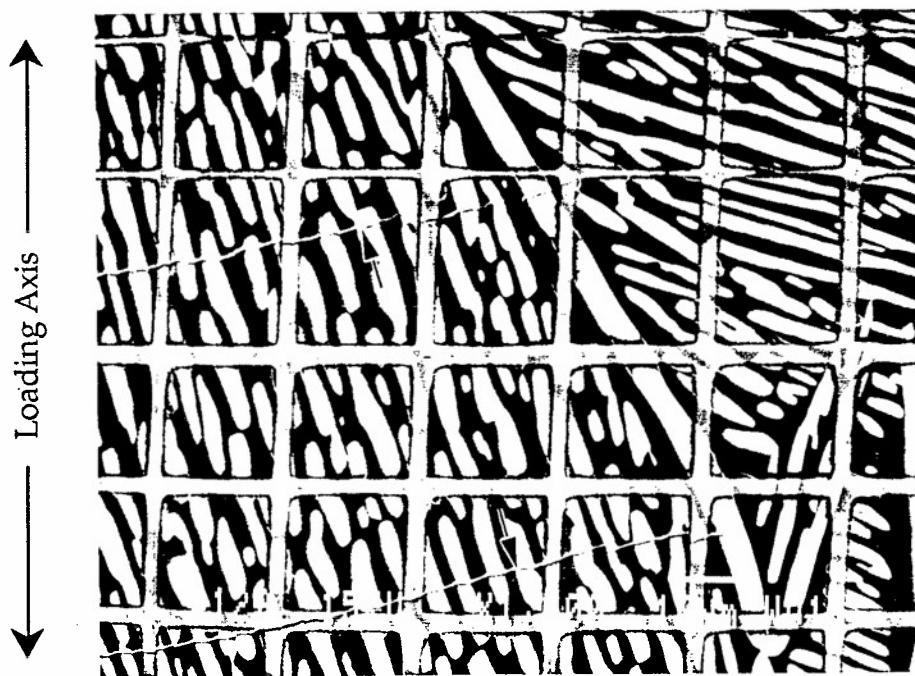


Fig. 54 Optical micrograph of α - β Ti-8.1V alloy specimen after tensile deformation. Vertical lines are gold reference grid lines.

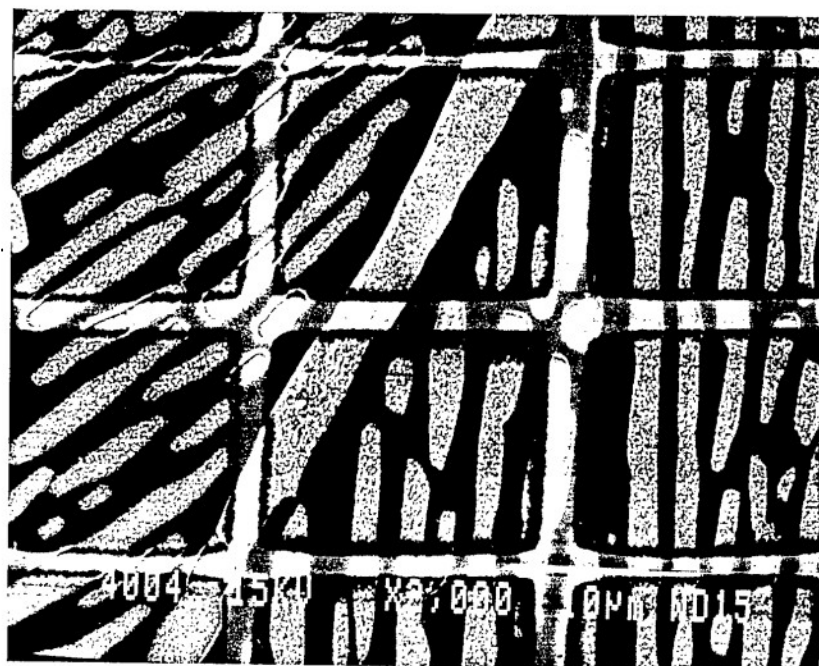
Fig 55 Microstructure of Ti-8.1V (~ 51% α - 49% β) alloy: (a) before creep deformation, (b) the same area after creep deformation, note slip lines, (c) another area of the same specimen before creep deformation and (d) after creep deformation, note slip lines crossing α - β boundaries. The total creep strain is 0.57% in 280 h at 95% YS. The alloy was heat treated for 2 h at 1173 K, FC to 963 K, annealed for 200 h and water quenched.



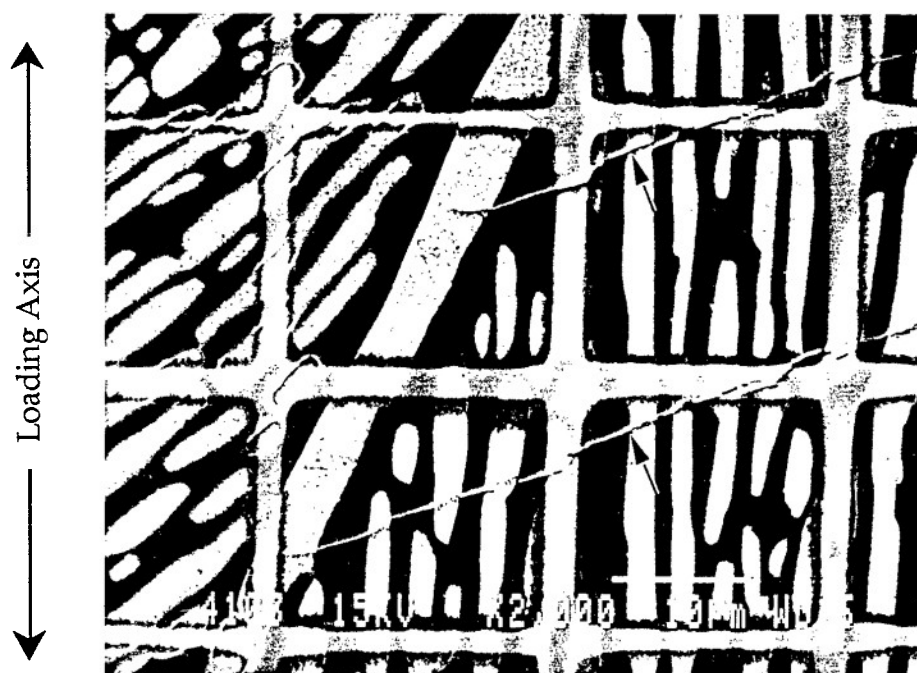
(a)



(b)



(c)



(d)

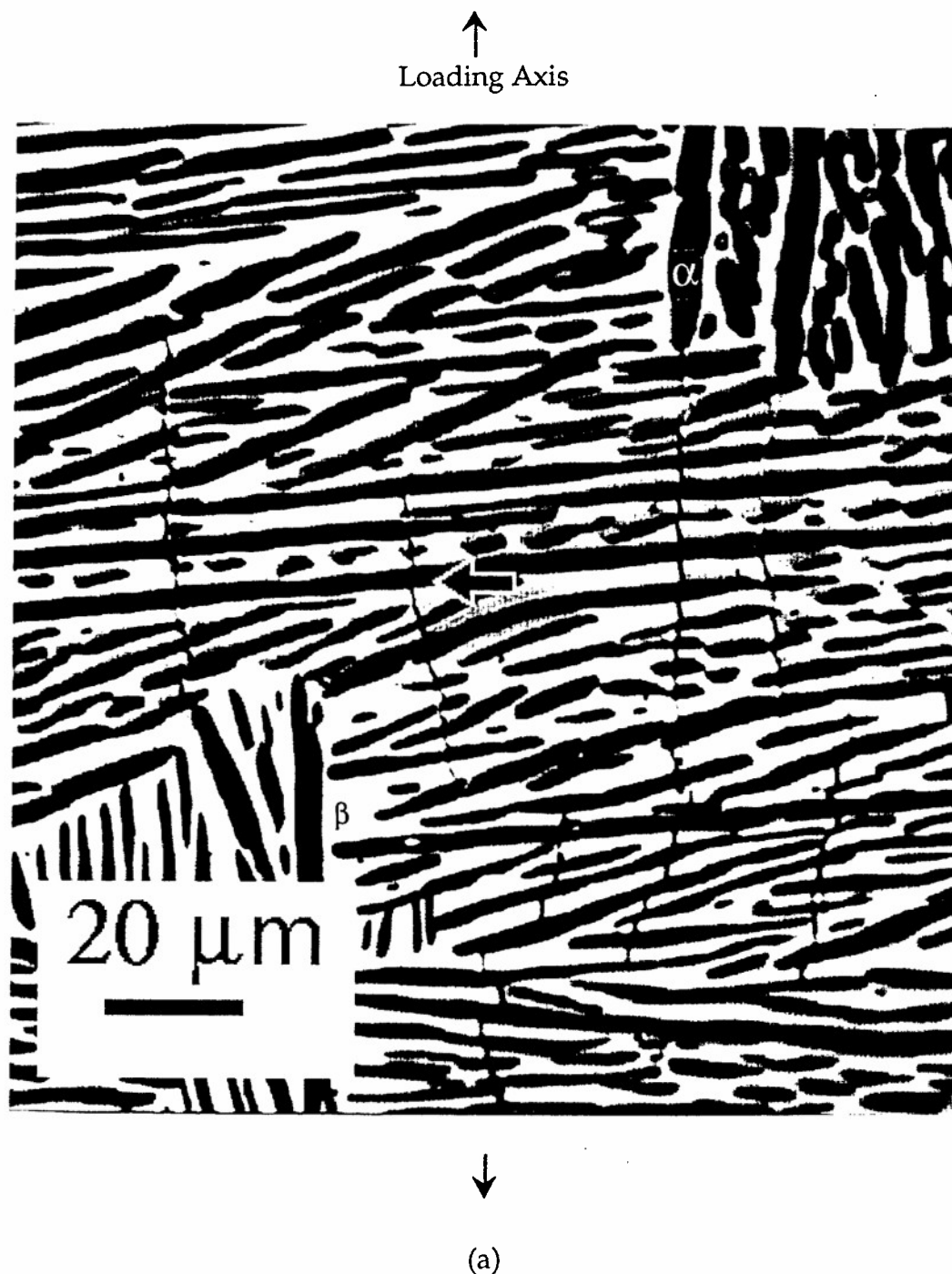
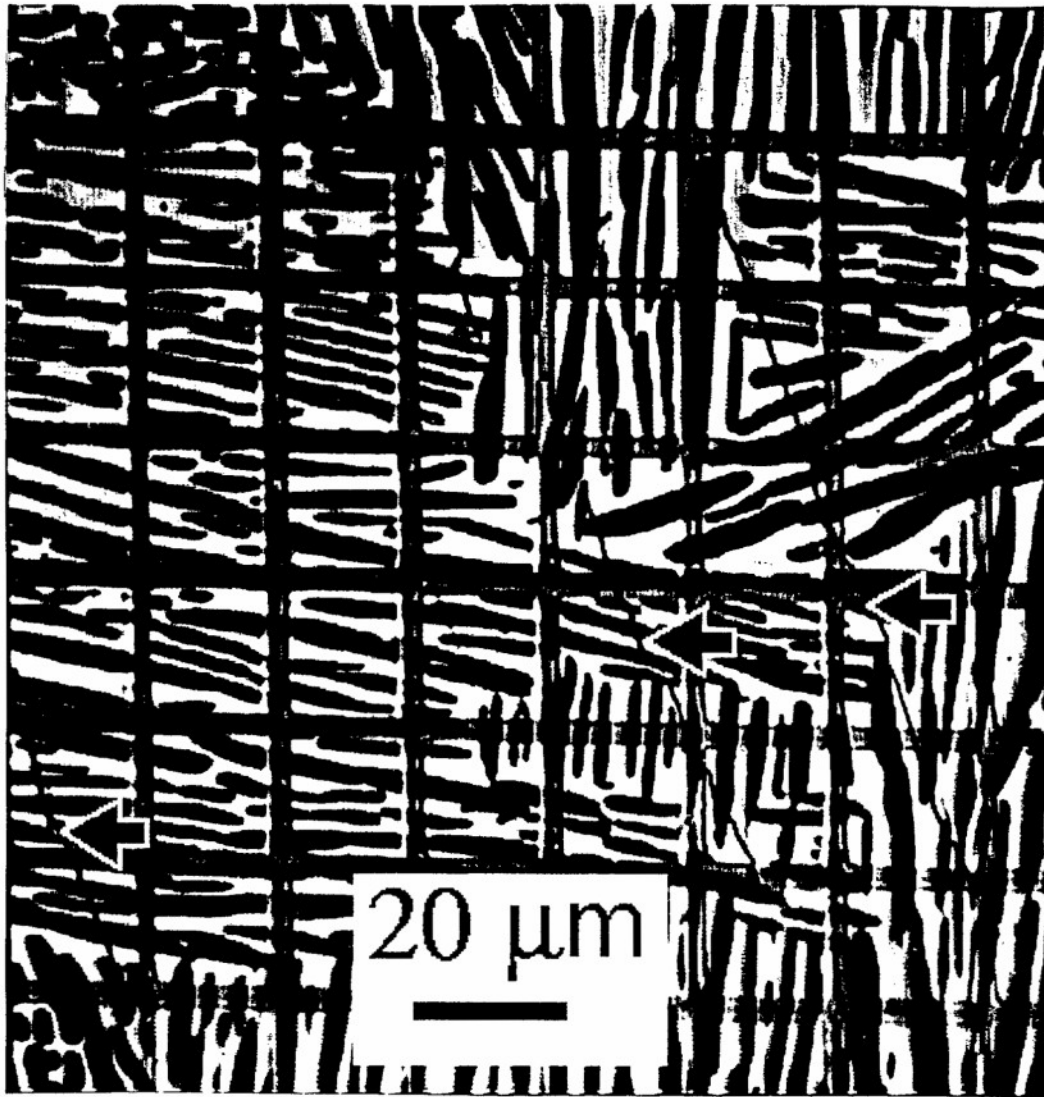


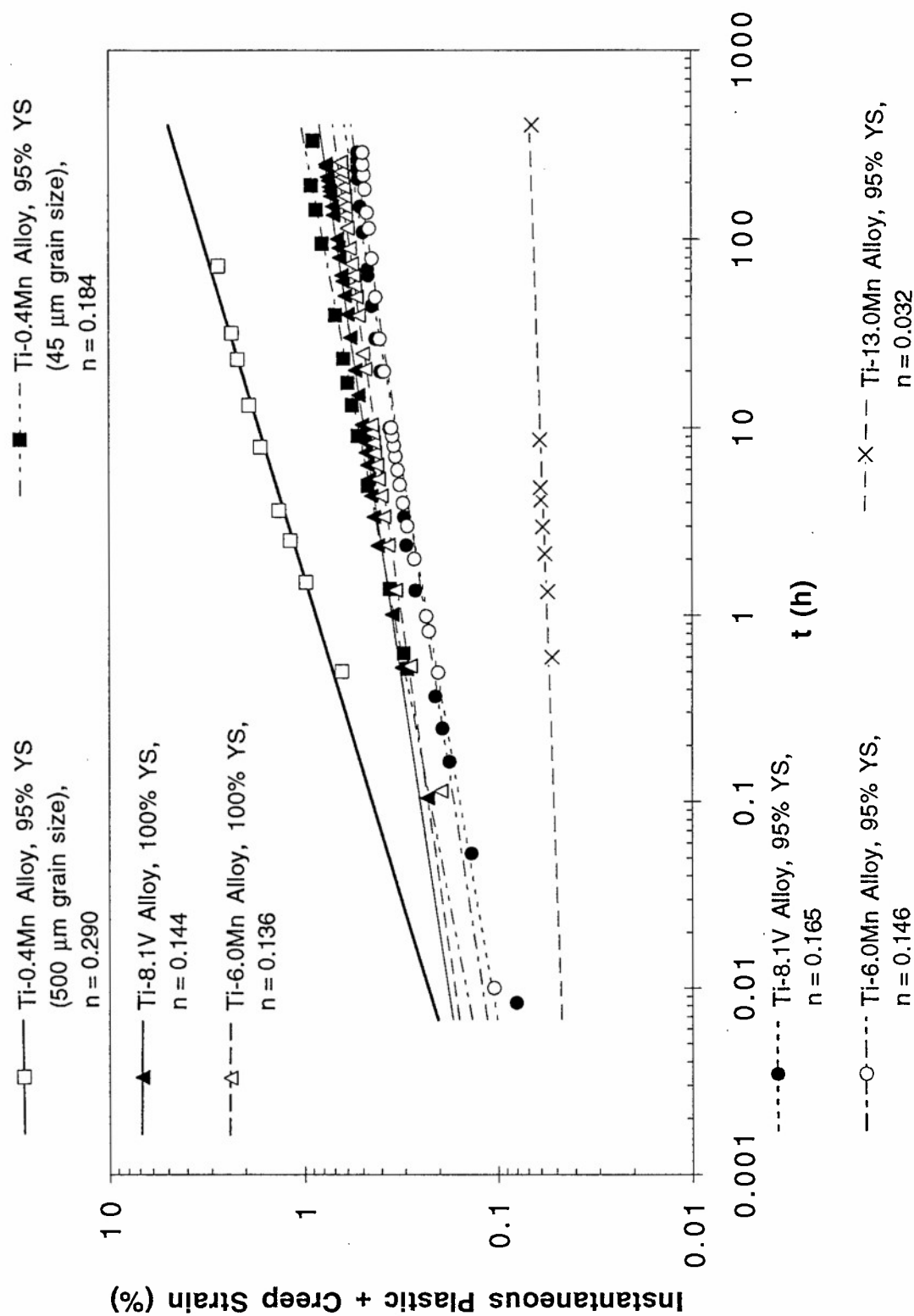
Fig. 56 Optical micrograph of Ti-8.1V ($\sim 51\% \alpha$ - $49\% \beta$) alloy after creep deformation, (a) without reference grid and (b) with reference grid. Note slip lines. The total creep strain was 0.57% in 280 h at 95% YS.

↑
Loading Axis



(b)

Fig. 57 Log-log plot of creep strain, ϵ_c , versus time, t . Slope is time exponent, n , from equation $\epsilon_c = At^n$.



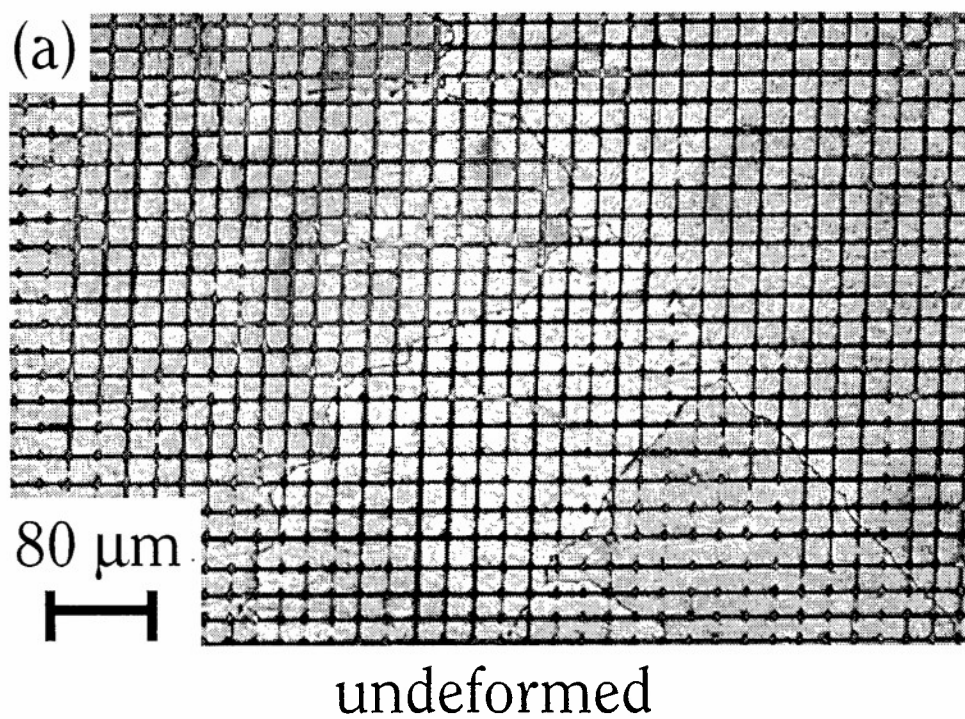
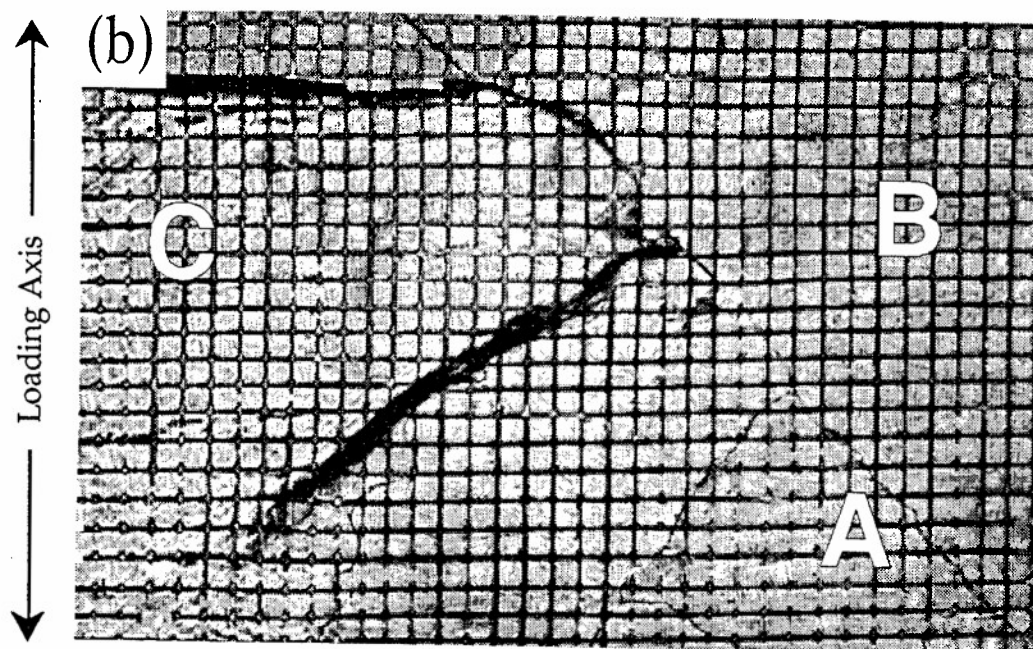
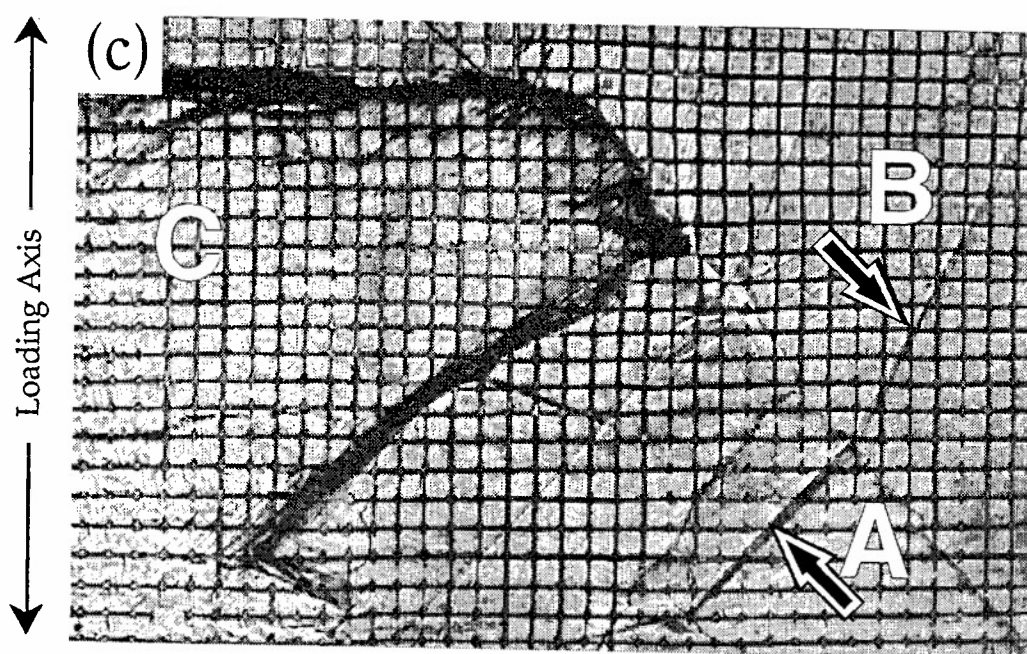


Fig. 58 Optical micrograph of another area of Specimen B. Note elongation of grid lines in direction of loading at "A" and "B" in (b), (c) shows twin formation at locations "A" and "B", i.e. twin triggering another twin in a neighboring grain, (c) also reveals coarse slip at "C".



creep strain = 1.73%, time = 17.7 h



creep strain = 2.82%, time = 115 h

Fig. 59 Transmission electron micrograph of 500 μm grain size α Ti-0.4Mn alloy after creep strain to 2.7% at 298 K. Note twin/dislocation interaction at "A".



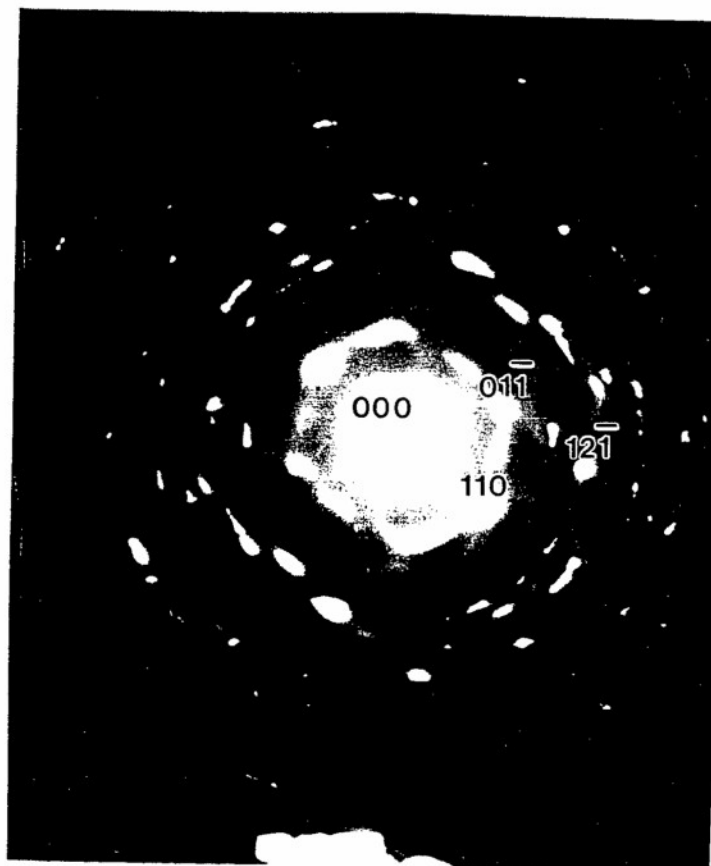


Fig. 60 Pre ω phase streaking in the SADP of β phase in the α - β Ti-6.0Mn alloy.

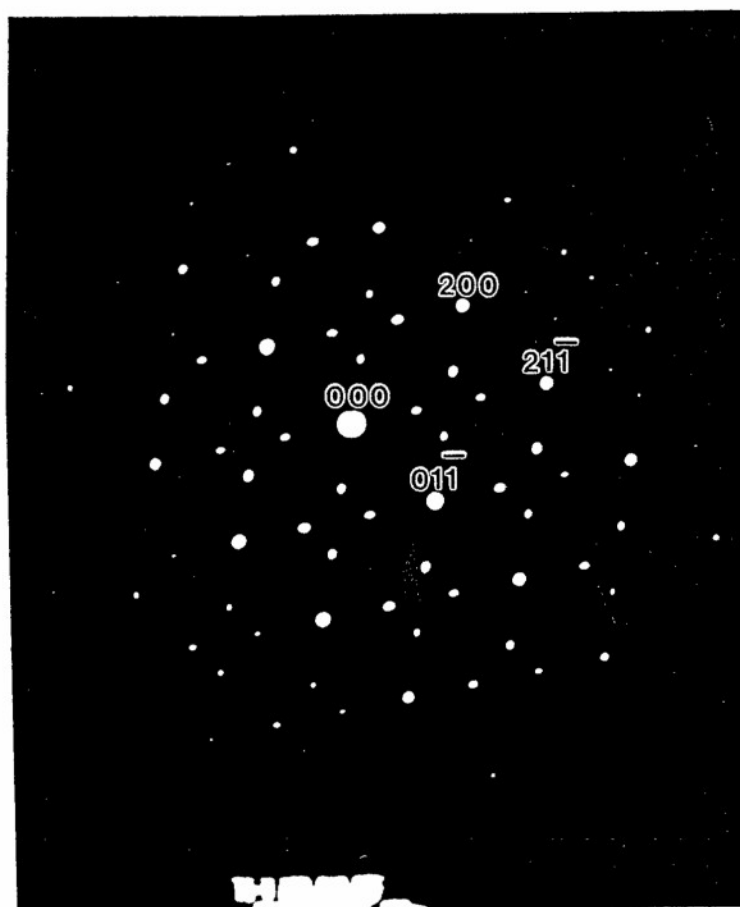


Fig. 61 Athermal ω phase evident in the SADP of β phase in the α - β Ti-8.1V alloy.

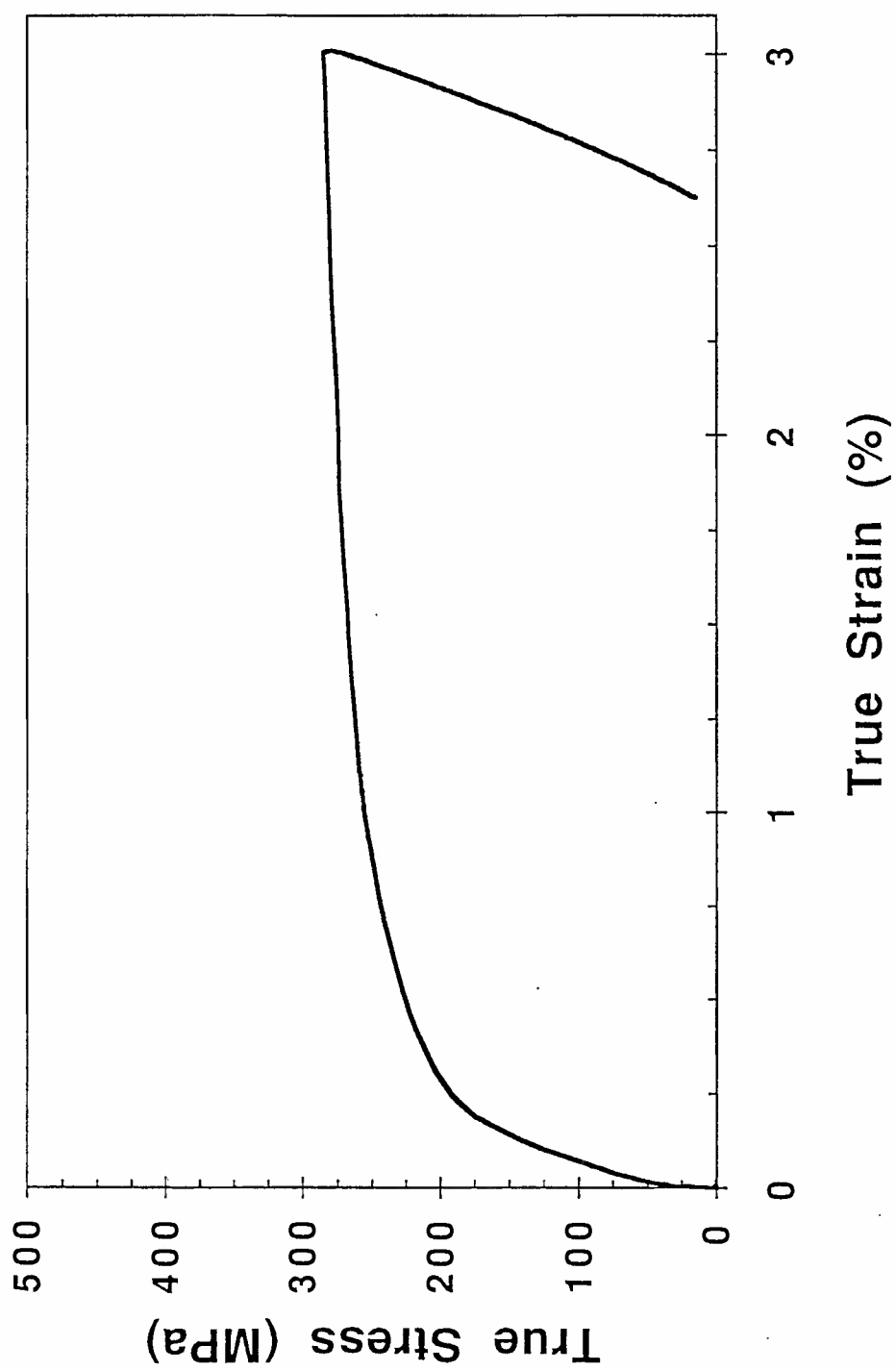


Fig. 62 Ambient temperature true stress - true strain curve of α Ti-1.5V alloy [98].

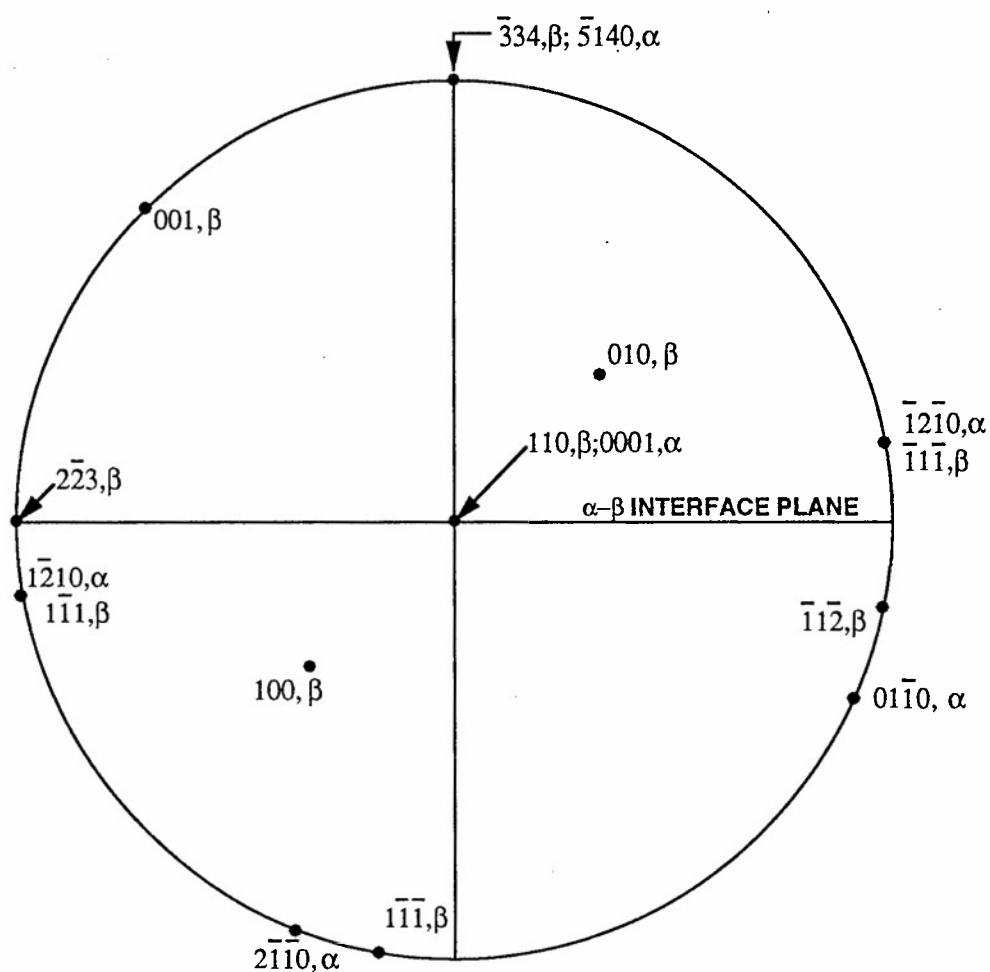


Fig. 63 A stereographic projection showing the interface plane, $(\bar{5}140)_{\alpha'}$, $(\bar{3}34)_{\beta}$ and the Burgers orientation relationship $\langle \bar{1}210 \rangle_{\alpha} // \langle \bar{1}\bar{1}1 \rangle_{\beta}$ for α - β phases in two phase titanium alloys with Widmanstatten type microstructure.

8. REFERENCES

1. B. P. Bannon, D. M. Strollo and D. E. Thomas, *Industrial Applications of Titanium and Zirconium*, edited by R. T. Webster and C. S. Young, p. 66, ASTM, Philadelphia, PA (1984).
2. K. Wang, L. Gustavson and J. Dumbleton, *Beta Ti Alloys for the 1990s*, edited by D. Eylon, R. R. Boyer and D. A. Koss, p. 49, TMS, Warrendale, PA (1993).
3. A. K. Mishra, J. A. Davidson, P. Kovacs and R. A. Poggie, *Beta Ti Alloys for the 1990s*, edited by D. Eylon, R. R. Boyer and D. A. Koss, p. 61, TMS, Warrendale, PA (1993).
4. F. C. Holden, H. R. Ogden and R. I. Jaffee, *Trans. AIME*, **200**, 169 (1954).
5. H. Conrad, *Canad. J. Phys.*, **45**, 581 (1967).
6. S. Ankem and H. Margolin, *Metall. Trans.*, **17A**, 2209 (1986).
7. C. A. Greene and S. Ankem, *Beta Ti Alloys for the 1990s*, edited by D. Eylon, R. R. Boyer and D. A. Koss, p. 309, TMS, Warrendale, PA (1993).
8. D. Sil, C. A. Greene and S. Ankem, *International Workshop on β Titanium Alloys*, Societe Française de Metallurgie et de Materiaux, Paris, March 14-16, 1994.
9. A. Akhtar and E. Teghtsoonian, *Metall. Trans.*, **6A**, 2201 (1975).
10. A. Akhtar, *Metall. Trans.*, **6A**, 1105 (1975).

11. F. D. Rossi, C. A. Dube and B. H. Alexander, *J. of Metals Trans. AIME* Feb., 257 (1953).
12. W. J. McG. Tegart, 1964, *Phil. Mag.*, **9**, 339 (1964).
13. H. Numakura, Y. Minonishi and M. Koiwa, *Scripta. Metall.*, **20**, 1581 (1986).
14. H. Conrad, *Progress in Material Science*, **26**, 200 (1981).
15. M. H. Yoo, *Trans. of Metall. Soc. AIME*, **245**, 2051 (1969).
16. D. J. Bacon and A. Serra, *Mat. Res. Soc. Symp. Proc.*, **238**, 73 (1992).
17. J. Jinoch, S. Ankem and H. Margolin, *Mat. Sci. Eng.*, **34**, 203-211 (1978).
18. S. Ankem and H. Margolin, *Metall. Trans. A*, **14A**, 500-503 (1983).
19. S. Ankem and H. Margolin, *Metall. Trans.*, **13A**, 603 (1982).
20. M. K. Koul and J. F. Breedis, *Acta Metall.*, **18**, 579-588 (1970).
21. T. S. Kuan, R. R. Ahrens and S. L. Sass, *Metall. Trans.*, **6A**, 1767 (1975).
22. R. R. Boyer, *Beta Ti Alloys for the 1990s*, edited by D. Eylon, R. R. Boyer and D. A. Koss, p. 335, TMS, Warrendale, PA (1993).
23. H. P. Chu, *J. of Mater.*, **5**, 633 (1970).
24. M. A. Imam and C. M. Gilmore, *Metall. Trans.*, **10A**, 419 (1979).
25. W. H. Miller, Jr., R. J. Chen and E. A. Starke, Jr., *Metall. Trans.*, **18A**, 1451 (1987).
26. G. Y. Gao and S. C. Dexter, *Metall. Trans.*, **18A**, 1125 (1987).
27. D. Eylon and J. A. Hall, *Met Trans.*, **8A**, 981 (1977).
28. W. J. Evans and C. R. Gostelow, *Met Trans.*, **10A**, 1837 (1979).

29. J. E. Hack and G. R. Leverant, *Met Trans.*, **13A**, 1729 (1982).
30. W. H. Riemann, *J Mater*, **6**, 926 (1971).
31. A. J. Hatch, J. M. Partridge and R. G. Broadwell, *J Mater*, **2**, 111 (1967).
32. B. C. Odegard and A. W. Thompson, *Met Trans*, **5**, 1974, 1207.
33. G. R. Yoder, C. A. Griffis, and T. W. Crooker, *Trans. AIME*, **96**, 268 (1974).
34. S. Wapniarsky, A. I. Rotem and A. Rosen, *Strength of Metals and Alloys*, **1**, (Proc.), Haifa, Israel, 437 (1991).
35. H. Adenstedt, *Metal Progress*, **56**, 658 (1949).
36. N. R. Kiessel and M. J. Sinnott, *Trans. AIME*, **197**, 331 (1953).
37. D. R. Luster, W. W. Went and D. W. Kaufman, *Materials and Methods*, **37**, 100 (1953).
38. R. Zeyfund, R. Martin and H. Conrad, *Mat. Sci. and Eng.*, **8**, 134 (1971).
39. K. Stetina, *Scripta Met.*, **3**, 57 (1969).
40. S. Agrawal, G. Sargent and H. Conrad, *Metall. Trans.*, **4**, 2613 (1973).
41. S. Agrawal, G. Sargent and H. Conrad, *J. Less Common Met.*, **34**, 201 (1974).
42. W. J. Evans, *Creep and Fracture of Engineering Materials and Structures*, (Proc.) Swansea, UK, 5-10 Apr. 1987, Inst. of Metals, 603 (1987).
43. G. F. Harrison, P. H. Tranter, M. R. Winstone and W. J. Evans, *Creep and Fracture of Engineering Materials and Structures*, (Proc.) Swansea, UK, 5-10 Apr. 1987, Inst. of Metals, 615 (1987).

44. A. W. Thompson and B. C. Odegard, *Metall. Trans.*, **4**, 899 (1973).
45. Max Hansen, *Constitution of Binary Alloys*, p. 616, McGraw-Hill Book Company (1965).
46. G. Grewal and S. Ankem, *Metall. Trans.*, **20**, 334 (1989).
47. D. G. Attwood and P. M. Hazzledine, *Metallography*, **9**, 483 (1976).
48. M. Kikukawa, M. Jono and M. Adachi, *Mechanical Behavior of Materials*, *JSMS*, **1**, (Proc), Kyoto, Japan, August 21-24, 307 (1974).
49. H. Margolin and J. P. Neilsen, *Modern Materials*, **2**, p. 225, Academic Press, 1960.
50. Directions for Microposit™ 2400 Series Photoresist, Shipley Company, tel. 800-345-3100, Whitehall, PA (1991).
51. COHU 4810 Series Monochrome Solid-State Cameras Installation and Operation Instructions, Document No. 6X-845(A), COHU, Inc., Electronics Div., tel. 619-277-6700, San Diego, CA 92138-5623.
52. PCVISION plus™ Hardware Reference Manual, Imaging Technology Inc., tel. 800-874-1888, Document No. 47-H00010-02 (1989).
53. JAVA®, Jandel Video Analysis Software, Jandel Scientific, tel. 800-874-1888, Carte Madera, CA (1988).
54. R. A. Spurling, *Metall. Trans.*, **6A**, 1660 (1975).
55. J. W. Edington, *Practical Electron Microscopy in Materials Science*, p. 77, TechBooks, Herndon, VA, (1976).
56. P. G. Partridge, *Metall. Rev.*, **12**, 169 (1967).
57. Analog Connection Jr. Manual, Data Acquisition & Control Sys,

Strawberry Tree, Inc., tel. 408-736-8800, Sunnyvale, CA (1988).

58. P. R. Bevington, *Data Reduction and Error Analysis for the Physical Sciences*, p.64, McGraw-Hill Book Company, New York (1969).
59. R. J. Lederich, S. M. L. Sastry, J. E. O'Neal and B. B Rath, *Mat. Sci. and Eng.* **33**, 183 (1978).
60. H. Conrad, *Progress in Material Science* **26**, p. 123 (1981).
61. G. E. Dieter, *Mechanical Metallurgy 3rd ed.*, p.448, McGraw-Hill, New York (1986).
62. J. R. Hauber and O. D. Sherby, *J. of Mater.* **5**, 251 (1970).
63. M. Oka and Y. Taniguchi, *Metall. Trans.*, **10A**, 651 (1979).
64. R. W. Armstrong, *Deformation Twinning*, p. 356, Gordon & Breach, New York (1964).
65. A. K. Chakrabarti and E. S. Nichols, *Titanium '80*, Science and Technology, p. 1081, AIME, Warrendale, PA (1981).
66. J. D. Lubahn and R. P. Felgar, *Plasticity and Creep of Metals*, pp. 157, 239, 259, John Wiley & Sons, New York (1961).
67. Y. Lii, V. Ramachandran and R. E. Reed-Hill, *Metall. Trans.*, **1447** (1970).
68. M. V. Klassen-Neklyudova, *Mech. Twinning of Crystals*, p. 101, Consultants Bureau, New York (1964).
69. M. H. Yoo, *Metall. Trans.*, **12A**, 409 (1981).
70. R. W. Cahn, *Deformation Twinning*, p. 1, Gordon & Breach, New York (1964).

71. G. F. Bolling and R. H. Rickman, *Acta Metall.*, **13**, 745 (1965).
72. K. Jagannadham and R. W. Armstrong, *Scripta Metall.*, **21**, 1459 (1987).
73. S. Mahajan and D. F. Williams, *Int. Metall. Rev.*, **18**, 43 (1973).
74. C. J. Beevers and J. L. Robinson, *J. Less-Common Metals*, **17**, 345 (1969).
75. S. Ankem, C. A. Greene and S. Singh, *Scripta Metall.*, **30**, 803 (1994).
76. A. P. Young, R. I. Jaffee and C. M. Schwartz, *Acta Metall.*, **11**, 1097 (1963).
77. J. C. Williams, *Titanium Science and Technology*, edited by R. I. Jaffee and H. M. Burte, p. 1433, Plenum Press, New York (1973).
78. D. de Fontaine, N. Paton and J. C. Williams, *Acta Metall.*, **19**, 1153 (1971).
79. F. W. Ling, E. A. Starke, Jr. and B. G. LeFevre, *Metall. Trans.*, **5A**, 179 (1974).
80. S. Hanada and O. Izumi, *Trans. Japan Inst. Metals*, **23**, No. 2, 85 (1982).
81. S. Hanada, A. Takemura and O. Izumi, *Trans. Japan Inst. Metals*, **23**, No. 9, 507 (1982).
82. S. Hanada and O. Izumi, *J. Mater. Sci.*, **21**, 4131 (1986).
83. S. Hanada, T. Yoshio, O. Izumi, *Trans. Japan Inst. Metals*, **27**, No. 7, 496 (1986).
84. S. Hanada and O. Izumi, *Metall. Trans.*, **18A**, 265 (1987).
85. S. Ankem, J. G. Shyue, M. N. Vijayshankar, and R. J. Arsenault,

- Mat. Sci. & Eng.*, **A111**, 51, (1989).
86. M. N. Vijayshankar and S. Ankem, *Mat. Sci. & Eng.*, **A129**, 229, (1990).
 87. D. Sil and S. Ankem, *Unpublished Research*, (1994).
 88. J. C. Williams, B. S. Hickman and C. H. Leslie, *Metall. Trans.*, **2A**, 477 (1971).
 89. S. Ankem and S. R. Seagle, *Beta Titanium Alloys in the 1980s*, edited by R. R. Boyer and H. W. Rosenberg, p. 107, TMS, Warrendale, PA (1984).
 90. C. H. Wells and C. P. Sullivan, *Trans. ASM*, **62**, 263 (1969).
 91. M. A. Greenfield and H. Margolin, *Metall. Trans.*, **3**, 2649 (1972).
 92. D. Eylon, et. al., *Metall. Trans.*, **7A**, 1817 (1976).
 93. D. Eylon and J. A. Hall, *Metall. Trans.*, **8A**, 981 (1977).
 94. D. Shechtman and D. Eylon, *Metall. Trans.*, **9A**, 1018 (1978).
 95. D. Eylon and P. J. Bania, *Metall. Trans.*, **9A**, 1273 (1978).
 96. S. Ankem and H. Margolin, *Metall. Trans.*, **11A**, 963 (1980).
 97. C. A. Greene, *M. S. Paper*, University of Maryland, College Park (1992).
 98. S. Singh and S. Ankem, *Unpublished Research*, 1994.
 99. P. A. Albert, *Trans. AIME*, **197**, 1449 (1953).
 100. C. G. Rhodes and J. C. Williams, *Metall. Trans*, **6A**, 2103 (1975).
 101. C. G. Rhodes and N. E. Paton, Final Report submitted to ONR, Contract No. N00014-76-C-0598 (1979).
 102. D. A. Porter and K. E. Easterling, *Phase Transformations in Metals*

and Alloys, 2nd edition, Chapman and Hall, London, 1992, p. 145.

CURRICULUM VITAE

Name: Charles Arthur Greene

PII Redacted

Degree and date to be conferred: Ph.D., 1994

PII Redacted

PII Redacted

Secondary Education: Sandy Spring Friends School, Sandy Spring,
Maryland, 1980

Collegiate institutions attended:

<u>INSTITUTION</u>	<u>DATES ATTENDED</u>	<u>DEGREE</u>	<u>DATE OF DEGREE</u>
--------------------	-----------------------	---------------	-----------------------

University of Maryland	8/89 - 8/94	Ph.D.	1994
Major:	Engineering Materials		
Minor:	Physics of Materials		

University of Maryland	8/89 - 12/92	M.S.	1992
Major:	Materials Science		

Towson State University	8/81 - 5/88	B.S.	1988
Major:	Physics		
Minors:	Chemistry, Mathematics		

Kenyon College	8/80 - 5/81		
Major:	Chemistry		

Professional Publications:

1. C. A. Greene and S. Ankem, "Ambient Temperature Tensile and Creep Deformation Behavior of Alpha and Beta Titanium Alloys" in *Beta Titanium Alloys in the 1990's* (edited by D. Eylon, R. R. Boyer and D. A. Koss), published by TMS, 1993, pp. 309-319
2. S. Ankem, C. A. Greene and S. Singh, "Time Dependent Twinning During Ambient Temperature Creep of α Ti-Mn Alloy", *Scripta. Met.*, Vol. 30-6, March, 1994, pp. 803-808

3. S. Ankem, C. A. Greene, S. Singh and D. Sil, "Recent Developments in Ambient Temperature Creep Deformation Behavior of Alpha, Alpha-Beta and Beta Titanium Alloys", Proceedings of the *Harold Margolin Symposium on Microstructure/Property Relationships of Titanium Alloys*, TMS Annual Meeting, San Francisco, February 27 - March 3, 1994
4. D. Sil, C. A. Greene and S. Ankem, "The Effect of Alloying Element on the Tensile Deformation Behavior of β Titanium Alloys", Proceedings of the *International Workshop on β Titanium Alloys*, Societe Française de Metallurgie et de Materiaux, Paris, March 14-16, 1994

Professional positions held:

- Oct. 94-Oct. 96 National Research Council Associateship at the Naval Research Laboratory in Washington, DC
- Sept. 91-Aug. 94 National Defense Science and Engineering Graduate Fellow and Research Assistant at the University of Maryland, College Park, Maryland
- June 90-Aug. 91 Graduate Research Assistant at the University of Maryland, College Park, Maryland
- Aug. 89-May 90 Graduate Teaching Assistant at the University of Maryland, College Park, Maryland
- June 88-July 89 Senior Research Technician in the Biophysics Department at The Johns Hopkins University School of Medicine, Baltimore, Maryland